EFFICIENCY ESTIMATION OF INDUCTION MACHINES WITH LIMITED MEASUREMENTS

Arbi Gharakhani Siraki

A Thesis

In the Department

of

Electrical and Computer Engineering

Presented In Partial Fulfillment of the Requirements

for The Degree of

Doctor of Philosophy (Electrical and Computer Engineering) at

Concordia University

Montreal, Quebec, Canada

AUGUST 2012

CONCORDIA UNIVERSITY

SCHOOL OF GRADUATE STUDIES

This is to certify that the thesis prepared

By: **Arbi Gharakhani Siraki**

Entitled: **Efficiency Estimation of Induction Machines with Limited Measurements**

and submitted in partial fulfillment of the requirements for the degree of

DOCTOR OF PHILOSOPHY (Electrical & Computer Engineering)

complies with the regulations of the University and meets the accepted standards with respect to originality and quality.

Signed by the final examining committee:

_____ Chair
Dr. R. Zmeureanu

_____ External Examiner
Dr. J. O. Ojo

_____ External to Program
Dr. M. Paraschivoiu

_____ Examiner
Dr. A. G. Aghdam

_____ Examiner
Dr. L. A. C. Lopes

_____ Thesis Supervisor
Dr. P.Pillay

Approved by _____
J.X. Zhang, Graduate Program Director

August 13, 2012

_____
Dr. Robin A.L. Drew, Dean
Faculty of Engineering and Computer Science

ABSTRACT

Efficiency Estimation of Induction Machines with Limited Measurements

Arbi Gharakhani Siraki, Ph.D.

Concordia University, 2012

The first goal of this thesis is to develop a non-intrusive in-situ efficiency estimation technique, which is capable of dealing with unbalanced supplies and under- or overvoltage conditions. For the purpose of this thesis, non-intrusiveness refers to electrical measurements at terminals only, with no mechanical measurements, not even speed. This requirement imposes limitations on the available data, which brings challenges to the efficiency estimation problem. To have the lowest possible intrusion level, only two line voltages and currents are allowed to be measured, and all the required information, such as input and output power, speed, temperature, and the motor parameters, must be calculated or estimated solely based on these measurements.

The second goal of this thesis is to develop a simple method for full load efficiency estimation from no-load uncoupled testing, which can be used in refurbishment centers to estimate the efficiency of induction machines without performing expensive dynamometer testing.

ACKNOWLEDGMENTS

I would like to thank my supervisor, Prof. P. Pillay, for his kind support and guidance during these four years. I have learned a lot from his critical thinking, scientific knowledge, and precision, all of which will help me, for sure, in my future career. Our weekly meetings enabled me to develop my capabilities as a researcher and to improve my capacity to handle different tasks in a proper manner.

I thank Dr. L. Lopes and Dr. S. Williamson for encouraging me to participate in a variety of activities during the Ph.D. program.

My sincere gratitude is extended to my family, specifically my father, Mr. Aghanoor Gharakhani, and my mother, Mrs. Manoosh Torosian, for their unconditional love and support throughout my life.

I would also like to thank my fiancée, Miss Edna Tarverdian, for her emotional support and encouragement.

Many thanks to my colleagues and friends in the Power Electronics and Energy Research (PEER) group of Concordia University for the wonderful research environment I have experienced during these four years.

I would like to thank and acknowledge the support of the Natural Sciences & Engineering Research Council of Canada and Hydro-Québec for this work.

This work was supported in part by the R&D program of the NSERC Chair entitled Energy efficiency in electrical machines for small renewable energy production systems established in 2009 at “Concordia University”

TABLE OF CONTENTS

LIST OF FIGURES

LIST OF TABLES

NOMENCLATURE

AGT	Air-Gap Torque Method
CVUF	Complex Voltage Unbalance Factor
EVB	Evolutionary-Based Algorithm
FFT	Fast Fourier Transformation
GA	Genetic Algorithm
IM	Induction Motor
MCSA	Machine Current Signature Analysis
MAGT	Modified Air-Gap Torque Method
MNAGT	Modified Non-intrusive Air Gap Torque Method
MEE	Maximum Error Estimation
NAGT	Non-intrusive Air-Gap Torque Method
OVU	Overvoltage Unbalanced Condition
PU	Per Unit
RVU	Rated Voltage Unbalanced Condition

RMS	Route Mean Square
REE	Realistic Error Estimation
UVU	Undervoltage Unbalanced Condition
VUF	Voltage Unbalance Factor
WCEE	Worst Case Error Estimation

LIST OF SYMBOLS

$A(t)$	The signal's magnitude
E_1	Percentage of the error between estimated temperature at the rated condition and the assumed rated temperature
$E_{2,i}$	Percentage of the positive sequence input current estimation error at operating point "i"
$E_{3,i}$	Percentage of the positive sequence input active power estimation error at operating point "i"
f	Frequency
f_0	Frequency of the desired sinusoidal component
f_s	Supply frequency
f_{sdh}	Frequency of the largest speed-dependent component
$i(t)$	Current signal
$i_f(t)$	Fundamental component of the current signal
i_a , i_b , i_c	Instantaneous values of the current signal at phases a, b, and c
$I_{a,Est}$, $I_{b,Est}$, $I_{c,Est}$	Estimated currents based on the GA-estimated parameters
$I_{a,Meas}$, $I_{b,Meas}$, $I_{c,Meas}$	Measured values of the currents
I_{In}	Input current
$I_{In,Eff}$	Effective input current
$I_{In,Meas}$	Measured input current
$I_{In,N}$	Magnitude of the negative sequence input current
$I_{In,N,\ Est}$	Estimated magnitude of the negative sequence input current of the motor
$I_{In,N,\ Meas}$	Measured magnitude of the negative sequence input current of the motor
$I_{In,Noload}$	No-load input current
$I_{In,P}$	Magnitude of the positive sequence input current
$I_{In,P,\ Est}$	Estimated magnitude of the positive sequence input current

$I_{In,P,\ Meas}$	Measured magnitude of the positive sequence input current
$I_{In,Rated}$	Rated input current
$I_{In,VLR}$	Input current at low voltage virtual locked rotor test
I_M	The magnetizing current
$I_{M,P,Est}$	Estimated magnitude of the positive sequence magnetizing current
$I_{M,N,Est}$	Estimated magnitude of the negative sequence magnetizing current
I_R	Rotor current
$I_{R,N,Est}$	Estimated magnitude of the negative sequence rotor current
$I_{R,P,Est}$	Estimated magnitude of the positive sequence rotor current
$I_{R,Rated}$	Rotor current at the rated load
$\overline{I_a}, \overline{I_b}, \overline{I_c}$	Three-phase current phasor quantities
$\overline{I_0}, \overline{I_P}, \overline{I_N}$	Zero, positive and negative sequence current phasor quantities
IC_I	Influence coefficient of the current
IC_V	Influence coefficient of the voltage
IC_T	Influence coefficient of the torque
IC_S	Influence coefficient of the speed
K_{FW}	Coefficient of friction and windage losses
K_{Th}	Thermal coefficient of the machine
K_H	Coefficient of the hysteresis losses
K_E	Coefficient of the eddy current losses
m_1, m_2, m_3	Constants in the non-linear adaptive filter
$n(t)$	Noise signal
N_{Sync}	Mechanical synchronous speed
N_{Rated}	Mechanical rated speed
N_{Meas}	Measured speed
P	Number of poles
P_C	Core losses
P_{Conv}	Converted electrical to mechanical power
P_E	Eddy current losses

P_{FW}	Friction and Windage losses
P_{H}	Hysteresis losses
P_{In}	Input active power
$P_{In,Est}$	Estimated input power
$P_{In,Meas}$	Measured input power
$P_{In,N}$	Negative sequence input power
$P_{In,N,Est}$	Estimated negative sequence input power of the motor
$P_{In,N,Meas}$	Measured negative sequence input power of the motor
$P_{In,P}$	Positive sequence input power
$P_{In,P,\ Est}$	Estimated positive sequence input power of the motor
$P_{In,P,\ Meas}$	Measured positive sequence input power of the motor
$P_{In,VLR}$	Input power at low voltage virtual locked rotor test
$P_{L,Est}$	Estimated total losses of the machine
$P_{L,N,Est}$	Estimated losses in the negative sequence circuit
$P_{L,P,Est}$	Estimated losses in the positive sequence circuit
P_{Out}	Mechanical output power
$P_{Out,\ N}$	Negative sequence output power
$P_{Out,\ N,Est}$	Estimated negative sequence output power
$P_{Out,\ P}$	Positive sequence output power
$P_{Out,\ P,\ Est}$	Estimated positive sequence output power
$P_{Out,Rated}$	Rated mechanical output power
P_{SLL}	Stray load loss
$P_{SLL,\ Rated}$	Stray load loss at rated load
R_{1}	Stator resistance
R_{2}	Rotor positive sequence resistance
R_{3}	Rotor negative sequence resistance
R_{a}	Resistance at the ambient temperature
R_{M}	Resistance representing the core loss
R_{Rated}	Resistance at rated temperature
R_{SLL}	Resistance representing the stray load loss

S_{Est}	Estimated Slip
S_{Meas}	Measured slip
S_{Rated}	Rated slip
T	Machine's temperature
T_a	Ambient temperature
T_{AG}	Air-gap torque
T_{Rated}	Rated temperature of the machine
$T_{Rated,\ Est}$	Estimated temperature for the rated condition
v_{ab}, v_{bc} , v_{ca}	The instantaneous values of the line-to-line voltage signals
$V_{In,\ N}$	Negative sequence voltage magnitude
$V_{In,\ P}$	Positive sequence voltage magnitude
$V_{In,Min}$	Minimum voltage which gives the largest possible slip
$V_{In,Rated}$	Rated input voltage
$V_{In,Meas}$	Measured input voltage
$V_{In,VLR}$	Phase voltage at low voltage virtual locked rotor test
$V_{ab,}$ $V_{bc,}$ V_{ca}	Line to line voltages
$V_{a,}$ $V_{b,}$ V_c	Phase voltages
V_{Avg}	Average voltage of the three phases
V_M	Voltage across the magnetizing branch
V_N	Magnitude of the negative sequence component of the voltage signal
V_P	Magnitude of the positive sequence component of the voltage signal
$\overline{V_a}, \overline{V_b}, \overline{V_c}$	Phasors of the per phase voltages
$\overline{V_{ab}}, \overline{V_{bc}}, \overline{V_{ca}}$	Phasors of the line to line voltages
$\overline{V_{P,LL}}, \overline{V_{N,LL}}$	Phasors of the line to line positive and negative sequence voltages
$\overline{V_P}, \overline{V_N}$	Phasors of the per phase positive and negative sequence voltages
$X_{In,Min}$	Input reactance at the minimum voltage
$X_{In,Max}$	Maximum input reactance

$X_{In,Rated}$	Input reactance at the rated voltage
X_M	Mutual reactance
X_{Sum}	Sum of the stator and rotor leakage reactances
X_1	Stator reactance
X_2	Rotor positive sequence reactance
X_3	Rotor negative sequence reactance
$\overline{Y}_M$	Complex admittance of the magnetizing branch
$\overline{Y}_1$	Complex admittance of the stator branch
$\overline{Y}_{2,P}$	Complex admittance of the rotor branch in positive sequence circuit.
ΔT	Temperature rise
η	Efficiency
θ_P	Phase angle of the positive sequence component of the voltage signal
θ_N	Phase angle of the negative sequence component of the voltage signal
φ_N	Phase angle between the negative sequence input voltage and current
ε_η	Relative error of the measured efficiency
ε_I	Relative error of the measured current
ε_{Pout}	Relative error of the measured output power
ε_{Pin}	Relative error of the measured input power
ε_S	Relative error of the measured speed
ε_T	Relative error of the measured torque
ε_V	Relative error of the measured voltage
$\omega(t)$	Frequency
$\alpha(t)$	Phase angle of the current signal
B	Flux density

1. INTRODUCTION

1.1 Research Background

Environmental concerns, as well as an increasing demand for energy, provide strong motivation for further investment and research in demand side energy management techniques. Improving the efficiency of loads is one area [1] in which available funds are designated to find and replace old and less efficient systems with higher efficiency counterparts.

Electrical motors, and more specifically, induction motors are the main loads in the electrical power systems of industrialized countries. The enormous number of electrical motors represents a significant potential for the application of demand side energy management techniques. In addition, the efficient operation of the motors can bring direct and significant savings in consumed energy levels and indirectly reduce greenhouse gas emissions, as well as requirements for the installation of new power plants, transmission lines, and distribution systems.

The importance of the efficient operation of electrical motors became more evident with the enactment of the Energy Policy Act of 1992 [2], which focuses on the efficient operation of motors and covers all induction motors with the following specifications:

- Power range of 1 to 200 hp
- General purpose T-frame
- Single-speed

- Foot-mounted
- Poly-phase squirrel-cage design A and B
- Working under 230/460 volts and 60 Hz power
- Continuous-rated
- 2, 4 or 6 pole machines

Based on this Act, all manufacturers must indicate the efficiency of their motors, both on the nameplate and in all documents related to the motor. In addition, motors must have a nominal full load efficiency of not less than the values indicated there. As a result of this Act, manufacturers have to construct, and industries have to buy, more efficient motors, both for new installations and replacement purposes.

In an attempt to encourage the industrial sector to adopt demand side energy management techniques in their plants, the US Department of Energy developed a software tool called "Motor Master + 4" [3], which facilitates the management of motors in an industrial facility. It contains features that make it possible to identify motors with poor efficiencies, calculate lifetime energy savings (in case of replacement of an old motor with a new one), and make decisions over the replacement or repair of an existing motor. In short, by using this tool, different scenarios can be compared so that the most economical solution can be found.

Energy-saving calculations and the relevant decisions, such as the replacement of an existing motor, are strongly dependent on accurate knowledge of motor efficiency. The efficiency of an induction motor can be affected by many factors, such as supply voltage

unbalance [4], over- or undervoltage conditions [5], non-critical motor internal faults, the effects of rewinding and repair of the motor [6], [7], or simply due to over- or underloading (due to inappropriate sizing of the motor) conditions. Therefore, in-situ efficiency monitoring of installed motors is essential to detect motors with poor efficiencies and to take appropriate action.

The IEEE standard 112 [8] offers different methods to measure the efficiency of an induction motor in a laboratory environment. The most common practice for motors in the range of 1-300 kW is the IEEE standard112 method B, which is an input-output method with loss segregation. This method requires dynamometer testing combined with speed and torque readings using an installed sensor. For a higher rated machine, IEEE standard 112 method E/F are recommended. These methods are too intrusive to be applicable in an industrial environment.

As a result, different techniques have been proposed to measure the efficiency of an induction machine in situ. However, few of these are really practical considering the level of intrusion and accuracy. Besides, very little has been done to make these methods compatible with actual industrial conditions, where unbalanced supplies exist together with over- or undervoltage conditions.

Based on the NEMA MG 1 standard, induction motors can operate under up to 5% unbalance voltage [9]. In weak power systems, the voltage unbalance factor can be even greater during some periods of a day. In addition, up to ±10% over- and undervoltage supply conditions are commonly seen in industrial facilities.

Based on [10] and [11], an unbalanced voltage, combined with over- or undervoltage conditions, can significantly affect the working efficiency of motors. Therefore, it is essential to use a method that is specifically developed to deal with the unbalanced supply conditions. This will assure a reliable estimation of motor efficiency under real industrial conditions.

1.2 Objectives

The first goal of this thesis is to develop a non-intrusive in-situ efficiency estimation technique for induction machines, which will be capable of dealing with unbalanced voltages and can be combined with under- or overvoltage conditions. For the purpose of this thesis, non-intrusiveness refers to electrical measurements at the terminals only, with no mechanical measurements, not even speed. This requirement imposes limitations on the available data, which introduces some challenges to the efficiency estimation problem. To have the lowest possible intrusion level, only two line voltages and currents are allowed to be measured, and all the required information, such as input and output power, speed, temperature, and motor parameters, are calculated or estimated based solely on these measurements.

It should be emphasized that the goal is not to replace the accurate standard efficiency estimation techniques for standard test conditions. But rather, it is to develop a method that can be used for in-situ efficiency estimations where standard test methods are not applicable due to their intrusive nature.

The second goal of the thesis is the estimation of full load efficiency from no-load uncoupled testing. The idea is to develop a simple method that can be used in refurbishment centers to estimate the efficiency of an induction machine without performing expensive dynamometer testing. Like the in-situ efficiency estimation problem, the challenge is to estimate the efficiency of the machines with very limited measurements. This will help machine repair facilities to assess the quality of their work, and it can also assist industrial facilities to make better decisions over the future replacement or repair of their existing machines.

In the following sections, the available in-situ efficiency estimation techniques in literature are first reviewed and compared, based on their accuracy and intrusion levels. Special attention is paid to optimization based techniques, which form the basis of the proposed efficiency estimation method in this thesis. Thereafter, the available definitions and the effects of the unbalanced voltages on the performance of the machine are introduced. A detailed discussion is presented on the only available method in literature for in-situ efficiency estimation under unbalanced supplies. Finally, a literature review is done to find the available methods that might address the problem of full load efficiency estimation from no-load uncoupled testing. The outline of this thesis and the contributions are presented in the last sections of this chapter.

1.3 Literature Survey on In-Situ Efficiency Estimation Techniques

In this section, the available methods in literature for an in-situ efficiency assessment of induction machines are classified and briefly reviewed. The section starts with the simplest and least accurate techniques, and it concludes with the most accurate ones.

1.3.1 Slip Method

This method works based on the assumption that the slip of the motor changes linearly with the load as shown in (1.1) [12].

$$\eta = \frac{P_{Out,Rated}}{P_{In,Meas}} \times \left(\frac{N_{Sync} - N_{Meas}}{N_{Sync} - N_{Rated}} \right) \tag{1.1}$$

where

$P_{Out,Rated}$: is the rated mechanical output power

$P_{In,Meas}$: is the measured input power

N_{Sync} : is the mechanical synchronous speed

N_{Rated} : is the mechanical rated speed

N_{Meas} : is the mechanical measured speed

Although this method is completely non-intrusive and simple, it does not provide an accurate estimation of efficiency due to the following reasons:

1) In reality, the slip of the motor does not change linearly with the load.
2) In the NEMA MG 1 standard, it is stated that the real speed of the motor at full load conditions may have 20% variation with the nameplate speed [12].
3) The slip of the motor is influenced by the ambient temperature [13].
4) The rated speed indicated on the nameplate of the machine is at the nominal voltage condition. However, in real applications, voltage can deviate to some extent from the rated value indicated on the nameplate.

For the abovementioned reasons, this method is not suitable for efficiency estimation purposes.

1.3.2 Slip Method with Voltage Compensation

To compensate for the effects of voltage variation on the estimated efficiency, the modified version of the slip method was proposed in [14] and is shown in (1.2).

$$\eta = \frac{P_{Out,Rated}}{P_{In,Meas}} \times \left(\frac{N_{Sync} - N_{Meas}}{N_{Sync} - N_{Rated}} \right) \times \left(\frac{V_{Meas}}{V_{Rated}} \right)^2 \tag{1.2}$$

where

$P_{Out,Rated}$: is the rated mechanical output power

$P_{In,Meas}$: is the measured input power

N_{Sync} : is the mechanical synchronous speed

N_{Rated} : is the mechanical rated speed

N_{Meas} : is the mechanical measured speed

V_{Meas} : is the measured voltage

V_{Rated} : is the rated voltage of the machine.

The more accurate version of this equation was proposed in [13], as shown in (1.3), which is claimed to better reflect the relation between the slip and load of the machine.

$$\eta = \frac{P_{Out,Rated}}{P_{In,Meas}} \times \left(\frac{S_{Meas} - S_{Meas}^{\,2}}{S_{Rated} - S_{Rated}^{\,2}} \right) \times \left(\frac{V_{Meas}}{V_{Rated}} \right)^2 \qquad (1.3)$$

where

$P_{Out,Rated}$: is the rated mechanical output power

$P_{In,Meas}$: is the measured input power

S_{Meas} : is the measured slip of the machine

S_{Rated} : is the rated slip of the machine

V_{Meas} : is the measured voltage

V_{Rated} : is the rated voltage of the machine.

Although the modified version has less error in comparison to the basic slip method, it still suffers from high inaccuracies, and it is not recommended for accurate efficiency estimation.

1.3.3 Current Method

In this method, it is assumed that the input current of the machine changes linearly with the load. Thus, the efficiency can be estimated by (1.4).

$$\eta = \frac{P_{Out,Rated}}{P_{In,Meas}} \times \left(\frac{I_{In,Meas}}{I_{In,Rated}} \right) \tag{1.4}$$

where

$P_{Out,Rated}$: is the rated mechanical output power

$P_{In,Meas}$: is the measured input power

$I_{In,Meas}$: is the measured input current

$I_{In,Rated}$: is the rated current of the machine

As shown in [12], this assumption works better for heavy load conditions where the current of the machine is higher. This is due to the fact that the no-load current of the machine is not equal to zero, as assumed in (1.4). This is illustrated in Fig. 1.1 [12]. As can be seen, this relationship always overestimates the load and thus the efficiency.

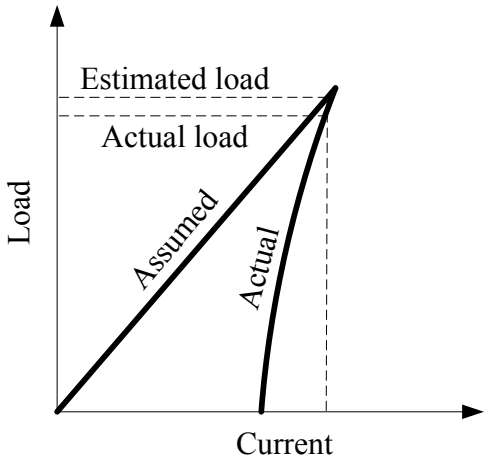

Fig. 1.1 Load vs. current relationship in current method [12].

1.3.4 Modified Current Method

It is possible to improve the accuracy of this relationship by considering the no-load current as shown in (1.5) and Fig. 1.2 [12].

$$\eta = \frac{P_{Out,Rated}}{P_{In,Meas}} \times \left(\frac{I_{In,Meas} - I_{In,Noload}}{I_{In,Rated} - I_{In,Noload}} \right) \tag{1.5}$$

where

$P_{Out,Rated}$: is the rated mechanical output power

$P_{In,Meas}$: is the measured input power

$I_{In,Meas}$: is the measured input current of the machine

$I_{In,Rated}$: is the rated input current of the machine

$I_{In,Noload}$: is the no-load current of the machine

This will increase the intrusiveness of the method since the no-load current is not known before doing the no-load test.

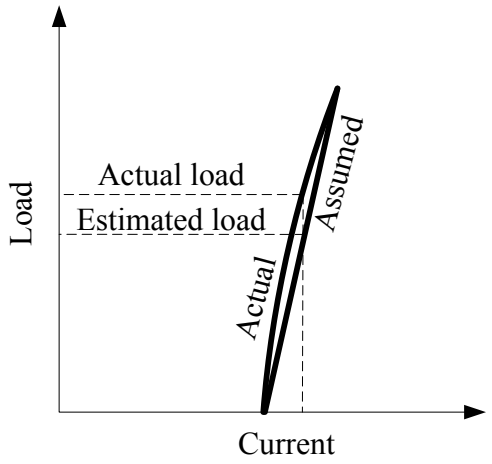

Fig. 1.2 Load vs. current relationship in modified current method [12].

In [14], the non-linearity of the current curve has been considered to improve the current vs. load linear relation, as shown in (1.6).

$$\eta = \frac{P_{Out,Rated}}{P_{In,Meas}} \times \left(\frac{2I_{In,Meas} - I_{In,Noload}}{2I_{In,Rated} - I_{In,Noload}} \right) \tag{1.6}$$

where

$P_{Out,Rated}$: is the rated mechanical output power

$P_{In,Meas}$: is the measured input power

$I_{In,Meas}$: is the measured input current of the machine

$I_{In,Rated}$: is the rated input current of the machine

$I_{In,Noload}$: is the no-load current of the machine

As can be seen in Fig. 1.2, this method generally underestimates the load and thus the efficiency of the machine. In [15], use of the average of the two current methods to improve the result is recommended. Although current based methods offer better accuracy in comparison to the slip methods, they still have an unacceptable range of error. This is mainly due to the fact that the nameplate value of the rated current is expected to have up to 10 % deviation from the real value [12]. In addition, the relationship represented by (1.5) or (1.6) does not perfectly represent what happens inside the machine.

1.3.5 Standard and Simplified Equivalent Circuit Based Methods

Theoretically, if the parameters of the equivalent circuit of an induction motor are known, it is possible to use (1.7) and estimate the efficiency of the motor under different loading conditions.

$$\eta = \frac{P_{Conv} - P_{FW} - P_{SLL}}{P_{In,Meas}} \tag{1.7}$$

where

P_{Conv} : is the converted electrical to mechanical power

P_{FW} : is the sum of friction and windage losses

P_{SLL} : is the stray load loss

$P_{In,Meas}$: is the measured input power

Method F and method F1 of the IEEE standard 112 [8] are based on this assumption. IEEE standard 112 method F requires a variable voltage no-load test, impedance test (locked rotor test at low frequency), and the stray load loss measurement. IEEE standard 112 method F1 is the simplified version of IEEE standard 112 method F in which an empirical value is assumed for the stray load loss. As mentioned earlier, these methods are too intrusive to be applicable for field conditions.

The Oak Ridge National Laboratory offers a nameplate-based equivalent circuit method, which is more suitable for in-situ measurements. In this method, known as ORMEL96 [16], the locked rotor test is avoided by assuming a locked rotor current considering the NEMA code letters (such as D, E, . . . L) on the nameplate. In detail, the parameters of a machine are found based on an iterative approach with the goal of obtaining the same rated efficiency and locked rotor current using the rated slip, total input resistance and reactance, the assumed magnitude of the locked rotor impedance, and the ratio of X_1/X_2 [16]. Use of empirical data, such as the locked rotor current, assumed rated slip, and the rated efficiency, in the parameter estimation process degrades the accuracy of this method. Moreover, the rated efficiency, which in fact should be the final outcome of the method, is already used in the algorithm to find the parameters of the machine. This

means that the rated efficiency of the machine is assumed to be equal to the nameplate value, which is the main problem with this technique.

In [17], an equivalent circuit-based method is proposed, which requires a no-load and a loaded operating point to estimate the parameters of the machine. The necessity of doing the no-load test means that this method does not provide a realistic solution for the in-situ efficiency estimation problem.

The main advantage of the equivalent circuit-based methods is that the efficiency of the machine can be estimated for operating points and conditions rather than measured ones.

1.3.6 Segregated Loss Method

This method is based on the measurement and separation of the different losses of the machine. The IEEE standard 112 method E [8] is based on this principle. This method includes the removed rotor and the reversed rotation tests for direct stray load loss measurements. Due to the intrusive nature of these tests, this method is not appropriate for in-situ efficiency estimation. The simpler version of this method, IEEE standard 112 method E1, avoids the direct stray load loss measurements by use of an empirical value which takes into account the machine size. However, this method is still too complicated for in-situ efficiency estimation due to the requirement for variable voltage no-load and multiple points loaded tests.

The simplified version of IEEE standard 112 method E1, which can be used for in-situ applications, was proposed by Ontario Hydro [18]. This method assumes an empirical

value for the no-load rotational losses and therefore does not require the no-load test to be performed. Although this assumption makes the method more applicable for an in-situ efficiency measurement, it degrades the accuracy of the results.

1.3.7 Conventional and Non Intrusive Air-Gap Torque Methods

The conventional air-gap torque method works based on the estimation of the air-gap torque value with use of the measured current and voltage signals, as shown in (1.8) [19], [20].

$$T_{AG} = \frac{P}{2\sqrt{3}}\left[(i_a - i_b)\int\left[v_{ca} - R_1(i_c - i_a)\right]dt - (i_c - i_a)\int\left[v_{ab} - R_1(i_a - i_b)\right]dt\right] \tag{1.8}$$

where

T_{AG} : is the air-gap torque

P : is the number of the poles of the machine

R_1 : is the stator resistance

i_a, i_b, i_c : are the instantaneous values of the current signal at phases a, b, and c

v_{ab}, v_{bc}, v_{ca} : are the instantaneous values of the line-to-line voltage signals

When the air-gap torque is known, it is possible to find out the shaft torque and consequently the efficiency by (1.9).

$$\eta = \frac{1}{P_{In,Meas}} \times \left[T_{AG} \frac{2\pi . N_{Meas}}{60} - P_{FW} - P_C - P_{SLL} \right] \tag{1.9}$$

where

η : is the efficiency

T_{AG} : is the air-gap torque

N_{Meas} : is the measured mechanical speed

P_{FW} : is the friction and windage loss

P_{SLL} : is the stray load loss

P_C : is the core loss

$P_{In,Meas}$: is the measured input power

This method requires the motor to be disconnected from the load to perform the no-load test in order to find the core, friction, windage, and stray load losses, and is a highly intrusive requirement. In [21], the non-intrusive air-gap torque method is proposed in which some empirical values are assumed for the no-load losses in order to avoid the intrusive no-load test. As is shown in Chapter 4, these assumptions can significantly degrade the accuracy of the results.

The accuracy of the air-gap torque method is significantly dependent on the accurate measurement of the stator resistance at the operating temperature. This is an intrusive

requirement. In addition, the efficiency estimation is only possible for the measured field condition, and no conclusion can be made for any other operating point.

The major advantage of this method over previous techniques is its capability of dealing with unbalanced supply voltages [19]. The air-gap torque calculated with (1.8) consists of the positive and negative sequence torque components, and it leads to more accurate efficiency estimation in the case of induction machines working under unbalanced supply conditions. An illustration of the method is shown in Fig. 1.3.

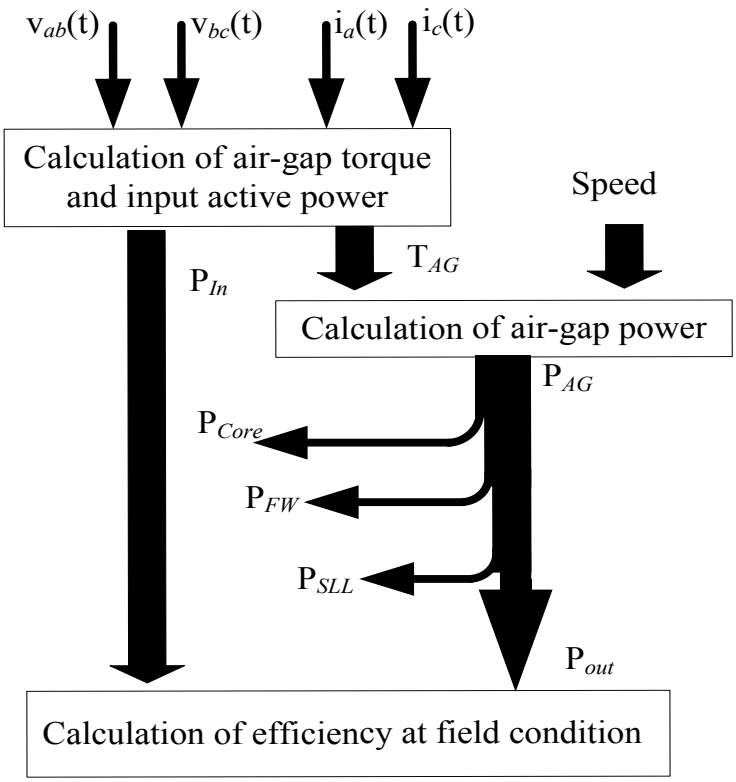

Fig. 1.3 The air-gap torque method

More accurate analyses, based on experimental results, are presented in Chapter 4 where the non-intrusive air-gap torque method and its modified version are compared with the method proposed in this thesis.

1.3.8 Optimization Based In-Situ Efficiency Estimation Methods

In the literature, there is another in-situ efficiency assessment technique, which is a modified version of the equivalent circuit-based method for an in-situ application. In this method, the parameters of the equivalent circuit of an induction machine are estimated with the help of a search (optimization) algorithm, i.e., Genetic Algorithm (GA), based on limited available data, which can be the motor's voltage, current, speed, power factor, or input electrical power. From the estimated parameters, it is possible to estimate the efficiency of an induction machine at any desired operating condition.

Research work has previously been done in this area with the aim of using the GA as a tool to estimate the parameters and, consequently, the efficiency of an induction machine.

In [22], the authors used a GA program with binary representation to solve the nonlinear equations, and estimate the parameters and efficiency of the machine. Since the available data was less than the unknown parameters, a unique set of solutions was not achievable. Therefore, the average value of the results was considered to be the final solution. In addition, the friction and windage losses were combined with the core loss, the total amount of which was estimated by GA through the estimation of resistance in the magnetization branch. This is not an appropriate assumption due to the fact that friction and windage losses are mechanical losses, and they affect (increase) the slip of an

operating point. Therefore, these losses are already included in the amount of the converted power calculated by (1.10).

$$P_{Conv} = 3\frac{1-S}{S} R_2 {I_R}^2 = P_{Out} + P_{FW} \tag{1.10}$$

where

P_{Conv} : is the converted electrical to mechanical power

S : is the slip of the machine

R_2 : is the rotor's resistance

I_R : is the rotor current

P_{Out} : is the output power of the machine

P_{FW} : is the friction and windage losses

In addition, the stator resistance of the machine is measured from the machine terminals at ambient temperature. The value of the resistance is corrected based on the estimated operating temperature, the value of which is in turn based on a linear approximation as shown below:

$$T = \frac{I_{In,Meas} - I_{In,Noload}}{I_{In,Rated} - I_{In,Noload}} \times (T_{Rated} - T_a) + T_a \tag{1.11}$$

where

$I_{In,Meas}$: is the measured input current.

$I_{In,Rated}$: is the rated (full load) input current

$I_{In,Noload}$: is the no-load input current

T_a : is the ambient temperature

T_{Rated} : is the rated temperature based on the insulation class of the machine [22]

There are some problems with this proposed temperature estimation method:

1) The temperature of the machine in a no-load condition is assumed to be equal to the ambient temperature, which is not true.
2) The value of the no-load current is required in this method. However, the no-load current is not known without performing a no-load test, which is not permitted due to its intrusiveness.
3) The temperature of the machine is assumed to change linearly with the current. However, it is well known that the copper losses change with the square of the current.

In Chapter 3, a non-linear temperature estimation technique is proposed, which calculates the temperature rise through estimation of the losses and the machine's thermal coefficient.

The problem of non-convergence to a unique solution was solved in [23] through use of multiple data points; however, it still has the same problem as [22] regarding friction and windage losses.

In [24] and [25], a floating point GA was used instead of the GA with binary representation. In [26], the same algorithm has been used with two operating points instead of one. No temperature estimation techniques were reported in these works.

In [27], the same technique as [22] is proposed with some modifications to reduce the intrusiveness of the method. Firstly, the speed of operation was estimated with a machine current signature analysis (MCSA)-based technique, which uses embedded eccentricity and slot harmonics inside the current. Secondly, the value of the stator resistance was measured at the operating temperature with help of a metal oxide semiconductor field-effect transistor (MOSFET)-controlled DC injection circuit. Finally, windage and friction losses were claimed to be computable by GA, as shown in (1.12).

$$P_{In} = 3{I_{In}}^2 R_1 + 3{I_M}^2 R_M + 3{I_R}^2 \left[R_2 + \frac{1-S}{S} R_2 \right] + P_{SLL} + K_{FW} N_{Meas} \tag{1.12}$$

where

P_{In} : is the input power of the machine

I_{In} : is the input current

I_M : is the magnetizing current

R_2 : is the rotor's resistance

R_M : is the resistance representing the core loss

I_R : is the rotor current

P_{FW} : is the sum of friction and windage losses

S : is the slip of the machine

K_{FW} : is the coefficient of the friction and windage losses

N_{Meas} : is the measured mechanical speed

Some comments can be made regarding this work:

1) The speed measurement technique proposed in this work had an accuracy of ±5 rpm, as stated in [27]. Based on our observations, however, the parameter estimation problem is too sensitive to the speed value. This uncertainty can cause a bigger error in parameter estimation and, consequently, in the efficiency estimation process.
2) Installation of a DC injection circuit specifically in series with the power supply of the motor requires a shutdown of the motor. The intrusion level of this method, if not more, is not less than the measurement of cold resistance. Besides, it is not clear how this device is going to be installed temporarily in a motor control center cabinet, or if this is allowed by the relevant safety codes.
3) As discussed earlier, the effects of the friction and windage losses are already included in the magnitude of the converted power as shown in (1.10). The addition of

the term "$K_{FW}.N_{Meas}$" into (1.12) is simply considering the friction and windage losses twice. Therefore this equation is not correct, and basically, the friction and windage losses cannot be estimated separately with this technique.

Reference [28] is one of the latest works that has been published in this area. This work is very similar to [22] with the main difference that a multi-objective GA was used instead of the common single objective technique. It was shown that this technique gave a set of non-dominant optimum solutions. The final solution was selected by calculating the Euclidian distance between non-dominated solutions and the origin [28]. This work has almost all the same problems that have been mentioned with respect to the other publications. Furthermore, based on the claimed results, it can be concluded that multi-objective optimization did not lead to any significant advantage regarding the estimation error.

In [29], the bacterial foraging algorithm has been used instead of the genetic algorithm to solve the same problem, and almost the same results have been achieved.

In addition to the discussed limitations and weaknesses, the common denominator with all these works is the assumption that the machines are supplied through rated balanced voltages. Unfortunately, this is not the case in practice. As mentioned earlier, unbalanced and over- or undervoltage conditions may exist in industrial facilities for many reasons. Therefore, it is essential to use a method that is specifically developed to deal with these conditions in order to assure a reliable estimation of the efficiency under real industrial conditions.

Before trying to come up with any solution to this problem, it is essential to know more about this phenomenon and its effects on induction machines.

It is also informative to have an idea about the accuracy of the existing non-intrusive in-situ efficiency estimation tools in the market. This will help to assess and compare the performance of our developed algorithm. In [30] the efficiency estimation results of the three different commercially available instruments are compared for the case of 50 hp, 100hp and 200hp induction machines. Based on the achieved results, it was concluded that the estimated values with these instruments are within ±3 percent of the real efficiencies.

1.4 Unbalanced Voltages and Their Effects on the Induction Machines

1.4.1 Available Definitions for the Voltage Unbalance Factor

Voltage unbalance is defined as the discrepancy in phase or line voltages. The difference can be in magnitude, phase, or both. Unbalanced voltages can exist for different reasons, such as [10] or [11]:

- Incomplete transposition of transmission lines
- Open delta transformers
- Blown fuses on three-phase capacitor banks
- Unequal distribution of single-phase loads
- Defective transformers in power systems
- Operation of single-phase loads at different times

There are three different definitions for the voltage unbalance factor (VUF) in the standards. The NEMA MG 1 standard defines the voltage unbalance factor as shown in (1.13) [9].

$$VUF = \frac{Max\left[\left(V_{ab} - V_{Avg}\right),\left(V_{bc} - V_{Avg}\right),\left(V_{ca} - V_{Avg}\right)\right]}{V_{Avg}} \times 100 \tag{1.13}$$

$$V_{Avg} = \frac{V_{ab} + V_{bc} + V_{ca}}{3} \tag{1.14}$$

where

V_{ab}, V_{bc}, V_{ca}: are the line-to-line rms voltages

V_{Avg}: is the average voltage of the three lines

In this definition, no limitation is considered for the average voltage value. The IEEE standard offers almost the same definition with the exception that the phase values have been used instead of the line values, as shown in (1.15) [11].

$$VUF = \frac{Max\left[\left(V_{a} - V_{Avg}\right),\left(V_{b} - V_{Avg}\right),\left(V_{c} - V_{Avg}\right)\right]}{V_{Avg}} \times 100 \tag{1.15}$$

$$\mathrm{V_{Avg}} = \frac{\mathrm{V_a} + \mathrm{V_b} + \mathrm{V_c}}{3} \tag{1.16}$$

where

V_a, V_b, V_c: are the phase rms voltages

V_{Avg}: is the average voltage of the three phases

The definition of the IEEE standard is not really practical due to the fact that, in most industrial applications, it is not possible to measure the phase values [31].

The IEC standard uses the true definition of the voltage unbalanced factor, which is the ratio of the negative sequence to positive sequence components, as shown in (1.17) [11].

$$VUF = \frac{V_N}{V_P} \times 100 \tag{1.17}$$

where

V_P: is the magnitude of the positive sequence component of the voltage signal

V_N: is the magnitude of the negative sequence component of the voltage signal

Like the NEMA standard, no limitation is considered for the value of the positive sequence component in the IEC standard.

In [31], it is shown that the definitions of the IEC and NEMA standards lead to almost the same results for up to 5% of voltage unbalance factors (which is the acceptable limit of voltage deviation stipulated by the NEMA standard) [9]. Thus, for practical values of the voltage unbalance factor, each of these definitions can be used.

In this thesis, the IEC definition has been used to define the existing VUF.

1.4.2 Different Types of Unbalanced Voltage Conditions

Since no limitation has been introduced for the values of the average voltage or the positive sequence component, there can be at least eight different types of unbalanced voltage conditions with the same value of VUF [10], [11]. These unbalanced conditions are:

- Single-phase undervoltage unbalanced condition (1Ph-UV)
- Two-phase undervoltage unbalanced condition (2Ph-UV)
- Three-phase undervoltage unbalanced condition (3Ph-UV)
- Single-phase angle unbalanced condition (1Ph-AU)
- Two-phase angle unbalanced condition (2Ph-AU)
- Single-phase overvoltage unbalanced condition (1Ph-OV)
- Two-phase overvoltage unbalanced condition (2Ph-OV)
- Three-phase overvoltage unbalanced condition (3Ph-OV)

As discussed in [10] and [11], the value of the voltage unbalance factor, if used alone, cannot provide adequate information about the existing unbalanced condition. Therefore, it is proposed to use the per-unit value of the positive sequence component as well as the VUF to clearly define the situation.

In [32] and [33], it is shown that the angle of the VUF can influence and change the distribution of the currents and consequently the distribution of the copper losses inside the machine. Different sets of unbalance line voltages can be presented with the same VUF and the same positive sequence component. However, with a known angle of VUF,

a unique set of unbalanced line voltages can be found. A complex voltage unbalance factor (CVUF) is proposed in [33] and shown in (1.18).

$$CVUF: \frac{V_N}{V_P} \times 100 \angle(\theta_N - \theta_P) = VUF \angle(\theta_N - \theta_P) \tag{1.18}$$

where

V_P : is the magnitude of the positive sequence component of the voltage signal

V_N : is the magnitude of the negative sequence component of the voltage signal

θ_P : is the phase angle of the positive sequence component of the voltage signal

θ_N : is the phase angle of the negative sequence component of the voltage signal

Based on [32] and [33], a complex VUF should be used to derate the machines under unbalanced supplies. However, as discussed in [34], the magnitude of the total copper losses remains the same for different angles of the CVUF. Consequently, the data of the VUF and the V_P is sufficient for the efficiency estimation problem.

1.4.3 Effects of Unbalanced Voltages on the Induction Machines

Negative sequence voltage components create a negative sequence current in a machine. The negative sequence current, which has a noticeable value due to the small negative sequence impedance, generates a magnetic field with a rotating direction opposite to the motor's speed. This magnetic field makes a magnetic torque which opposes the main

(positive sequence) torque of the machine [31]. An unbalanced voltage raises the amount of the input power, and at the same time, it decreases the level of the produced torque (output power), thereby reducing efficiency.

Based on [11], for the same value of VUF, a higher positive sequence component of voltage, V_P, will lead to a lower loss of efficiency. Therefore, unbalanced voltage cases can be ranked based on their severity (or loss of efficiency) as shown below [11]:

3Ph-UV > 2Ph-UV > 1Ph-UV > 2Ph-AU > 1Ph-AU > 3Ph-OV > 2Ph-OV > 1Ph-OV

The results of [11] are achieved without considering the core losses and the effect of the core saturation on the magnitude of the input currents. Investigations of [35] show that, in the case of a strongly saturated machine, an overvoltage condition can be worse than an undervoltage condition, while in the case of a weakly saturated machine, the results can be as predicted in [11]. Thus the magnetic design of the machine can significantly influence the efficiency variations due to unbalanced and over- or undervoltage supply conditions. Finally, higher temperatures due to the significant amount of negative sequence currents, even with small values of voltage unbalance factors, can significantly shorten the life of machines [36].

Under unbalance voltage condition, the input and output powers contain an average and a time varying component which oscillates with a frequency equal to double of the fundamental frequency. Due to the existence of the time varying component in both input and output powers, the efficiency if defined as the ratio of the instantaneous output power to the instantaneous input power will also contain a time varying component.

In this thesis, only the average value of the input and output powers are considered in efficiency estimation and calculation process. The possible effect of these power oscillations on the machine's efficiency is not investigated in this thesis.

Based on discussions to this point, it is evident that the operation of induction machines under unbalanced voltages that are combined with over- or undervoltage conditions, has a considerable impact on their efficiency and performance. Thus, any in-situ efficiency estimation algorithm should consider these effects in order to improve estimation accuracy.

Based on the literature review, there is only one published research work, [37], that deals with in-situ efficiency estimations of induction machines under unbalanced supply conditions using the optimization-based method. This work is discussed in the next section.

1.5 An In-Situ Efficiency Estimation Algorithm for Induction Machines Working under Unbalanced Supplies

As discussed, [37] is the only work available in the literature that combines GA with an equivalent circuit method to deal with the efficiency estimation problem under unbalanced supply conditions.

In [37], GA was used to estimate eight unknown parameters of positive and negative sequence equivalent circuits. Line voltages, phase currents, active and reactive powers,

stator resistance at the ambient temperature, and the speed were considered to be known through measurements.

The speed of the machine was measured by use of an optical tachometer. The value of stator resistance was measured at an ambient temperature, and it is corrected to the specific (rated) temperature based on the recommendations of the IEEE standard 112 [8].

As stated in this work, the sum of the absolute values of the average errors of the input current, input power, core losses, and friction and windage losses is used as an objective function for the GA as shown below [37]:

$$F_1 = \frac{\left(I_{a,Est} - I_{a,Meas}\right)}{I_{a,Meas}} \times 100 \tag{1.19}$$

$$F_2 = \frac{\left(I_{b,Est} - I_{b,Meas}\right)}{I_{b,Meas}} \times 100 \tag{1.20}$$

$$F_3 = \frac{\left(I_{c,Est} - I_{c,Meas}\right)}{I_{c,Meas}} \times 100 \tag{1.21}$$

$$F_4 = \frac{\left(P_{In,Est} - P_{In,Meas}\right)}{P_{In,Meas}} \times 100 \tag{1.22}$$

$$F_5 = \frac{\left(P_{cte} - P_o\right)}{P_o} \times 100 \tag{1.23}$$

$$Error = \sum_{i=1}^{5} |F_i| \tag{1.24}$$

where

$I_{a,Est}$, $I_{b,Est}$, $I_{c,Est}$: are the estimated currents based on the GA-estimated parameters

$I_{a,Meas}$, $I_{b,Meas}$, $I_{c,\ Meas}$: are the measured values of the currents

$P_{In,Est}$: is the estimated input power based on the GA-estimated parameters

$P_{In,Meas}$: is the measured input power

P_o : is the estimated combined core, and friction and windage losses

P_{cte} : is the calculated combined core, and friction and windage losses based on the GA-estimated parameters

Some comments can be made regarding this work:

1) The number of unknown parameters is more than the number of equations. This means that an infinite set of solutions could be the answer to the parameter estimation problem. This is the same problem that was reported in [22].
2) In three-phase three-wire systems, the value of each phase is not independent on the other two phases. Therefore, (1.21) cannot be used as an independent equation simply because it does not bring to light any new information.

3) In (1.23), P_o is introduced as sum of estimated core, and friction and windage losses. However, it is not clear how this estimation was done and why an estimated value can be used in an objective function instead of a measured value.
4) As discussed earlier, windage and friction losses cannot be considered together with core losses.
5) The speed measurement with an optical tachometer is not a general solution because there might not be any access to the motor's shaft.
6) In [37], it is assumed that the measurements are always done at the rated temperature. That is the reason no temperature estimation method has been used for partially loaded conditions. Both in industry and the vast majority of cases, machines are not working at their rated loading condition. Consequently, in case of an in-situ measurement, the temperature will not be equal to the assumed rated temperature. Since it is not possible to measure the machine's temperature non-intrusively, a temperature estimation algorithm should be employed.

1.6 Literature Survey on Full Load Efficiency Estimation Techniques from the No-Load Uncoupled Testing

As discussed up to this point, various techniques have been proposed for efficiency estimation with different requirements. The accepted standard routine tests are introduced in the IEEE standard 112 [8]. Numerous other works have also been published with aim of estimating the efficiency of the machines in situ under the loaded condition without disturbing their operation.

However, very little has been done to find a simple yet reliable technique to estimate the efficiency of induction machines after the refurbishment process in workshops.

It is well known that quite a significant number of the machines in industry are repaired at least once in their lifetime. Studies have shown that repaired and rewound motors often suffer from efficiency changes. Being able to estimate the full load efficiency of a machine after its repair will help machine repair facilities to assess the quality of their work. In addition, it would also help industrial facilities to make more informed decisions regarding the future replacement or repair of their existing machines.

Most electrical machine refurbishment centers cannot afford to test their machines with the well-accepted efficiency test, IEEE standard 112 method B, which requires dynamometer testing. In fact, in these facilities, machines can only be started with the help of auto-transformers and run under no-load conditions. Thus, typically, these facilities cannot provide any information about the efficiency of a machine following its repair.

It would be useful to know if any of the available methods can be used for this specific application. In [14], the slip and current methods are proposed for in-service testing. As discussed in [12], these methods are not accurate and are highly dependent on nameplate data and the aforementioned rated efficiency, which is not valid after repair. Loss segregation based methods, such as IEEE standard 112 method E/E1 [8] or the simplified version proposed by Ontario Hydro [18], are also not appropriate for workshop testing since they require the rated load test, which cannot be undertaken in workshops. The

more accurate methods, such as the air-gap torque method [19], [20] or even the available optimization-based methods discussed in previous sections [22]-[29], cannot be the solution due to the same constraints.

In [38], a method is proposed for efficiency determination from the start-up transient data. This method requires the nominal voltage start up test as well as data of one loaded point, which is not applicable in refurbishment centers.

Synthetic loading is another approach, proposed in [39] and [40], which does not require loading of the machine. Instead, it requires the machine to be supplied either through a power electronic converter, or an auxiliary generator and a transformer. It therefore is not simple to apply this method in ordinary motor repair centers.

The equivalent circuit-based methods, such as IEEE standard 112 method F/F1 [8] or a simplified equivalent circuit method, e.g., the Oak Ridge National Laboratory method which is also known as ORMEL96 [16], are alternatives for the efficiency estimation problem.

The classic IEEE standard 112 method F/F1 requires a low voltage, low frequency locked rotor test to estimate the rotor parameters. The low frequency power supply and rotor locking requirements make this method unfeasible in workshop applications.

As explained previously, ORMEL96 [16] is a nameplate-based equivalent circuit method in which the locked rotor test is avoided by assuming a locked rotor current based on the NEMA code letters, e.g., D, E, . . . L, on the nameplate. In this method, the rated

efficiency, which in fact should be the final outcome of the algorithm, is already used to find the parameters of the machine. This means that the rated efficiency of the machine is assumed to be equal to the nameplate value. In addition to inaccuracy of the nameplate data, it is unlikely to have exactly the same nameplate values after the repair process.

In [17], an equivalent circuit-based method is proposed, which requires a no-load and a loaded operating point to estimate the parameters of the machine. Like the previous methods, the necessity of loading the machine makes it an unrealistic solution for this problem.

Another potential routine that can be used along with the standard no-load test method to find the parameters of the machine, is the third impedance test method proposed in the IEEE standard 112 [8]. This method does not depend on the low frequency locked rotor test to estimate the motor parameters. Instead, as stated in the standard, it works on low voltage no-load or light load test data. In this method, the voltage of the machine is reduced until a full load slip is achieved. Then the parameters of the rotor are calculated based on an iterative approach. This method seems very promising for workshop testing applications. However, some practical concerns were raised after testing the method, and these are discussed in detail in Chapter 5.

In this thesis, a simple method is proposed for full load efficiency estimation from uncoupled no-load testing. The method is a modified version of IEEE standard 112 method F1, which is designed with due consideration of the available data from the uncoupled no-load testing, namely:

1) Two voltage and current signals under a no-load testing condition.
2) Value of the stator resistance at an ambient temperature.
3) Nameplate data of the machine.

1.7 Thesis Outline

The thesis is organized as follows:

Chapter 2 discusses a non-linear algorithm developed in [41] and proposes a new application of this algorithm in non-intrusive speed detection and symmetrical components extraction problems. The extracted speed information and the positive and negative sequence components are used as a set of input data in the developed efficiency estimation algorithms in the rest of the thesis. The main part of this chapter is extracted from [44], which has been published by the author of the thesis.

Chapter 3 presents a new evolutionary-based in-situ efficiency estimation algorithm developed for unbalanced supply conditions. In addition, a non-linear temperature estimation algorithm is presented to estimate the temperature of the machine in the event of a partial loading condition. The proposed concept has been verified through simulation results. Experimental results with two different machines are used to prove the effectiveness and generality of the proposed method. Measurement error analysis as well as repeatability tests have been done to determine the credibility of the proposed method. The main part of this chapter is extracted from [42] to [44], which are published by the author of the thesis.

Chapter 4 is an extension of the work of Chapter 3. In this chapter, an algorithm is introduced to estimate efficiency in unbalanced and under- and overvoltage conditions. The effects of machine saturation are considered in the developed algorithm. In addition, a comprehensive study is done on the functionality and accuracy of the non-intrusive air-gap torque (NAGT) method, which is claimed to be one of the most promising methods in the reviewed literature. This method is compared with the evolutionary-based method, and it is shown that the efficiency calculated by this method under field conditions cannot be used in the decision-making process regarding the replacement of existing machines or the relevant calculations regarding the payback period. The research is supported by experimental results on two different induction machines. The main part of this chapter is extracted from [45], which has been published by the author of the thesis.

In Chapter 5, a simple method is developed for full load efficiency estimation from no-load uncoupled testing, which can be used in refurbishment centers to estimate the efficiency of induction machines without performing expensive dynamometer testing. The full load efficiency of the machine is extracted, based on two voltage and current signals under no-load conditions, the value of stator resistance at an ambient temperature, and the nameplate data of the machine. The credibility of the results is validated through experiments with two different induction machines. The main part of this chapter is extracted from [46], which has been published by the author of the thesis.

The conclusions and the proposed future work are presented in Chapter 6.

1.8 Thesis Contributions

The first goal was to improve and extend the existing optimization-based in-situ efficiency estimation techniques so that the effect of unbalanced voltages, which may be combined with under- or overvoltage conditions, could be considered. As discussed earlier, the proposed algorithm can be used to estimate the efficiency of the installed machines in order to detect motors with poor efficiencies and to take appropriate action.

A simple method has also been developed for full load efficiency estimation from the no-load uncoupled testing, which can be used in refurbishment centers to estimate the efficiency of an induction machine without performing expensive dynamometer testing. It has the potential to help machine repair facilities to assess the quality of their repair work, and it can also assist industrial facilities to make more informed decisions regarding the future replacement or repair of their existing machines.

The specific contributions made in this thesis are summarized as follows:

Chapter 2:

- The development of a simple non-intrusive speed estimation technique through the use of a simple non-linear filter in order to reduce the intrusiveness of the in-situ efficiency estimation process.
- The application of a non-linear filter in the extraction of symmetrical components of the current, voltage, and input power from measured voltage and current signals.

Chapter 3:

- The development of an evolutionary-based in-situ efficiency estimation algorithm for induction machines, which is capable of dealing with unbalanced supply conditions.
- The development of a non-linear temperature estimation algorithm to estimate the temperature of a machine in partially loaded conditions.

Chapter 4:

- The extension of the proposed algorithm for efficiency estimation in unbalanced and over- or undervoltage conditions.
- A comprehensive study on the functionality and accuracy of the non-intrusive air-gap torque (NAGT) method for efficiency estimation problems.
- A comparison of the NAGT and evolutionary-based efficiency estimation methods regarding their capability in determining the standard condition's efficiency from the measurements in field conditions.

Chapter 5:

- The development of a simple method to estimate the full load efficiency of induction machines from uncoupled no-load testing.

Journal papers published, accepted or submitted:

1. A. Siraki and P. Pillay, "An in situ efficiency estimation technique for induction machines working with unbalanced supplies," *IEEE Trans. Energy Convers*., vol.27, pp.85-95, March 2012
2. A. Gharakhani Siraki, C. Gajjar, M. A. Khan, P. Barendse and P. Pillay, "An algorithm for non-intrusive in-situ efficiency estimation of induction machines operating with unbalanced supply conditions," *Accepted for publication in IEEE Trans. Ind. Appl*.
3. A. Gharakhani Siraki and P. Pillay, "Comparison of two methods for full load in-situ induction machine efficiency estimation from field testing in the presence of over/under voltages and unbalanced supplies," *Accepted for publication in IEEE Trans. Ind. Appl*.
4. A. Gharakhani Siraki and P. Pillay, "Full load efficiency estimation of refurbished induction machines from no-load testing," *Submitted to IEEE Trans. Energy Convers.*

Conference paper published, accepted:

1. A. Gharakhani Siraki and P. Pillay, "A novel evolutionary-based in-situ efficiency estimation technique for induction machines working with unbalanced supplies," in *Conf. Rec. IEEE Electric Machines & Drives*, 2011, pp.1563-1568

2. NON INTRUSIVE SPEED DETECTION AND SYMMETRICAL COMPONENTS EXTRACTION TECHNIQUES

2.1 Introduction

In this chapter, a new application is proposed for the adaptive non-linear filter developed in [41], in the non-intrusive motor speed detection algorithm, and in the extraction of the symmetrical components of the voltage, current, and input active power from the line voltage and current signals. This filter was originally developed for biomedical and communication engineering applications [41]. However, it was found to be useful in power applications such as motor fault diagnosis or power quality measurements [47]-[49].

In this thesis, the proposed filter is used in the speed detection process in order to track and extract the fundamental component (of any magnitude, phase, or frequency) of the current signal. The extraction of the main component of the signal is essential to reduce its masking effect on harmonics with smaller magnitudes and to facilitate detection of the speed-dependent current harmonics. The same non-linear filter is later used to extract the negative and positive sequence components of the voltage, current, and input active power from the measured current and voltage signals.

The extracted speed information and the value of the positive and negative sequence voltages, currents, and input active powers are used as the input data for the efficiency estimation algorithm, which is shown in Fig. 2.1.

In this chapter, firstly, the mathematics of the adaptive non-linear filter is reviewed and then its performance is validated by simulation results. The application of this algorithm in the non-intrusive speed estimation process is then discussed. Thereafter, the performance of the proposed speed estimation algorithm is validated through experimental results with two different induction machines. And, in the last part of the chapter, another application is proposed for extraction of the symmetrical components of the voltage, current, and input active power from the measured voltage and current signals. The accuracy of the method is also verified by simulation results.

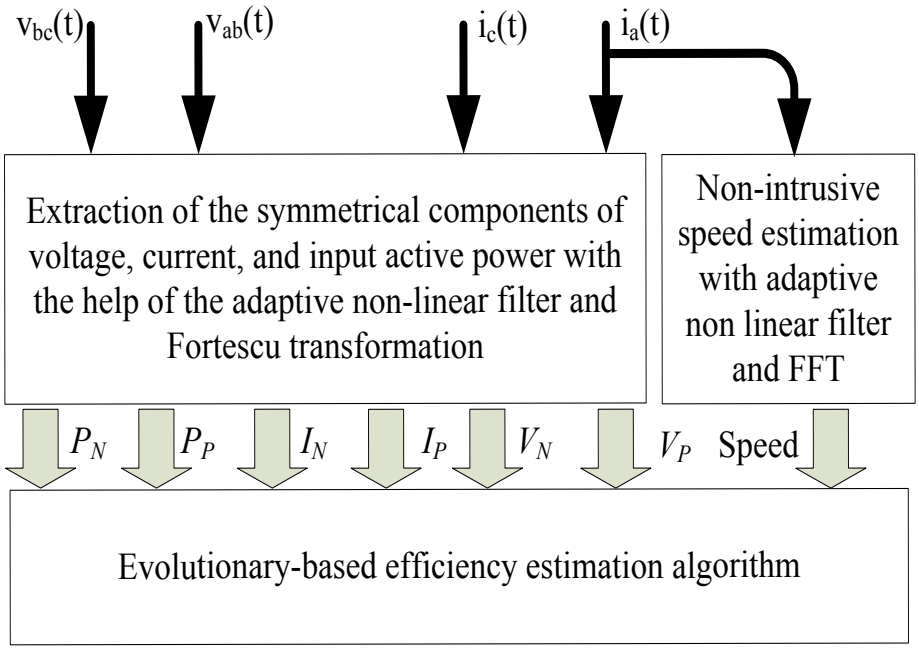

Fig. 2.1 Flowchart of the proposed efficiency estimation technique

2.2 Adaptive Non-Linear Filter for the Extraction of Non-Stationary Signals

2.2.1 Mathematics of the Adaptive Non-Linear Filter

Consider a dominant sinusoidal signal $i_f(t) = A(t).\sin\varphi(t)$ combined with other sinusoidal components and noise as shown in (2.1) as the input of the filter [41], [47], [49]:

$$i(t) = \sum_{i=0}^{\infty} A_i(t).\sin\varphi_i(t) + n(t) \tag{2.1}$$

$$\varphi_i(t) = \int^t \omega_i(t)dt + \alpha_i(t) \tag{2.2}$$

where

A(t) : is the signal's magnitude

ω(t) : is the frequency

α(t) : is the phase angle

n(t) : is the noise component

Let the output of the filter be as shown in (2.3)

$$i_f(t) = A(t).\sin\left(\int^t \omega(\tau)d\tau + \alpha(t)\right) \tag{2.3}$$

Consider M as manifold of all pure sinusoidal signals as shown in (2.4).

$$M = \left\{ \begin{array}{c} A(t).\sin\left(\int^{t} \omega(\tau) d\tau + \alpha(t) \right) \\ A(t) \in \left[A_{\min}, A_{\max} \right], \omega(\tau) \in \left[\omega_{\min}, \omega_{\max} \right], \alpha(t) \in \left[\alpha_{\min}, \alpha_{\max} \right] \end{array} \right\} \tag{2.4}$$

and $\theta(t) = \left[A(t), \omega(t), \alpha(t) \right]^T$ as the vector of parameters that belong to the parameter space as shown in (2.5).

$$\Theta = \left\{ \begin{array}{c} \left[A(t), \omega(t), \alpha(t) \right]^T \\ A \in \left[A_{\min}, A_{\max} \right], \omega \in \left[\omega_{\min}, \omega_{\max} \right], \alpha \in \left[\alpha_{\min}, \alpha_{\max} \right] \end{array} \right\} \tag{2.5}$$

The output which is the desired sinusoidal component can be defined as (2.6).

$$i_f(t, \theta(t)) = A(t).\sin\left(\int^{t} \omega(\tau) d\tau + \alpha(t) \right) \tag{2.6}$$

To extract the desired sinusoidal component, the solution should be the one which minimizes the distance function d , between the input i(t) and the desired output signal $i_f(t)$ as shown in (2.7).

$$\theta_{opt} = \arg\min d\left[i_f(t, \theta(t)), i(t) \right]^T \tag{2.7}$$

The distance function d is defined as

$$d\left(t, \theta(t)\right) = \left| i(t) - i_f(t) \right| \tag{2.8}$$

And finally the cost function is shown in (2.9)

$$J\left(t,\theta(t)\right)=d^{2}\left(t,\theta(t)\right) \tag{2.9}$$

As discussed in detail in [41], the gradient descent method is used to minimize the least square error by estimating the parameter vector θ as shown in (2.10),

$$\frac{d\theta(t)}{dt}=-\mu\frac{\partial\left[J\left(t,\theta(t)\right)\right]}{\partial\theta(t)} \tag{2.10}$$

where μ is a constant diagonal matrix as shown in (2.11), which controls the stability of the algorithm as well as the rate of convergence.

$$\mu=\begin{bmatrix} m_1 & 0 & 0 \\ 0 & m_2 & 0 \\ 0 & 0 & m_3 \end{bmatrix} \tag{2.11}$$

The estimated parameter vector is symbolized as

$$\hat{\theta}(t)=\left[\hat{A}(t),\hat{\omega}(t),\hat{\alpha}(t)\right]^{T} \tag{2.12}$$

It is possible to rewrite and expand (2.10) as shown in (2.13) [41]

$$\begin{bmatrix} \frac{d\hat{A}(t)}{dt} \\ \frac{d\hat{\omega}(t)}{dt} \\ \frac{d\hat{\alpha}(t)}{dt} \end{bmatrix} = \begin{bmatrix} m_1 & 0 & 0 \\ 0 & m_2 & 0 \\ 0 & 0 & m_3 \end{bmatrix} \begin{bmatrix} \frac{\partial}{\partial \hat{A}(t)} \left[u(t) - \hat{A}(t) \sin\left(\int^t \hat{\omega}(\tau) d\tau(t) + \hat{\alpha}(t) \right) \right]^2 \\ \frac{\partial}{\partial \hat{\omega}(t)} \left[u(t) - \hat{A}(t) \sin\left(\int^t \hat{\omega}(\tau) d\tau(t) + \hat{\alpha}(t) \right) \right]^2 \\ \frac{\partial}{\partial \hat{\omega}(t)} \left[u(t) - \hat{A}(t) \sin\left(\int^t \hat{\omega}(\tau) d\tau(t) + \hat{\alpha}(t) \right) \right]^2 \end{bmatrix} \quad (2.13)$$

As shown in [41], equations (2.14) to (2.16) are achieved by solving the differential equation.

$$\frac{d\hat{A}(t)}{dt} = 2m_1 e(t) \sin\left(\int^t \hat{\omega}(\tau) d\tau(t) + \hat{\alpha}(t) \right) \quad (2.14)$$

$$\frac{d\hat{\omega}(t)}{dt} = 2m_2 e(t) \hat{A}(t) t \cos\left(\int^t \hat{\omega}(\tau) d\tau(t) + \hat{\alpha}(t) \right) \quad (2.15)$$

$$\frac{d\hat{\alpha}(t)}{dt} = 2m_3 e(t) \hat{A}(t) \cos\left(\int^t \hat{\omega}(\tau) d\tau(t) + \hat{\alpha}(t) \right) \quad (2.16)$$

where e(t) is the error function defined as shown in (2.17).

$$e(t) = i(t) - \hat{A}(t) \sin\left(\int^t \hat{\omega}(\tau) d\tau(t) + \hat{\alpha}(t) \right) \quad (2.17)$$

Considering the fact that $\hat{\varphi}(t) = \int^t \hat{\omega}(t) dt + \hat{\alpha}(t)$, it is possible to write

$$\frac{d\hat{\varphi}(t)}{dt} = \hat{\omega}(t) + \frac{d\hat{\alpha}(t)}{dt} \quad (2.18)$$

As it can be seen, (2.15) has a factor of time t and thus it presents a time varying system. As stated in [41], this time varying system was found unstable and non useful. However, a heuristic method was employed where the time variable t was replaced by the constant m_4 in order to make the time variable system time-invariant which performed well in practice. Although the algorithm is inspired from the least square error minimization problem and the gradient descent method, the final derivation of the equations does not comply with the conditions of this method. Thus a mathematical proof is required for convergence of the algorithm. The mathematical proof of the convergence of the algorithm is out of the scope of this thesis. The detail proof based on Poincare theorem is presented in [41].

The governing equations of the proposed non-linear filter were taken from [41], where $\mu_1 = 2m_1, \mu_2 = 2m_2 m_4, \mu_3 = \frac{m_3}{m_2 m_4}$. These equations are shown below:

$$\frac{d\hat{A}(t)}{dt} = \mu_1 . e(t) . \sin \hat{\varphi}(t) \tag{2.18}$$

$$\frac{d\hat{\omega}(t)}{dt} = \mu_2 . e(t) . \hat{A}(t) . \cos \hat{\varphi}(t) \tag{2.19}$$

$$\frac{d\hat{\varphi}(t)}{dt} = \hat{\omega}(t) + \mu_3 . \frac{d\hat{\omega}(t)}{dt} \tag{2.20}$$

The convergence speed and the steady state error of the filter are dependent on the values of the constants μ_1, μ_2, and μ_3. In [41], it is stated that the value of the constants should be selected in order to roughly satisfy the two following conditions.

$$0 < \mu_1 < 4f_0 \tag{2.21}$$

$$0 < \mu_2 < 8\frac{f_0}{A}^2 \tag{2.22}$$

where A is the magnitude of the desired component (the fundamental component of the signal in this case) and f_0 is the frequency of the desired sinusoidal component

For instance, for a 60 Hz signal with unity amplitude, the constant, μ_1, should be smaller than 250, and the constant, m_2, should be smaller than 30,000. The choice of m_3 is dependent on μ_2. In [41], the selection of the value of m_3 is recommended such that the value of μ_2. μ_3 has the same order as μ_1. The value of the constant, μ_1, affects the tracking speed of the changes in the magnitude of the desired component, while μ_2 and m_3 affect the frequency and phase tracking capabilities. The value of these parameters is chosen based on a compromise between the steady state error and the speed of convergence. More details are provided in [41] about the characteristics of the algorithm and the effects of the constants. This algorithm acts as an adaptive notch filter in the sense that it passes a desired sinusoidal component and rejects all other components, including superimposed noise. This algorithm is capable of extracting the main component of a signal in the presence of other components, including noise, even if there are changes in the frequency or magnitude of the main component. Based on [41], little

computational effort due to the simplicity of the structure, immunity to noise, and the robustness of the filter, are the main features of the proposed algorithm.

The block diagram of the adaptive non-linear filter is shown in Fig. 2.2.

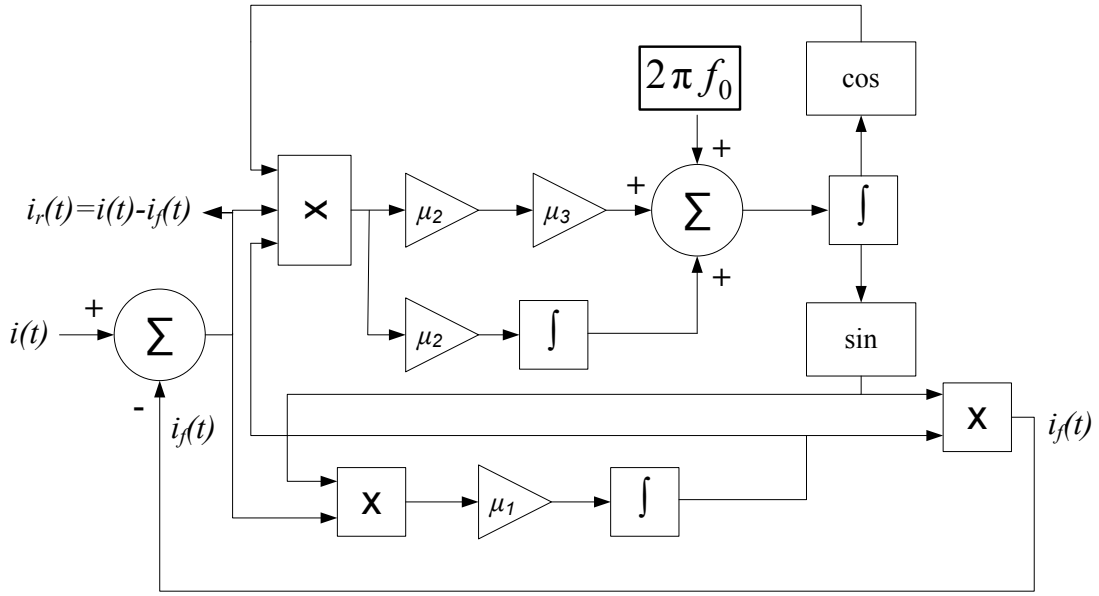

Fig. 2.2 Block diagram of the proposed non-linear filter

2.2.2 Examining the Performance of the Algorithm

In this section, the performance of the algorithm was evaluated by simulation with Matlab/Simulink software. The initial convergence of the algorithm was tested in Fig. 2.3. The input signal had a 60 Hz frequency with 1 pu magnitude. The initial condition for the frequency of the filter was set to 30 Hz. As can be seen, the output signal of the filter easily tracked the dominant sinusoidal component (with a frequency of 60 Hz) in a short period of time.

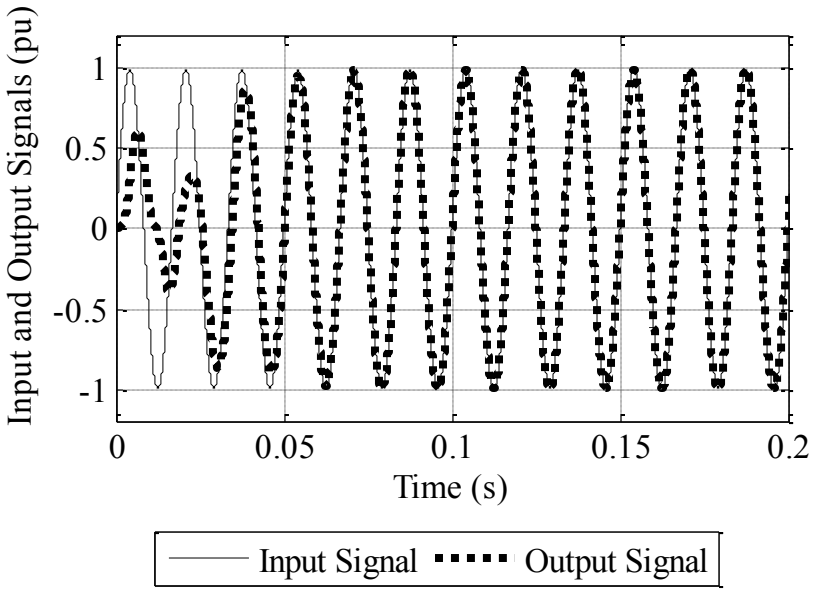

Fig. 2.3 Initial convergence of the proposed non-linear adaptive filter of [41]

The response of the filter to a 20% decrease in magnitude of the dominant sinusoidal signal and frequency change from 60 Hz to 30 Hz is shown in Fig. 2.4 and Fig. 2.5, respectively. The results verify the ability of the filter to track the changes in the magnitude and frequency of the input signal.

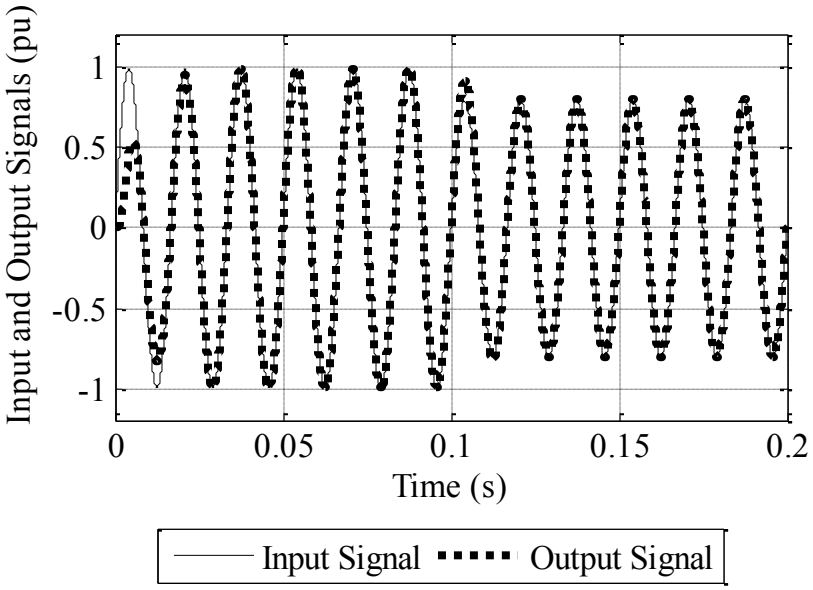

Fig. 2.4 Response of the filter to 20% magnitude change in the input signal

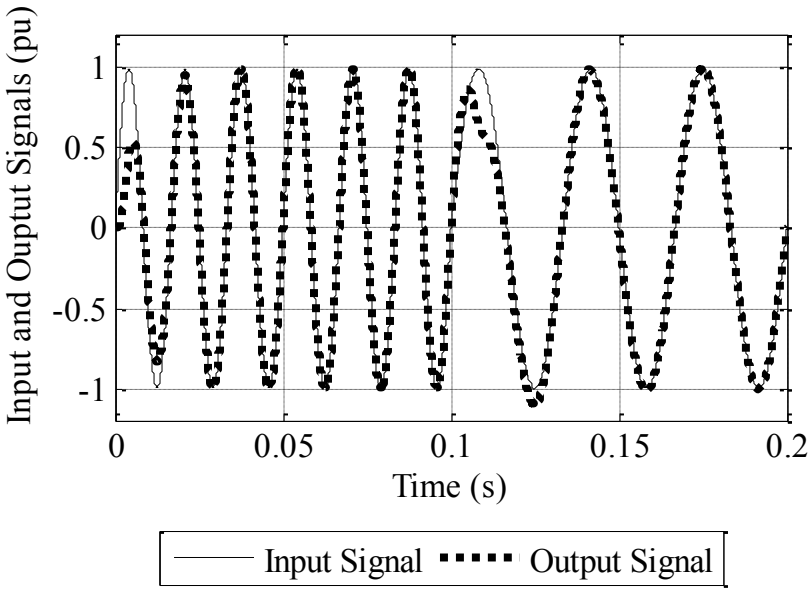

Fig. 2.5 Response of the filter to frequency change in the input signal

In Fig. 2.6, the noise cancelation characteristics of the proposed filter are illustrated. This can be useful in canceling measurement noises.

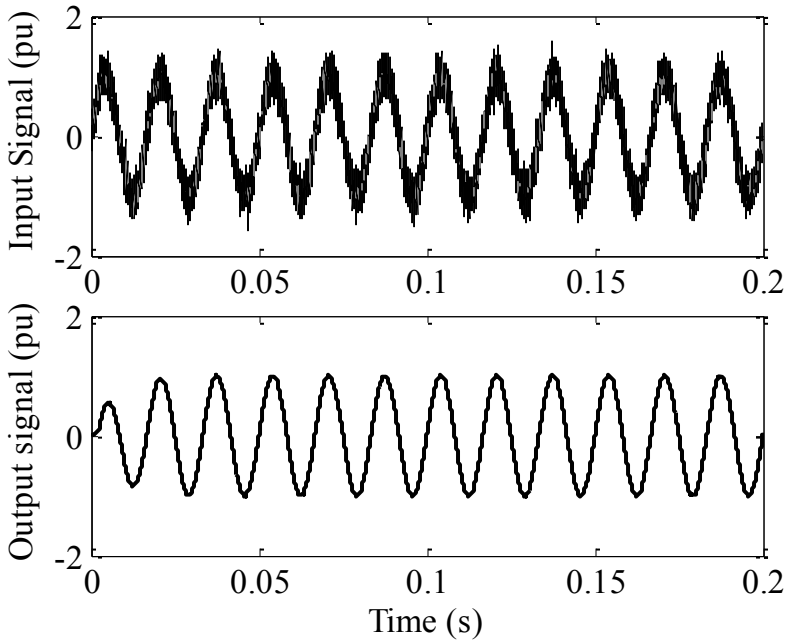

Fig. 2.6 Noise cancelation characteristics of the proposed filter by [41]

2.3 Application of the Adaptive Non-Linear Filter in the Non-Intrusive Speed Detection Process

To achieve an efficiency estimation technique with the lowest possible level of intrusion, the speed of the motor should be measured without the use of a speed sensor. Therefore, a machine current signature analysis (MCSA)-based speed detection technique that works with detection of eccentricity harmonics is proposed for this project. Other versions of this technique that use different approaches to detect the speed-dependent harmonics can be found in [50]-[52].

Based on [50], the eccentricity of the rotor (due to its oval shape) creates speed-dependent current harmonics. The largest (in magnitude) speed-dependent current harmonic has a frequency (f_{sdh}), which can be found by using (2.23).

$$f_{sdh} = \left(1 \pm \frac{1-S}{\frac{P}{2}} \right) . f_s \tag{2.23}$$

where f_s is the supply frequency, S is the slip and P is the number of poles.

Even the largest speed-dependent current harmonic is extremely small in comparison to the fundamental component of the current signal. This makes the detection process more complicated due to the masking effect of the fundamental component on the other harmonic orders.

For this reason, the introduced non-linear adaptive filter is used to extract the main component of the signal. After extraction of the main component, fast Fourier transform (FFT)-based harmonic analysis of the residual signal can be used to detect the speed-dependent current harmonics.

Using the frequency of the speed dependent current harmonic, frequency of the grid and the number of poles, (2.23) can be used to find the slip of the machine. The equivalent speed of the machine can be found based on (2.24).

$$N_{Meas} = (1-\mathrm{S}).\mathrm{N}_{\mathrm{sync}} \tag{2.24}$$

The block diagram of the proposed method is shown below.

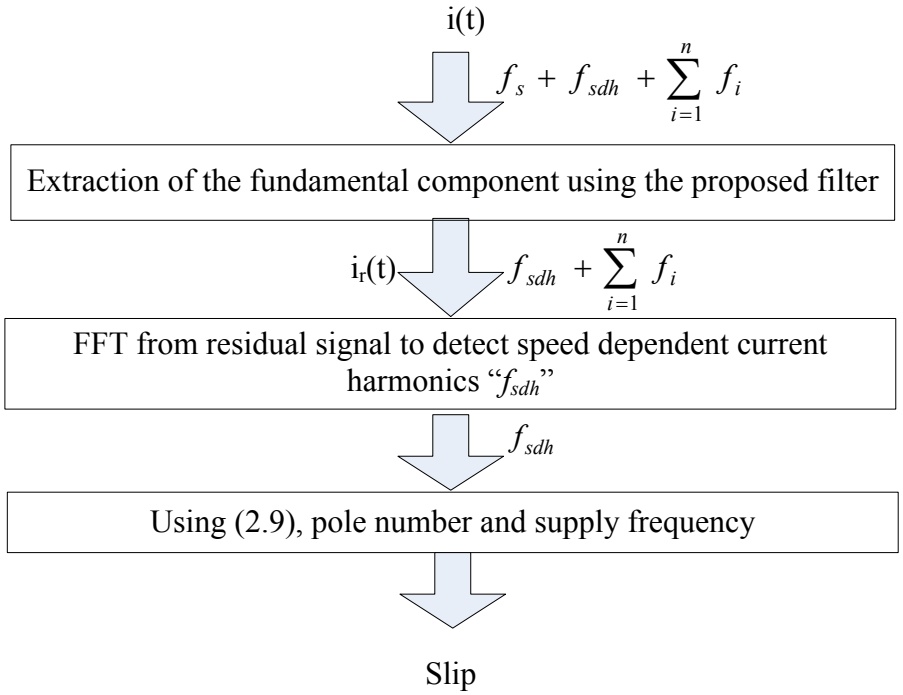

Fig. 2.7 The flowchart of the proposed non-intrusive speed estimation technique

2.3.1 Verification of the Proposed Non-Intrusive Speed Estimation Algorithm

To verify the credibility and accuracy of the proposed method, it was tested with a 3 hp induction motor. The nameplate data of the tested machine is provided in Table 2.1.

Table 2.1 Nameplate data of a 3 hp induction machine

f	60 Hz	Design class	B
V_{LL}	208 V	Insulation class	B
I	10.3 A	Nominal speed	1740 rpm
Connection	Y	Poles	4

Fig. 2.8 shows the measured input current of one of the phases of the tested 3 hp induction motor. The residual current after extraction of the main component is shown in Fig. 2.9.

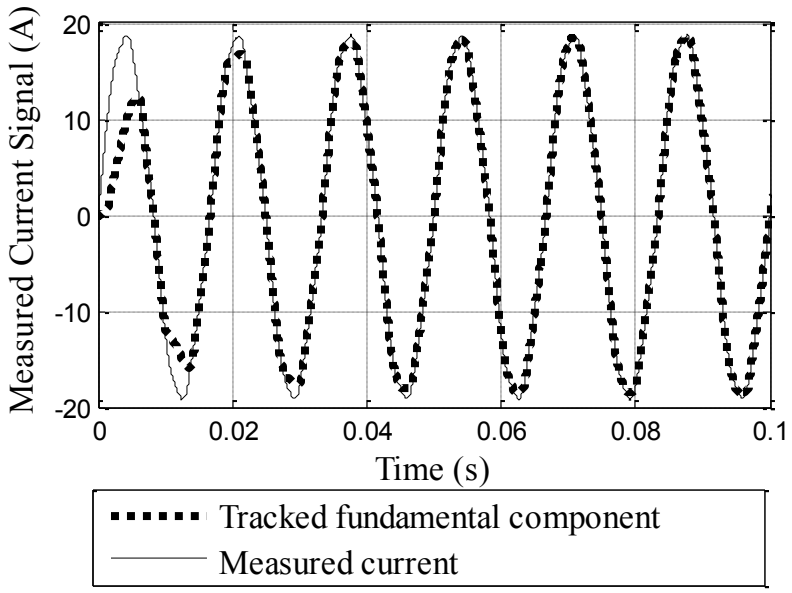

Fig. 2.8 Measured current signal and the tracked fundamental component

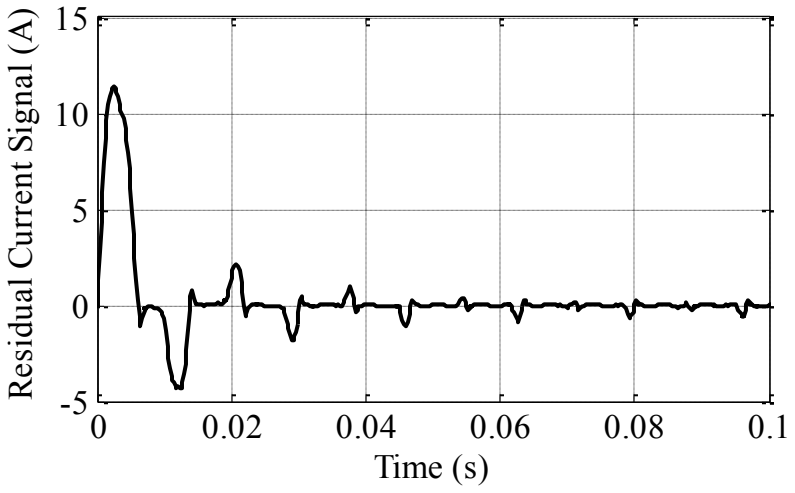

Fig. 2.9 Residual current signal $i_r(t)$ after extraction of the fundamental component

The harmonic spectra of the current signal before and after extraction of the main component are shown in Fig. 2.10 and Fig. 2.11, respectively. The smaller harmonics were detectable after extraction of the main component.

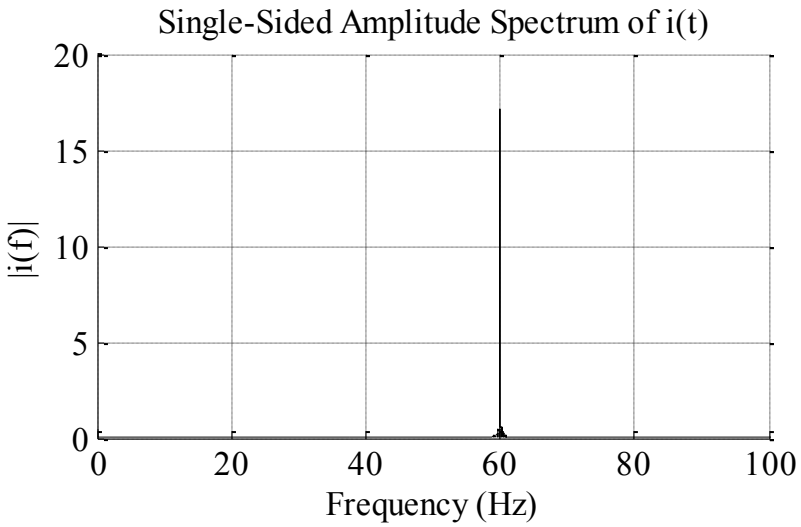

Fig. 2.10 Harmonic spectrum of the current signal i(t)

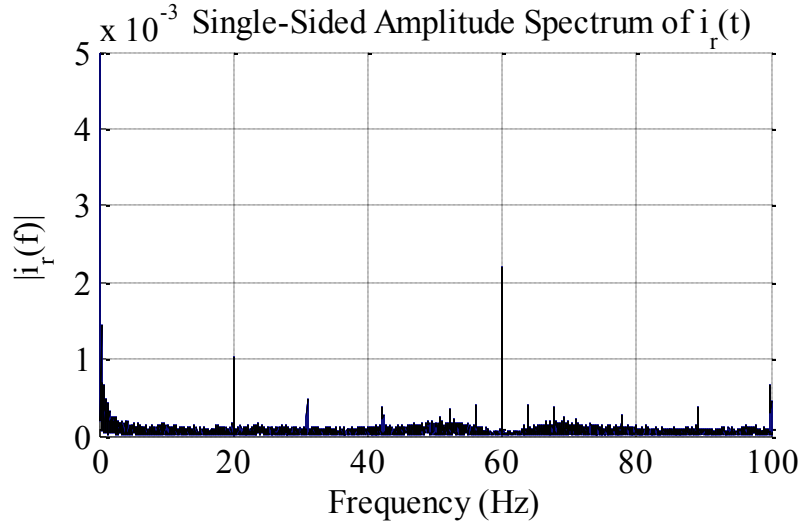

Fig. 2.11 Harmonic spectrum of the residual current signal $i_r(t)$

Based on the theory of induction machines, one can expect to have the speed value somewhere between the synchronous speed (1800 rpm in this case) and the rated speed (which is 1740 rpm for the machine). However, considering the possibility of working under an overload condition, the lowest possible speed is considered to be around 1700 rpm. Given that the number of the pole pairs equals 2, a supply frequency of 60 Hz, and a slip range from 0 to 0.055 (1700 rpm), it was anticipated that the speed-dependent current harmonic would be somewhere between 30 Hz and 31.67 Hz. The harmonic spectra of the residual currents of the tested 3 hp machine are shown in Fig. 2.12 at two different load points.

Based on (2.23), the frequency of 30.22 Hz is equivalent to slip of 0.0077 (1786.0 rpm), and 30.95 Hz is equivalent to slip of 0.032 (1742.3 rpm). A comparison of the estimated and measured speeds with tachometer results is presented in Table 2.2. The estimation was based on 60 seconds of data acquisition with 5 kHz sampling rate.

Table 2.2 Measured vs. estimated speeds for the 3 hp motor

% of rated load	Measured (rpm)	Estimated (rpm)	Error (%)
25	1785	1786.0	0.06
50	1772	1773.1	0.06
75	1759	1760.0	0.06
85	1751	1751.9	0.05
100	1741	1742.3	0.07

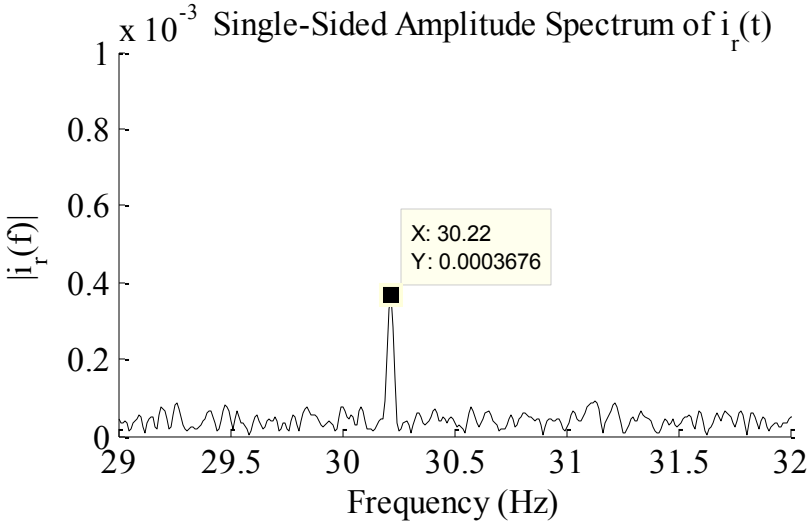

(a)

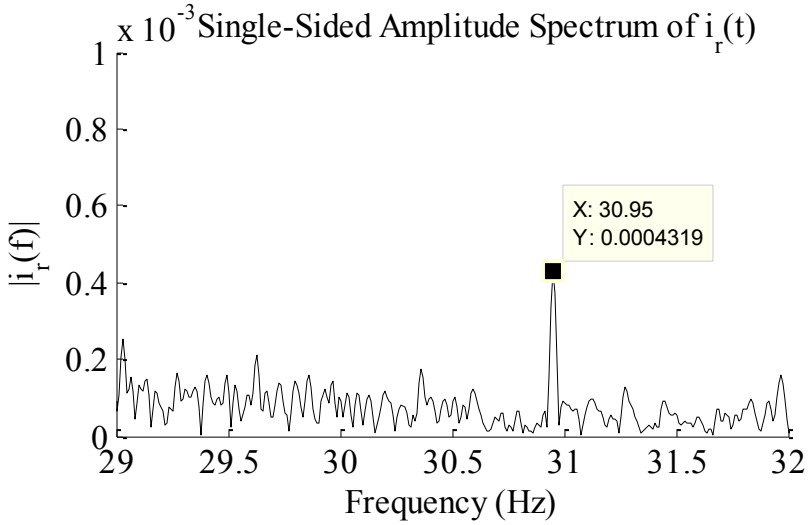

(b)

Fig. 2.12 Harmonic spectrum of the residual current signal at (a) around 25% of the rated load and (b) around the rated load

The same test was performed with a 10 hp premium efficiency induction machine to check the generality of the method. The nameplate of the machine is shown in Table 2.3. The estimated speeds are compared with the measured values in Table 2.4.

Table 2.3 Nameplate data of a 10 hp induction machine

f	50 Hz	Design class	B
V_{LL}	380 V	Insulation class	F
I	14.4 A	Nominal speed	1460 rpm
Connection	Δ	Poles	4

As can be seen, the results of this technique were highly congruent with the tachometer measurements.

Table 2.4 Measured vs. estimated speeds for the 10 hp motor

% of rated load	Measured (rpm)	Estimated (rpm)	Error (%)
25	1494	1493.9	-0.01
50	1486.2	1486.5	0.02
75	1481.9	1482.1	0.01
85	1474.8	1474.9	0.01
100	1466.7	1467.0	0.02

2.4 Application of the Adaptive Non-Linear Filter in the Extraction of the Symmetrical Components

The proposed non-linear filter can be used to track the fundamental component and to extract the phasor information (magnitude and phase shift) of a signal. The filter is capable of dealing with frequency fluctuations while estimating the phasor quantities. The block diagram of the proposed technique, which is based on a combination of the proposed filter and the Fortescue transformation matrix, inspired from [47], is illustrated in Fig. 2.13.

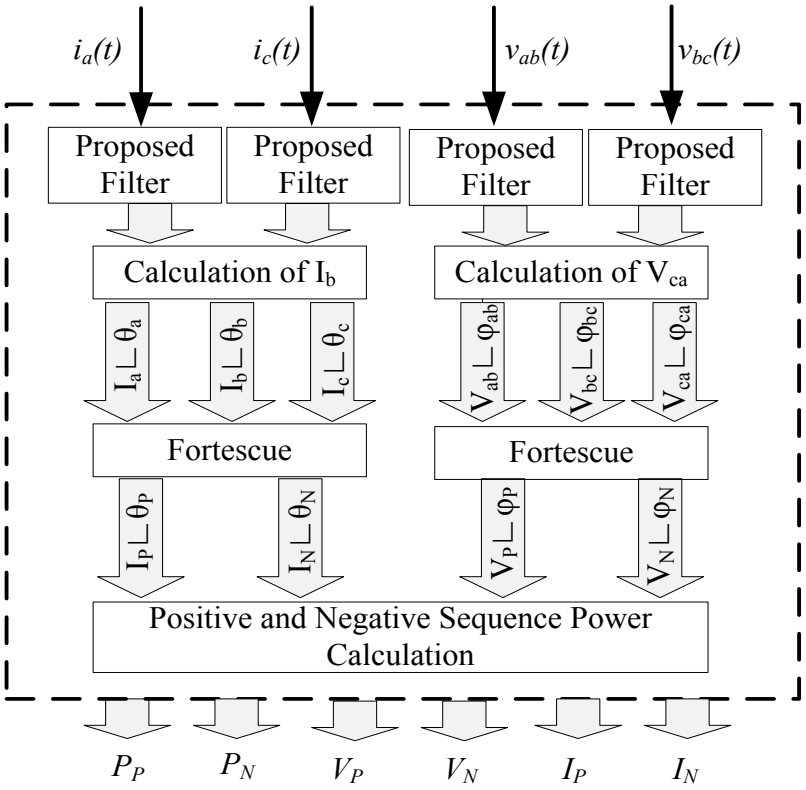

Fig. 2.13 Extraction of the positive and negative sequence components from two line voltage and current signals

The Fortescue transformation is shown in (2.25).

$$\begin{bmatrix} \overline{I_0} \\ \overline{I_P} \\ \overline{I_N} \end{bmatrix} = \frac{1}{3}\begin{bmatrix} 1 & 1 & 1 \\ 1 & e^{j\frac{2\pi}{3}} & e^{j\frac{4\pi}{3}} \\ 1 & e^{j\frac{4\pi}{3}} & e^{j\frac{2\pi}{3}} \end{bmatrix}\begin{bmatrix} \overline{I_a} \\ \overline{I_b} \\ \overline{I_c} \end{bmatrix} \tag{2.25}$$

where

$\overline{I_a}, \overline{I_b}, \overline{I_c}$: are three-phase current phasor quantities

$\overline{I_0}, \overline{I_P}, \overline{I_N}$: are zero, positive and negative sequence current phasor quantities

In a three-phase three-wire system, regardless of the connection type, under unbalanced conditions, the line voltages and line currents will only contain positive and negative sequence components. This means the sum of the line currents at all time is equal to zero, since there is no neutral conductor in a three-phase three-wire system. In addition, the sum of the three-phase line voltages at all time are also equal to zero, since the zero sequence voltage must be zero in absence of a fault. Consequently, two sets of filters are sufficient for the extraction of the phase and the magnitude of the symmetrical components of the voltage, current, and input active power from the voltage and current signals as shown in Fig. 2.13.

In most industrial applications, only the line voltages are accessible due to a Y connection with no access to the neutral or delta (Δ) connection. However, the phase

values of the positive and negative sequence components are required in the efficiency estimation process. Thus, phase values of the positive and negative sequence components should be found based on the accessible line voltage signals.

2.4.1 Transformation from Line to Phase Symmetrical Components

Let $\overline{V_a}$, $\overline{V_b}$, and $\overline{V_c}$ be a set of three-phase phasors of an unbalanced system defined with (2.26).

$$\begin{aligned}
\overline{V_a} &= V_P\angle(0°) + V_N\angle(0° + \varphi) \\
\overline{V_b} &= V_P\angle(-120°) + V_N\angle(+120° + \varphi) \\
\overline{V_c} &= V_P\angle(+120°) + V_N\angle(-120° + \varphi)
\end{aligned} \tag{2.26}$$

where

V_P : is the magnitude of the positive sequence components (phase quantity)

V_N : is the magnitudes of the negative sequence components (phase quantity)

φ : is the phase shift between the negative and positive sequence components

When the phase values are known, it is possible to find the line phasors as shown in (2.27).

$$\begin{aligned}
&\overline{V_{ab}} = \overline{V_b} - \overline{V_a} = V_P\angle(0°) + V_N\angle(0° + \varphi) - V_P\angle(-120°) - V_N\angle(+120° + \varphi) \\
&= \sqrt{3}V_P\angle(30°) + \sqrt{3}V_N\angle(-30° + \varphi) \\
&\overline{V_{bc}} = \sqrt{3}V_P\angle(-90°) + \sqrt{3}V_N\angle(90° + \varphi) \\
&\overline{V_{ca}} = \sqrt{3}V_P\angle(150°) + \sqrt{3}V_N\angle(210° + \varphi)
\end{aligned} \tag{2.27}$$

By substituting the line phasors into the Fortescue matrix, the line positive ($\overline{V_{P,LL}}$) and negative ($\overline{V_{N,LL}}$) sequence phasor components are found, as shown in (2.28).

$$\begin{aligned}\overline{V_{P,LL}} &= \frac{1}{3}\left[\overline{V_{ab}} + e^{j\frac{2\pi}{3}}.\overline{V_{bc}} + e^{j\frac{4\pi}{3}}.\overline{V_{ca}}\right] = \sqrt{3}V_P\angle(30°)\\ \overline{V_{N,LL}} &= \frac{1}{3}\left[\overline{V_{ab}} + e^{j\frac{4\pi}{3}}.\overline{V_{bc}} + e^{j\frac{2\pi}{3}}.\overline{V_{ca}}\right] = \sqrt{3}V_N\angle(-30° + \varphi)\end{aligned} \tag{2.28}$$

Based on (2.28), the magnitude of each line symmetrical component should be divided by $\sqrt{3}$ in order to have the magnitude of the per phase symmetrical values. The angle of the line positive sequence component should be shifted by -30° while, for the negative sequence component, 30° should be added to have the per-phase angles. This transformation is shown in a matrix form in (2.29).

$$\begin{bmatrix}\overline{V_P}\\ \overline{V_N}\end{bmatrix} = \begin{bmatrix}\frac{1}{\sqrt{3}}\angle -30 & 0\\ 0 & \frac{1}{\sqrt{3}}\angle +30\end{bmatrix}\begin{bmatrix}\overline{V_{P,LL}}\\ \overline{V_{N,LL}}\end{bmatrix} \tag{2.29}$$

In the case of a Y connection, the line voltage components are transferred to the phase components while, in the case of a Δ connection, the current components need to be transferred. The positive and negative sequence components of the input active power can be calculated based on extracted per-phase phasors of the symmetrical components of the voltage and current signals.

2.4.2 Verification of the Proposed Algorithm for the Extraction of Symmetrical Components

To verify the performance of the proposed technique, a set of hypothetical unbalanced three-phase line voltage and line current signals were created with phasor values as shown in (2.30).

$$\overline{V_{P,LL}} = \sqrt{3}\angle(0°),\quad \overline{V_{N,LL}} = \frac{\sqrt{3}}{5}\angle(30°),\quad \overline{I_{P,LL}} = 1\angle(-60°),\quad \overline{I_{N,LL}} = \frac{1}{5}\angle(30°) \tag{2.30}$$

The created hypothetical unbalanced line voltage and current signals are shown in Fig. 2.14 and Fig. 2.15, respectively.

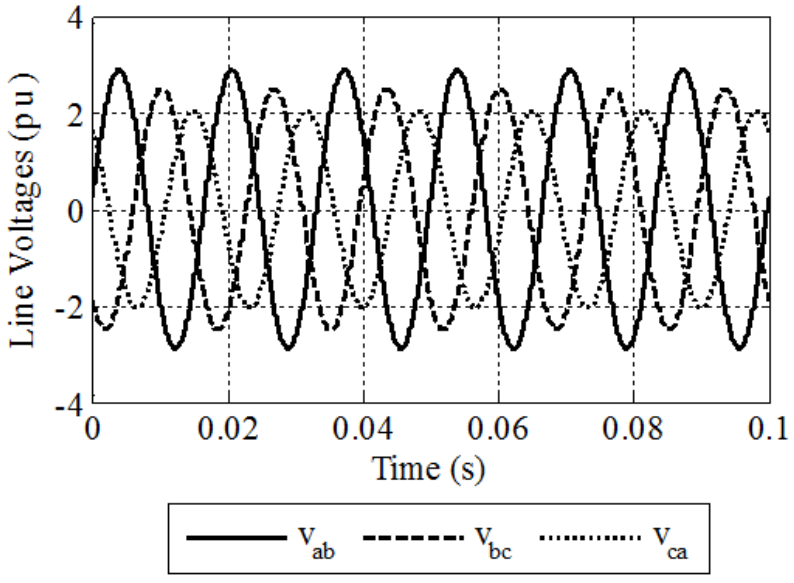

Fig. 2.14 Hypothetical three-phase unbalanced line voltages

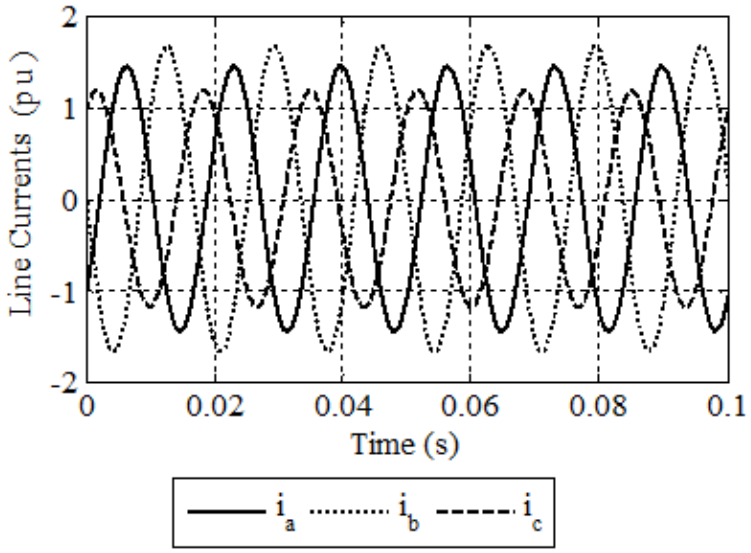

Fig. 2.15 Hypothetical three-phase unbalanced line currents

In (2.30), all the magnitudes are per unit values and the angles are in respect of positive sequence line voltage components. Considering a Y connection and (2.29), the line components were transformed to the phase components as shown in (2.31).

$$\overline{V_P} = 1\angle(-30°),\ \overline{V_N} = \frac{1}{5}\angle(+60°),\ \overline{I_P} = 1\angle(-60°),\ \overline{I_N} = \frac{1}{5}\angle(30°) \tag{2.31}$$

Based on (2.31), the positive sequence components of the active power should be around 2.598 pu while the negative sequence component is around 0.104 pu.

As can be seen from Fig. 2.16, the same results were obtained by using the proposed algorithm to extract the components of the hypothetical three-phase unbalanced signals. This verifies the accuracy and capability of the algorithm in the extraction of symmetrical components from voltage and current signals.

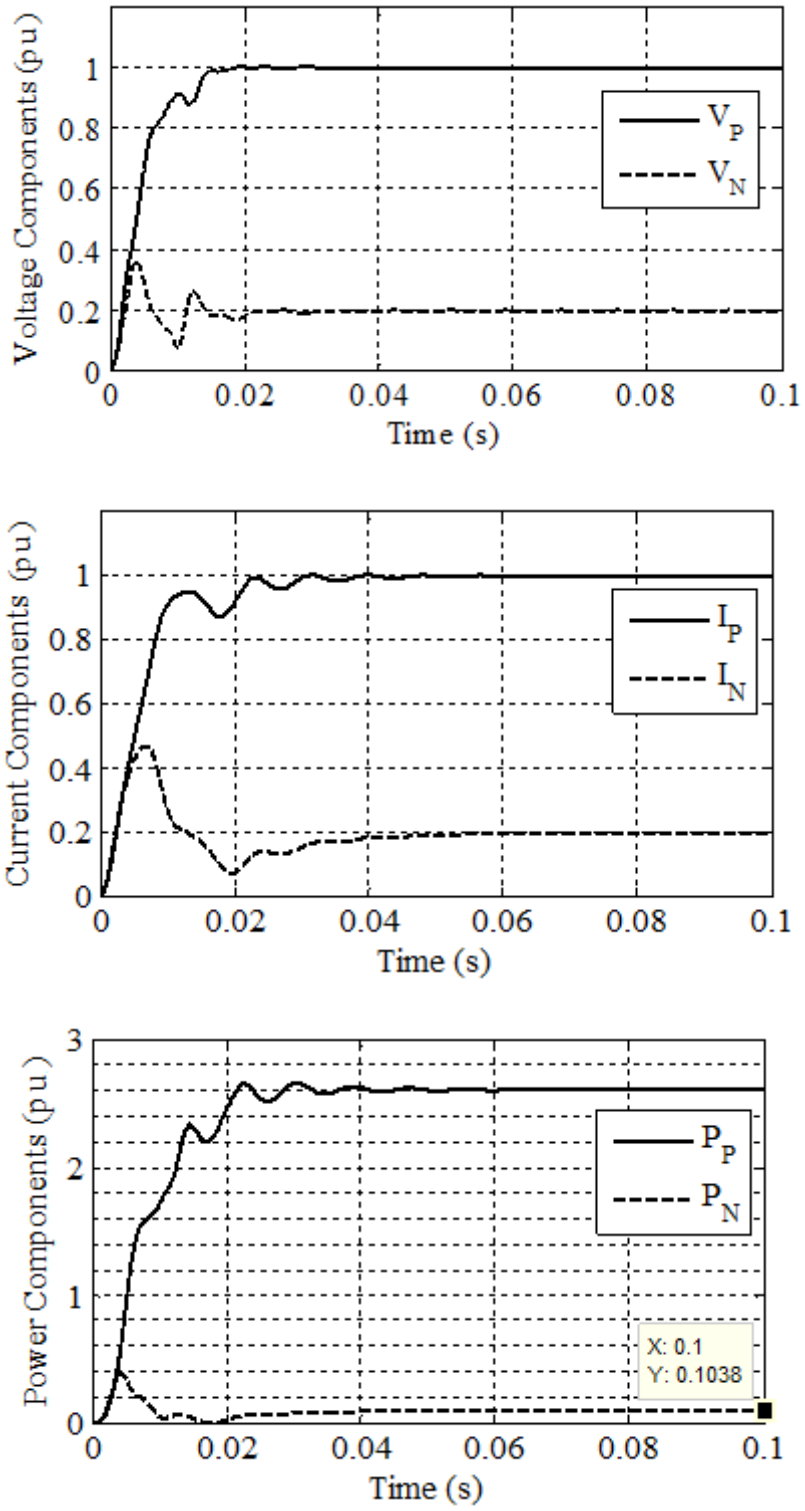

Fig. 2.16 Extracted symmetrical components of the hypothetical unbalanced signal using the proposed algorithm

Finally, the proposed algorithm was used to extract the symmetrical components of the voltage and current signals of the tested 3 hp induction machine under full load conditions with about 5% VUF, and this is shown in Fig.2.17 and Fig. 2.18.

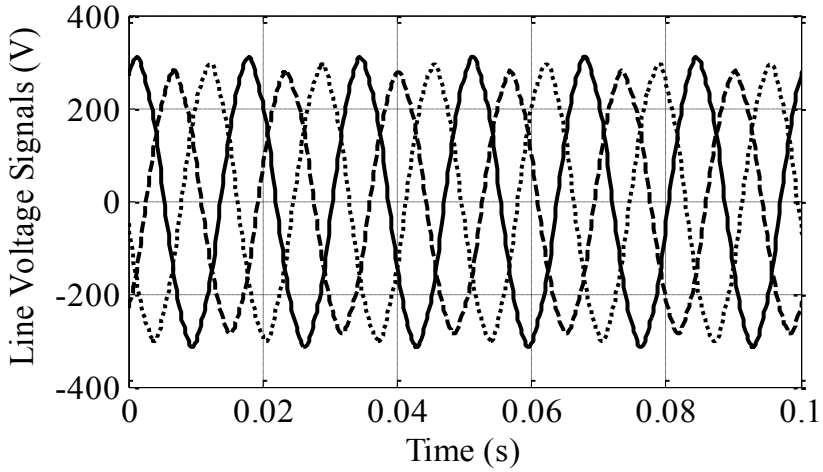

Fig. 2.17 Recorded line voltage signals of the 3 hp induction motor under 5% VUF

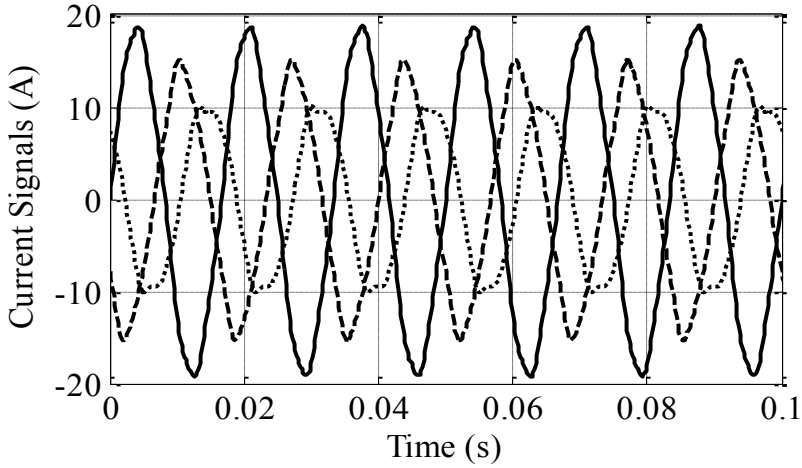

Fig. 2.18 Recorded line current signals of the 3 hp induction motor under 5% VUF and the rated load

The extracted components of the signals, as well as the estimated positive and negative sequence components of the input active power, are shown in Fig. 2.19.

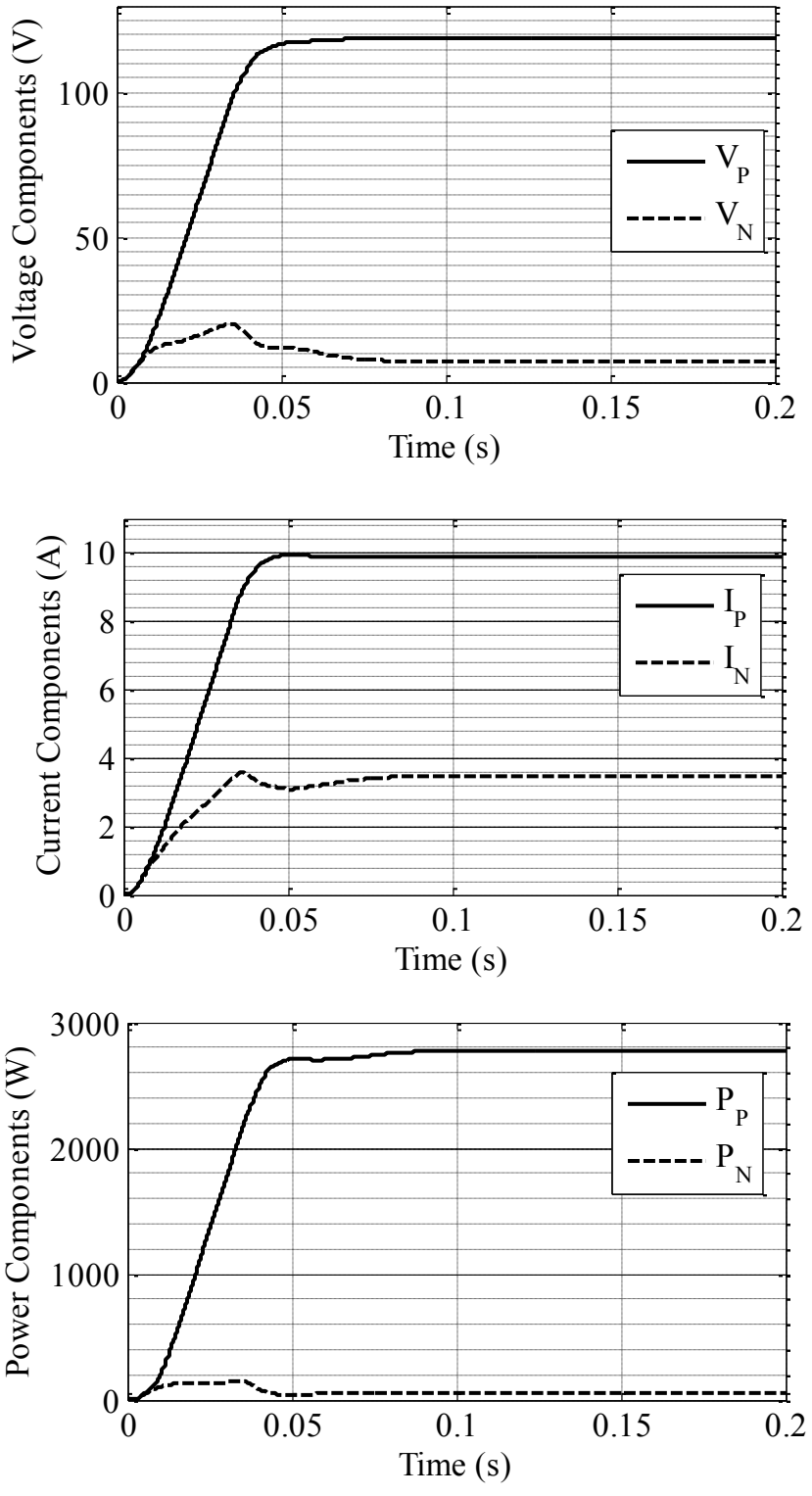

Fig. 2.19. Positive and negative sequence components of input voltage, input current, and input active power under 5% VUF and the rated load

2.5 Conclusions

In this chapter, two new applications for the adaptive non-linear filter of [41] were proposed in non-intrusive motor speed detection as well as symmetrical components extraction algorithms.

In the first application, the proposed filter was used to extract the fundamental component of the current signal in order to facilitate the speed detection process.

In the second application, the proposed filter was used to extract the negative and positive sequence components of the current, voltage, and input active power from the two line voltage and current signals.

The proposed methods were verified through simulation and experimental results. The extracted speed information and the values of the symmetrical components of the voltage, current, and input active power were used in the efficiency estimation process as is discussed in the following chapters.

3. IN-SITU EVOLUTIONARY- BASED EFFICIENCY ESTIMATION UNDER UNBALANCED SUPPLY CONDITIONS

3.1 Introduction

As discussed in Chapter 1, in-situ machine efficiency estimation techniques are increasing in importance due to pressures to improve performance and demand side energy management. Numerous techniques have been proposed to estimate the efficiency of an induction motor in situ; however, very little has been done to make these methods compatible with the unbalanced supply condition that exists in most industrial applications. Thus, in this chapter, a new evolutionary-based in-situ efficiency estimation technique is introduced, which is capable of dealing with unbalanced power supply conditions without the need for a no-load test.

The chapter is organized as follows: section 3.2 contains the problem statement. In section 3.3, the methodology and the assumptions are discussed in detail. The foundation of the proposed evolutionary-based efficiency estimation algorithm is presented in section 3.4, with a non-linear temperature estimation algorithm introduced in section 3.5. The proposed method is verified based on the simulation results which are shown in section 3.6. In section 3.7, the proposed algorithm is used to estimate the efficiency of a 3 hp squirrel cage induction machine, and the experimental results are compared with the measured values in order to validate the proposed method. In section 3.8, the effects of the input data are investigated in terms of efficiency estimation accuracy. The sensitivity of the efficiency estimation algorithm to the assumptions is interrogated in section 3.9.

The generality of the proposed method is validated through experimental results with another 10 hp induction machine in section 3.10. Measurement error analysis is done in section 3.11 to assure the accuracy of the measured efficiencies and, finally, the results of the repeatability tests have been provided in section 3.12 to demonstrate the consistency of the results and thus the credibility of the proposed method.

3.2 Problem Statement

Unbalanced power supply creates significant unbalanced currents in a machine. The unbalanced currents produce positive and negative sequence flux components. These fluxes generate positive and negative sequence torque components, which act against each other, and the net torque is reduced due to this interaction. The efficiency (η) of a machine in the presence of an unbalanced supply can be calculated by (3.1).

$$\eta = \frac{P_{Out}}{P_{In}} = \frac{\left|P_{Out,P}\right| - \left|P_{Out,N}\right| - P_{FW}}{\left|P_{In,P}\right| + \left|P_{In,N}\right|} \tag{3.1}$$

where

P_{FW} : is the friction and windage loss

P_{Out} : is the output power

P_{In} : is the input power

$P_{In,P}$: is the positive sequence component of the input power

$P_{In,N}$: is the negative sequence component of the input power

$P_{Out,P}$: is the positive sequence component of the output power

$P_{Out,N}$: is the negative sequence component of the output power

The value of the positive and negative sequence input active powers can be calculated non-intrusively with the measurement of only two line voltage and current signals at each operating point.

The value of the positive and negative sequence output powers can be estimated at each operating point if the parameters of the positive and negative sequence equivalent circuits of the induction machine are known. These equivalent circuits are shown in Fig. 3.1 [53].

Based on Fig. 3.1, it can be concluded that, in the worst case scenario, there are eight unknown parameters to be estimated by any search algorithm. These are R_1, X_1, X_M, R_M, R_2, X_2, R_3, and X_3. The slip of the induction machine at each operating point is known based on the proposed current signature analysis-based speed estimation technique discussed in detail in Chapter 2. The available data at each operating point are the magnitude of the positive sequence input current ($I_{In,P}$), the negative sequence input current ($I_{In,N}$), the positive sequence input active power ($P_{In,P}$) as well as the negative sequence input active power ($P_{In,N}$). Thus, for one operating point, there are four known values and, at most, eight unknown parameters.

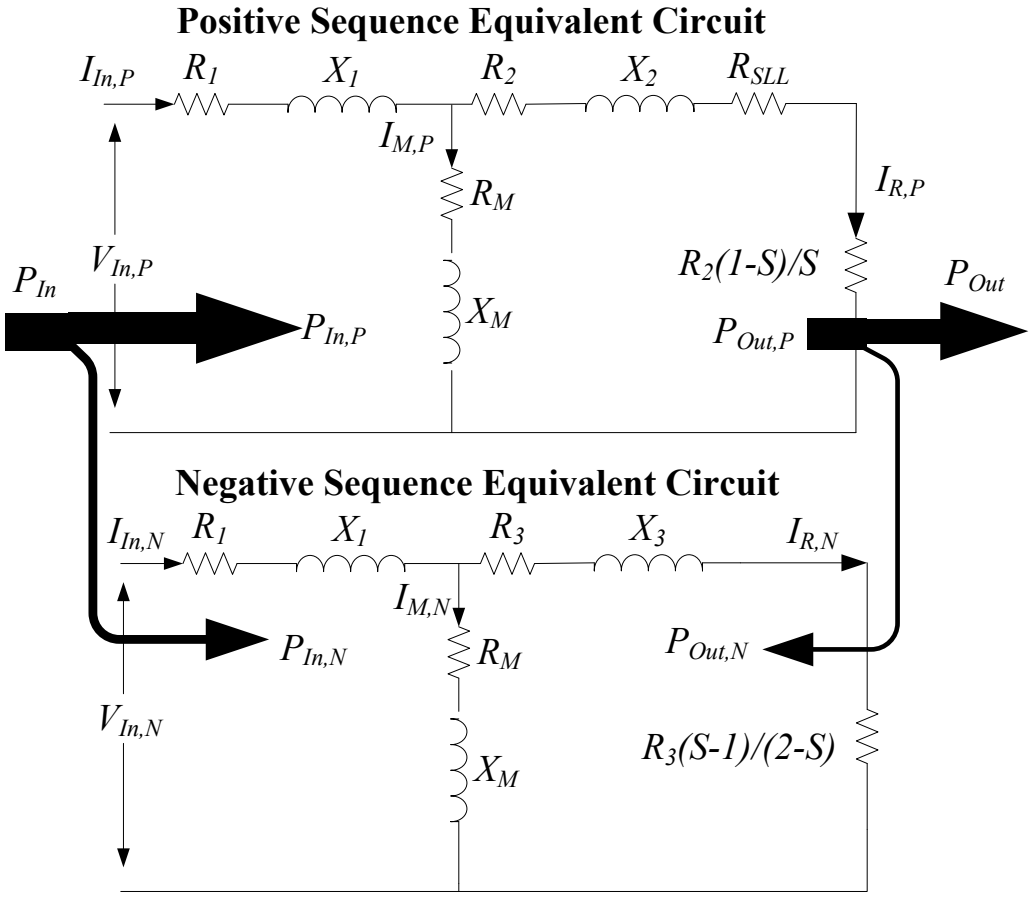

Fig. 3.1. Positive and negative sequence equivalent circuits of an induction machine [53]

where

R_1 : is the stator resistance

X_1 : is the stator leakage reactance

R_2: is the rotor positive sequence resistance

X_2 : is the rotor positive sequence leakage reactance

R_3 : is the rotor negative sequence resistance

X_3 : is the rotor negative sequence leakage reactance

X_M : is the mutual reactance of the machine

R_M : is the representative of the core losses

R_{SLL}: is the representative of the stray load losses defined, based on the IEEE standard 112 [8]

S: is the slip of the induction motor

One way of solving a non-linear system of equations is to take the least square minimization method and to try to fit an answer (a non-linear curve) to all the equations (in this case, operating points) in order to achieve a solution with the least square error. Since, in this problem, the number of known equations (available data) at one operating point was not sufficient, and different types of errors (measurement, methodology, etc.) exist, the data of multiple operating points were used to increase the number of equations and therefore facilitate the parameter estimation process. This forced the algorithm to converge to a unique set of parameters that had the least square error for all the operating points.

Non-linear least square minimization problems can be solved by using classic deterministic optimization methods, if the derivation of the objective function is available (which is not the case in this problem). Otherwise, a stochastic search technique can be

used instead. In [22]-[29], a genetic algorithm with binary representation was used as a promising tool to solve this type of problem. In this research work, a floating point evolutionary-based algorithm was used instead, as it was found to be more suitable for the efficiency estimation problem in terms of speed of convergence and accuracy.

3.3 Methodology and Assumptions

In order to be able to estimate the machine's parameters by using multiple sets of data from different operating points and an optimization-based search algorithm, these parameters should be constant at different operating conditions. Considering a constant input voltage, it is reasonable to assume that the parameters of the positive sequence equivalent circuit are almost constant at different loading conditions (excluding the temperature variation effect on the resistance values, which is discussed in section 3.5).

Based on the performed experiments as well as the published results in [12], it was observed that the negative sequence impedance was not a constant value at different loading conditions. Considering Fig. 3.1 and the fact that the positive sequence components were almost constant at different loading conditions (excluding the temperature effect on the resistance variations), it was concluded that the variation of the negative sequence components was due to the variation of the negative sequence rotor parameters, R_3 and X_3. In [12], it is claimed that this variation is due to the non-saturated tips of the rotor teeth. Since these two parameters are not constant at different operating points, it is not possible to use a search algorithm to find a unique set of parameters that will satisfy all the operating points. However, if the parameters of the positive sequence

components are known, it is possible to calculate the negative sequence output power and the rotor parameters based on the measured negative sequence voltage, current, and input active power at each operating point.

Therefore, in this work, the positive sequence parameters of the machine are estimated with the help of an evolutionary search algorithm based on the extracted positive sequence input currents and powers at five different operating points, while the effects of the negative sequence losses are considered on the machine's temperature rise. The negative sequence rotor components are calculated at each operating point based on the estimated positive sequence parameters and the measured negative sequence voltage, current, and input active power.

The algorithm uses data from multiple operating points. Two different scenarios are considered: firstly, the motor works under different loading conditions for a period of time with the result that each operating point has a different operating temperature. In the second scenario, the motor works most of the time under a main operating condition, e.g., 75% of the rated load; however, short term load fluctuations, e.g., with one minute duration, can be used as extra load points in the efficiency estimation process. In this case, the temperatures of all short term operating points are considered equal to the temperature of the main operating point. The proposed algorithm can be used in either scenario.

In addition to the above explanation, the following assumptions are in this work:

1) The value of the stator resistance is known at the ambient temperature. This could be achieved through the measurement from the motor control center with the lowest possible intrusion level at any time when the motor is in shutdown mode [22].
2) The ratio of X_1 over X_2 is known based on the design class of the machine and Table 3.1, which is adopted from the IEEE standard 112 [8]. As is shown in section 3.9, this ratio did not have a significant impact on the final results.

Table 3.1 Ratio of X_1/X_2 based on the design class of the machine [8]

Design class	X_1/X_2
A, D, wound rotor	1.00
B	0.67
C	0.43

3) The total amount of the friction and windage losses of the machine is equal to 1.2% of the input power [16], [54]. Since there is not a non-intrusive way to estimate the friction and windage losses of a loaded machine, an empirical value should be assumed for these losses. This is a common assumption in most of the non-intrusive in-situ efficiency estimation techniques in literature.
4) The rated temperature rise is known from the nameplate, or it can be assumed based on the recommendation of the IEEE standard 112 when the insulation class of the machine is known, as shown in Table 3.2 [8]. The rated temperature rise is used to estimate the temperature of the machine at other operating conditions, as shown in section 3.5.

Table 3.2 Specified (rated) temperature based on the insulation class of the machine [8]

Insulation class	T_{Rated} (C˚) (including 25˚C reference ambient)
A	75
B	95
F	115
H	130

5) The total amount of the full load stray load loss was assumed to be 1.8% of the rated power based on Table 3.3, which was adopted from the IEEE standard 112 for cases where the measurement of the stray load loss is not possible (such as methods E1, F1, and E1/F1).

Table 3.3 Assumed values for the stray load loss based on the IEEE standard 112 [8]

Machine rating (kW)	Stray load loss percent of rated load
1-90	1.8%
91-375	1.5%
376-1850	1.2%
1851 and greater	0.9%

This loss was considered as a resistance in the rotor circuit, so it changes with the loading condition according to the rotor's current, as recommended in the IEEE standard 112. The value of this resistance can be found by (3.2).

$$R_{SLL} = 0.01 \times 1.8 \times \frac{(1 - S_{Rated})}{S_{Rated}} R_2 \tag{3.2}$$

The sensitivity of the algorithm to these assumptions was investigated in section 3.9.

3.4 Fundamentals of the Floating Point Evolutionary Algorithm

In the floating point evolutionary algorithm, the genome and the phenome are exactly the same. In other words, there is no mapping from the genome space (which contains binary numbers in the case of the simple binary GA) to the phenome space (which contains the floating point numbers, which are the values of each parameter). This makes the process more efficient with faster convergence than binary GA [55].

Each individual of the population is made up of five parameters to be estimated with an evolutionary-based search algorithm, as shown in Fig. 3.2.

X_2	R_2	X_M	R_M	K_{Th}

Fig. 3.2. One individual of the population

where

K_{Th} : is the thermal coefficient of the machine

The total population consists of 250 individuals. The first generation of these individuals is selected randomly within a predefined period. The operators that were used in this work were:

- Recombination: Single arithmetic recombination
- Mutation: Non-uniform mutation with a fixed distribution
- Reproduction: Tournament-based selection combined with elitism

In the single arithmetic recombination technique, two parents were selected randomly with a probability of P_c. Then, one parameter of each parent (the same one for each) was selected at random and changed with the arithmetic average of the parent one and parent two, as shown in Fig. 3.3. The newly-created individuals were the offspring of those parents, and they participated in the pool of potential individuals for the next generation.

Parent 1

$X_{2,Parent1}$	$R_{2,Parent1}$	$X_{M,Parent1}$	$R_{M,Parent1}$	$K_{Th,Parent1}$

Parent 2

$X_{2,Parent2}$	$R_{2,Parent2}$	$X_{M,Parent2}$	$R_{M,Parent2}$	$K_{Th,Parent2}$

Offspring 1

$X_{2,Parent1}$	$R_{2,Parent1}$	$\sigma.X_{M,Parent1}+(1-\sigma).X_{M,Parent2}$	$R_{M,Parent1}$	$K_{Th,Parent1}$

Offspring 2

$X_{2,Parent2}$	$R_{2,Parent2}$	$\sigma.X_{M,Parent2}+(1-\sigma).X_{M,Parent1}$	$R_{M,Parent2}$	$K_{Th,Parent2}$

Fig. 3.3. Single arithmetic recombination in floating point evolutionary algorithm.

Sigma was defined as shown in (3.3), which is based on the fitness of parent one and two.

$$\sigma = \frac{Fitness\ of\ Parent\,1}{Fitness\ of\ Parent\,1 + Fitness\ of\ Parent\,2} \tag{3.3}$$

In a non-uniform mutation with a fixed distribution, one parameter of each individual was selected with the probability of P_m, and it was changed based on (3.4).

$$Mutated\ Parameter = Old\ Parameter \pm N \tag{3.4}$$

where

N : is a random number selected from a range that is decreased during generations

Finally, the parent pool selection and the survival selection were based on a tournament-based selection mechanism. Elitism, i.e., selection of the best parents to participate in the next generation, was used as an option to assure the existence of the best parents in the next generation.

In order to avoid premature convergence to a local minimum, it is recommended to keep a high diversity level in the population. This was achieved here by decreasing the elitism rate to the two best parents out of 250 old ones. At the same time, the tournament selection pool was limited to five individuals out of 250. This reduced the selection pressure and gave the opportunity for less fit individuals to exist for more generations. Considering the fact that multiple operating points were used to find the parameters of the positive sequence equivalent circuit, the fitness function (objective function) was defined

as shown in (3.5). This fitness function was inspired from a non-linear least square optimization technique.

$$F = \frac{1}{1 + {E_1}^2 + \sum_{i=1}^{n} \left({E_{2,i}}^2 + {E_{3,i}}^2 \right)} \tag{3.5}$$

where

n : is the number of operating points used in the efficiency estimation process

E_1 : is the percentage of the error between estimated temperature at the rated condition and the assumed rated temperature

As shown in (3.6),

$$E_1 = \frac{(T_{Rated} - T_{Rated,Est})}{T_{Rated}} \times 100 \tag{3.6}$$

where

$T_{Rated,Est}$: is the estimated temperature for the rated condition

T_{Rated} : is the assumed rated temperature

This helps the algorithm to find the thermal coefficient of the machine, which can later be used to estimate the machine's temperature at other operating conditions, as will be discussed in section 3.5.

$E_{2,i}$, as defined in (3.7), is the percentage of the positive sequence input current estimation error at operating point "i".

$$E_{2,i} = \frac{(I_{In,P,Meas,i} - I_{In,P,Est,i})}{I_{In,P,Meas,i}} \times 100 \tag{3.7}$$

$E_{3,i}$, presented in (3.8), is the percentage of the positive sequence input active power estimation error at operating point "i".

$$E_{3,i} = \frac{(P_{In,P,Meas,i} - P_{In,P,Est,i})}{P_{In,P,Meas,i}} \times 100 \tag{3.8}$$

As can be seen from (3.5), the magnitude of the fitness function, which is called the fitness value, is related to the magnitude of the errors between the measured and the estimated parameters. Therefore the fitness value can be used as a measure of the estimation quality and as a criterion to terminate the iterations. Based on several runs of the evolutionary-based algorithm, it was observed that the quality of the final result (in a predefined iteration level) was dependent on the quality of the initial population. Therefore, to avoid this problem, the fitness value was monitored after each generation and, based on that, it was decided whether to continue the iteration or stop the process, reset the initial population, and rerun the algorithm. The flowchart of the proposed method is shown in Fig. 3.4.

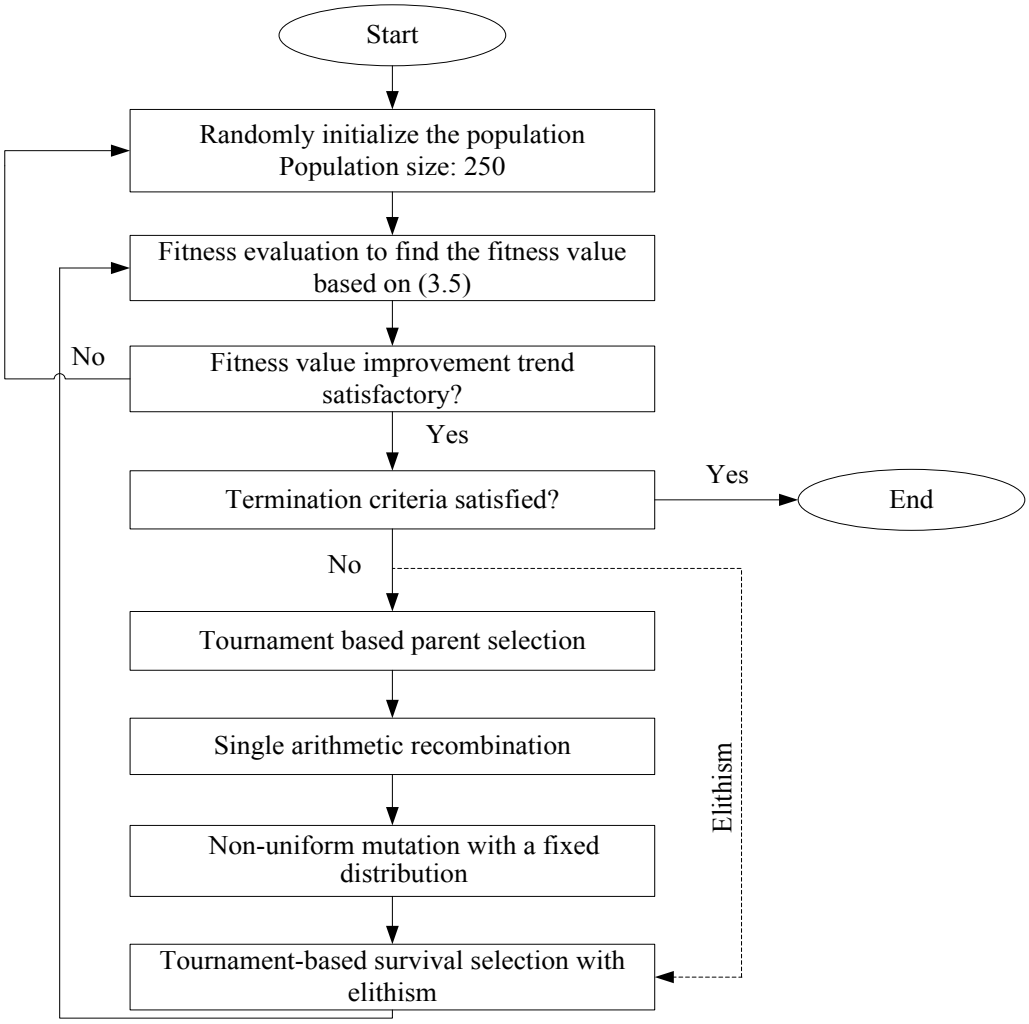

Fig. 3.4 Block diagram of the proposed algorithm

Based on the positive sequence equivalent circuit of Fig. 3.1, it is possible to write the following equations:

$$\overline{Y}_M = \frac{1}{R_M + jX_M} \tag{3.9}$$

$$\overline{Y}_1 = \frac{1}{R_{1,c} + jX_1} \tag{3.10}$$

$$\overline{Y}_{2,P} = \frac{1}{\frac{R_{2,c}}{s} + R_{SLL} + jX_2} \tag{3.11}$$

$$I_{M,P,Est} = \left| \frac{V_{In,P}.\overline{Y}_1.\overline{Y}_M}{\overline{Y}_1 + \overline{Y}_M + \overline{Y}_{2,P}} \right| \tag{3.12}$$

$$I_{In,P,Est} = \left| \frac{V_{In,P}.\overline{Y}_1.\left(\overline{Y}_M + \overline{Y}_{2,P}\right)}{\overline{Y}_1 + \overline{Y}_M + \overline{Y}_{2,P}} \right| \tag{3.13}$$

$$I_{R,P,Est} = \left| \frac{V_{In,P}.\overline{Y}_1.\overline{Y}_{2,P}}{\overline{Y}_1 + \overline{Y}_M + \overline{Y}_{2,P}} \right| \tag{3.14}$$

$$P_{In,P,Est} = 3\left(R_{1,c} {I_{In,P,Est}}^2 + \left(\frac{R_{2,c}}{s} \right) {I_{R,P,Est}}^2 + {I_{M,P,Est}}^2 . R_M \right) \tag{3.15}$$

$$P_{Out,P,Est} = 3\left(\left(\frac{R_{2,c}(1-S)}{S} \right) {I_{R,P,Est}}^2 \right) \tag{3.16}$$

where

$\overline{Y}_M$: is the complex admittance of the magnetizing branch

$\overline{Y}_1$: is the complex admittance of the stator branch

$\overline{Y}_{2,P}$: is the complex admittance of the rotor branch in positive sequence equivalent circuit

$I_{M,P,Est}$: is the estimated magnitude of the positive sequence magnetizing current

$I_{In,P,Est}$: is the estimated magnitude of the positive sequence input current of the motor

$I_{R,P,Est}$: is the estimated magnitude of the positive sequence rotor current of the motor

$P_{In,P,Est}$: is the estimated positive sequence input active power

$P_{Out,P,Est}$: is the estimated positive sequence output power

In these equations, the subscript "c" denotes the corrected resistances values based on the estimated temperature at each operating point.

Using these equations in combination with (3.6) to (3.8), the deviations of the positive sequence input currents and input active powers can be evaluated from the measured values at each operating point. Thus the fitness value of each individual can be specified, based on (3.5).

Knowing the negative sequence input active power ($P_{In,N}$), negative sequence voltage magnitude ($V_{In,N}$), and the negative sequence input current magnitude ($I_{In,N}$), one can use the negative sequence equivalent circuit and calculate the negative sequence rotor components at each operating point based on the following equations:

$$\varphi_N = \cos^{-1}\left(\frac{P_{In,N}}{3\times V_{In,N}\times I_{In,N}}\right) \tag{3.17}$$

$$I_{M,N,Est} = \left|\left(V_{In,N} - \frac{I_{In,N}.e^{-j\varphi_N}}{\overline{Y}_1}\right)\overline{Y}_M\right| \tag{3.18}$$

$$I_{R,N,Est} = \left|I_{In,N}.e^{-j\varphi_N} - \left(V_{In,N} - \frac{I_{In,N}.e^{-j\varphi_N}}{\overline{Y}_1}\right)\overline{Y}_M\right| \tag{3.19}$$

$$R_3 = \frac{(2-s)}{3I_{R,N,Est}^2}\left(P_{In,N} - 3R_{1c}{I_{In,N}}^2 - 3R_M I_{M,N,Est}^2\right) \tag{3.20}$$

where

φ_N : is the angle between the negative sequence input voltage and input current

$I_{M,N,Est}$: is the estimated magnitude of the negative sequence magnetizing current

$I_{R,N,Est}$: is the estimated magnitude of the negative sequence rotor current

S : is the slip of the induction motor

Once the value of R_3 is known at an operating point, the value of the negative sequence output power can be calculated at that specific operating point based on (3.21).

$$P_{Out,N,Est} = 3\left(\frac{R_{3,c}\cdot(S-1)}{(2-S)}\right)I_{R,N,Est}^2 \tag{3.21}$$

where

$P_{Out,N,Est}$: is the estimated negative sequence output power

$I_{R,N,Est}$: is the estimated magnitude of the negative sequence rotor current of the motor

S : is the slip of the induction motor

3.5 Temperature Compensation

The temperature of an induction machine changes with the loading condition. In addition, the resistances are dependent on the operating temperature. Therefore the temperature of each operating point should be known to be able to estimate the machine's parameters.

However, if thermocouples are not already embedded in the machine, it is not possible to measure the temperature of a machine non-intrusively or to find the thermal model (thermal equivalent circuit with its parameters) of a machine while estimating the efficiency of a loaded machine by measuring only the voltage and current signals.

In this work, a method was proposed to estimate the machine's temperature with very limited available data, which comprised the rated temperature rise, and the voltage and current signals at each operating point.

As the temperature rise originated from the machine losses, it seemed wise to relate it to the estimated losses in the positive ($P_{L,P,Est}$) and negative ($P_{L,N,Est}$) sequence circuits. The relevant equations are shown below.

$$P_{L,Est} = P_{L,P,Est} + P_{L,N,Est} \tag{3.22}$$

$$\Delta T = K_{Th}.P_{L,Est} \tag{3.23}$$

$$T = \Delta T + T_a \tag{3.24}$$

where

$P_{L,Est}$: is the estimated total losses of the machine

ΔT : is the temperature rise

T_a : is the ambient temperature

K_{Th} : is the thermal coefficient (C°/W) of the motor

The thermal coefficient was added to the unknown parameters of the machine (shown in Fig. 3.2), and it was chosen along with the other parameters using the proposed evolutionary search algorithm. The value of this coefficient was estimated with the goal of having the least square errors from measured currents, powers, and the rated temperature. This means that, for each individual (a set of possible machine parameters), the rated temperature was estimated based on the rated voltage and the rated speed. The individual that led to a closer value had a lower E_1 error, as shown in (3.6). This improved the fitness value and provided more opportunity for the individual to be selected for the next generation.

In order to estimate the temperature at a specific operating point, the amount of the total losses should be known at that point. To find the amount of total losses, the values of the resistors are required and this needs knowledge of the temperature, which is the unknown.

An iterative approach was used to solve this problem. For each operating point, an initial value was assumed for temperature based on (3.25) and (3.26).

$$I_{In,Eff} = \sqrt{I^2{}_{In,P} + I^2{}_{In,N}} \tag{3.25}$$

$$T = \frac{I_{In,Eff}}{I_{In,Rated}} \times (T_{Rated} - T_a) + T_a \tag{3.26}$$

where

$I_{In,P}$: is the magnitude of the positive sequence input current

$I_{In,N}$: is the magnitude of the negative sequence input current

$I_{In,Eff}$: is the effective input current

$I_{In,Rated}$: is the full load current

T_a : is the ambient temperature

T_{Rated} : is the rated temperature that is assumed based on the insulation class of the machine and Table 3.2 [8]

After this starting step, losses were found based on the assumed initial temperature. The value of the temperature was recalculated knowing the amount of losses, and this iterative approach was continued until a stable value was achieved for the temperatures. The mathematical proof of the convergence of the proposed method is out of the scope of the research. However, considering the limitations made on the range of the input parameters and the knowledge used in formulation of the algorithm, it is expected to have the initial value of temperature close to the final point which facilitates convergence of the method. The flowchart of the method is shown in Fig. 3.5.

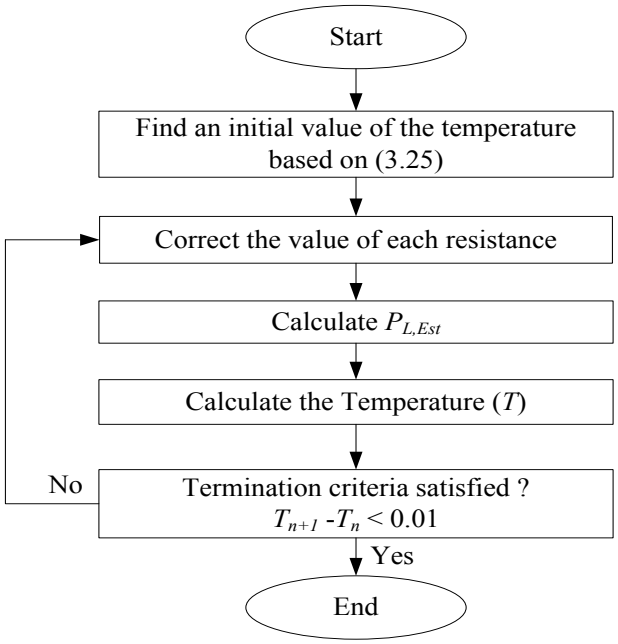

Fig. 3.5 Flowchart of the proposed temperature estimation method

The next step was to verify the effectiveness of the proposed evolutionary-based efficiency estimation algorithm through a simulated case where the efficiency and the

parameters of a 3 hp machine were estimated from the values of the active power and the input current at five different operating points.

3.6 Proof of Concept with Simulation

In this section, the capability of the proposed evolutionary-based efficiency estimation algorithm was verified based on the simulation results of a 3 hp induction machine with a nameplate, as shown in Table 2.1. The parameters of this machine are shown in Table 3.4.

Considering these parameters and 5% unbalanced supply, it was possible to calculate the currents and the input powers at five different operating points using the equivalent circuit of Fig. 3.1. The data of five operating points were then imported into the developed floating point evolutionary algorithm as a set of input data.

Table 3.4 Parameters of the tested induction machine

R_1	0.670 Ω	R_2	0.373 Ω
X_1	0.856 Ω	R_3	1.049 Ω
X_2	1.278 Ω	X_M	19.666 Ω
X_3	0.747 Ω	R_M	1.588 Ω
Thermal Coefficient 0.1365 (C°/W)			

The algorithm was then asked to estimate the actual parameters of the machine based on the imported power and current values at each point. The deviation from the original parameters was used to determine the capability of this algorithm to estimate the

parameters of the machine from the data of the power and current values. The algorithm was terminated after 20,000 generations, and the estimated parameters were tabulated in Table 3.5. The trend of the improvement of the fitness value (after each generation) is illustrated in Fig. 3.6.

Table 3.5 Comparison of the estimated and the actual parameters

Parameters	**Actual**	**Estimated**	**Error (%)**
X_2	1.278 Ω	1.275 Ω	-0.203
X_3	0.747 Ω	0.748 Ω	0.080
R_2	0.373 Ω	0.373 Ω	-0.027
R_3	1.049 Ω	1.049 Ω	-0.010
X_M	19.666 Ω	19.667 Ω	0.006
R_M	1.588 Ω	1.582 Ω	-0.365
K_{Th}	0.1365 C°/W	0.1366 C°/W	0.073

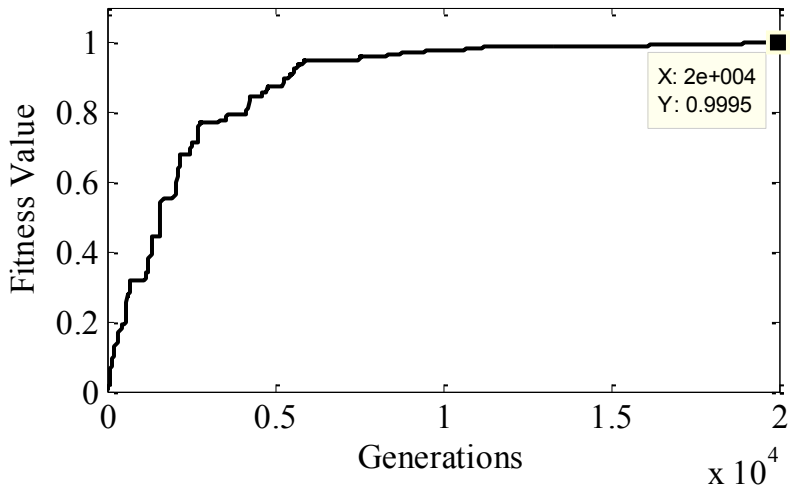

Fig. 3.6 Trend of the improvement of the fitness function's value.

Based on the achieved results, one can conclude that the developed algorithm is capable of accurately estimating the parameters and therefore the efficiency of a typical induction machine from only input current and active power data. The next step was to check the effectiveness of the proposed algorithm in the estimation of the efficiency of an induction motor from the actual measured data.

3.7 Experimental Results

In this section, the proposed algorithm was used to estimate the efficiency of the same 3 hp squirrel cage induction motor from the actual measured current and voltage signals under two different working scenarios as follows:

1) In the first scenario, the motor worked under different loading conditions for a considerable period of time. The temperature of the motor stabilized at each operating point, and consequently, each point had a different operating temperature.
2) In the second scenario, the motor worked most of the time under a main operating condition (75% of the rated load in the case of 3 hp machine). Short term load fluctuations, e.g., with one minute duration, were used as the extra required loading points in the efficiency estimation process. In this case, the temperature of all short term operating points was considered to be the same as the temperature of the main operating point.

An experimental setup with the schematic shown in Fig. 3.7 was used for this test. Fig. 3.8 shows the real experimental setup specifically assembled in the laboratory for in-situ efficiency estimation tests.

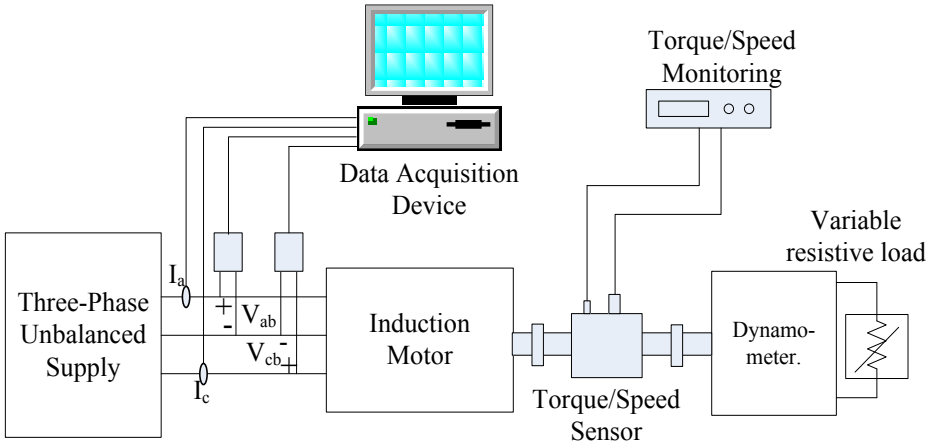

Fig. 3.7 Schematic of the test setup used for this experiment

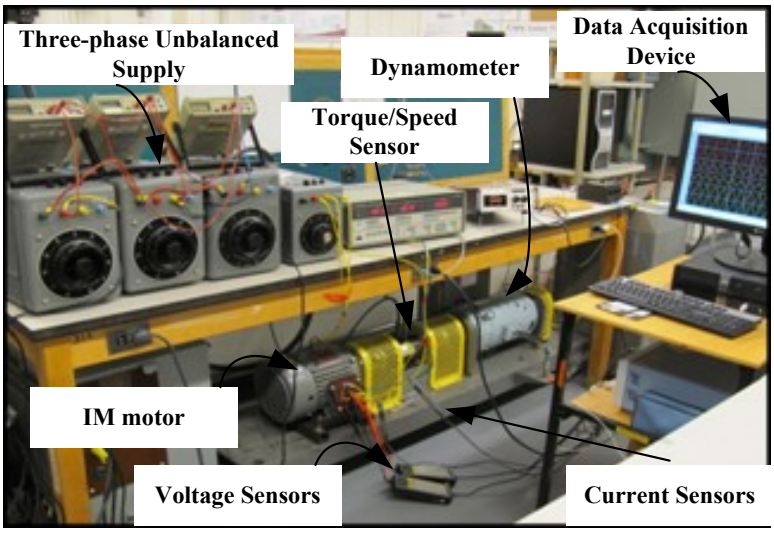

Fig. 3.8 The photo of the efficiency measurement test bench

As can be seen, the induction motor was coupled to a 7 hp dynamometer. Thus it was possible to impose different torque levels on the shaft of the induction motor. The three-phase unbalanced power supply was produced through the use of three single phase variacs as well as a transformer. Consequently three phase voltages with only magnitude unbalance were used for the test.

By supplying the induction machine with about 5% unbalanced voltages (V_{ab} = 205 V, V_{bc} = 219 V and V_{ca} = 199 V) and changing the load of the dynamometer, five different operating points were achieved. The line voltage and current waveforms at full load condition under the first scenario are shown in Fig. 3.9 and Fig. 3.10, respectively. As can be seen, 5% VUF created considerable unbalance in the line currents.

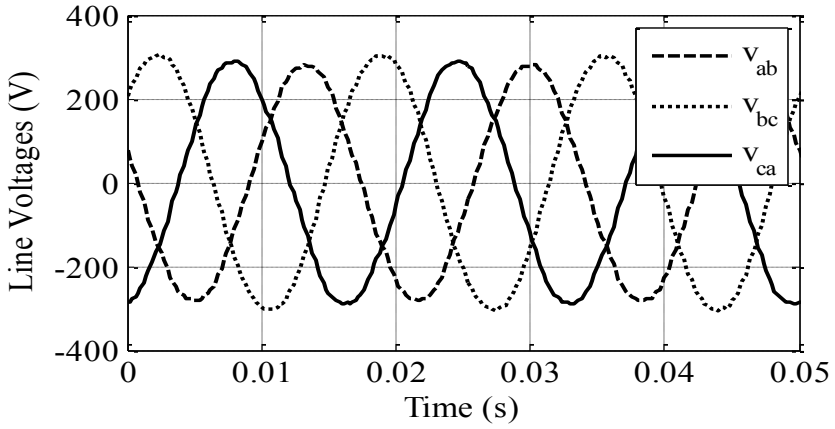

Fig. 3.9 Line voltage signals with 5% VUF at full load condition

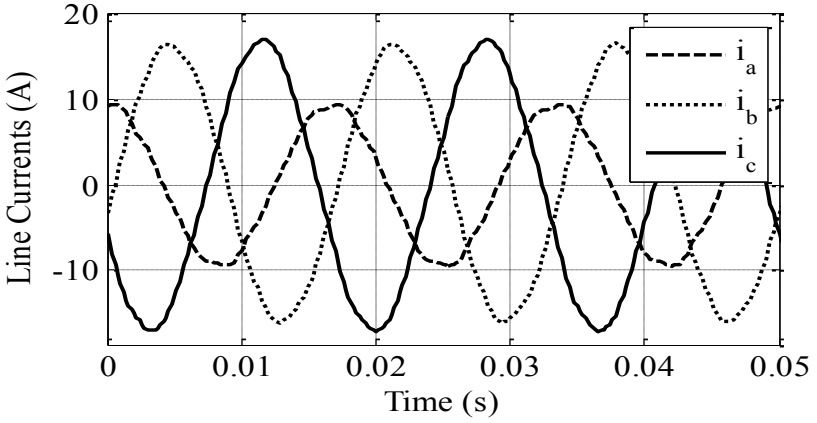

Fig. 3.10 Line current signals with 5% VUF at full load condition

The symmetrical components of the voltage, current, and input active power were extracted from the measured current and voltage signals under both working scenarios, and the results are tabulated in Table 3.6 and Table 3.7.

Table 3.6 Five different operating points with around 5% VUF under the first scenario

% of rated load	**25**	**50**	**75**	**85**	**100**
$V_{In,P}$ (V)	119.72	119.42	119.60	119.43	119.36
$V_{In,N}$ (V)	6.15	6.11	6.21	6.07	6.37
$I_{In,P}$ (A)	6.22	6.98	8.17	8.83	9.80
$I_{In,N}$ (A)	2.95	3.00	3.10	3.01	3.12
$P_{In,P}$ (W)	856.98	1438.43	2050.50	2350.35	2760.82
$P_{In,N}$ (W)	32.07	34.42	38.16	37.22	41.60
Speed (rpm)	1787.2	1774.2	1759.7	1752.6	1740.6

Table 3.7 Five different operating points with around 5% VUF under the second scenario

% of rated load	**25**	**50**	**75**	**85**	**100**
$V_{In,P}$ (V)	120.30	119.82	119.25	118.58	118.53
$V_{In,N}$ (V)	7.47	7.39	7.24	7.32	7.25
$I_{In,P}$ (A)	6.26	7.00	8.21	8.81	9.85
$I_{In,N}$ (A)	3.41	3.43	3.43	3.47	3.46
$P_{In,P}$ (W)	872.94	1468.32	2087.04	2359.50	2765.63
$P_{In,N}$ (W)	47.47	48.90	49.48	51.63	51.86
Speed (rpm)	1786.0	1773.1	1760.0	1751.9	1742.3

The extracted data under each scenario was imported into the developed evolutionary-based efficiency estimation algorithm as a set of input data in order to estimate the efficiency of the machine. The trend of the improvement of the fitness values is illustrated in Fig. 3.11 for both scenarios.

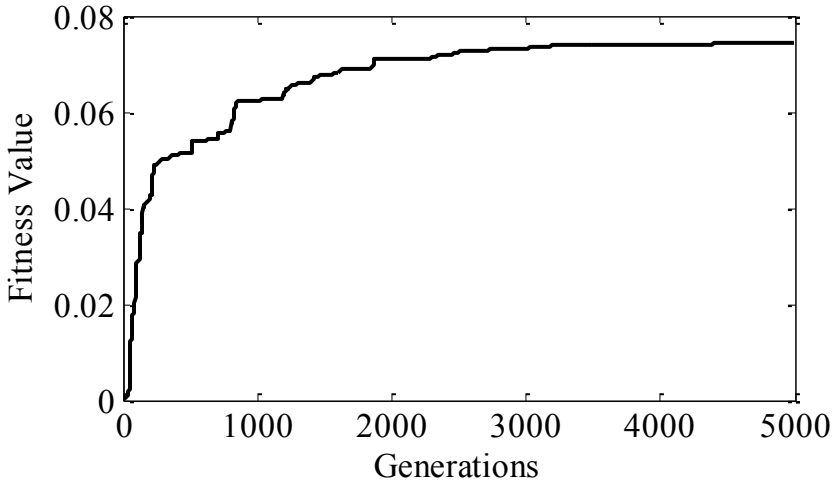

(a)

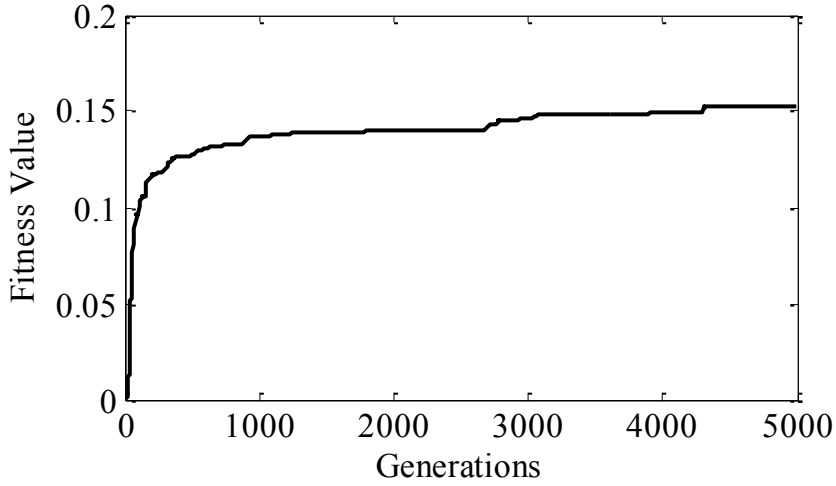

(b)

Fig. 3.11 Trend of the improvement of the fitness function's value under (a) the first scenario and (b) the second scenario

The value of the average error between estimated and measured positive sequence currents and powers at different operating points was around 1% for the first scenario and 0.74% for the second scenario, after the convergence of the algorithm. The efficiency of the machine was calculated after the estimation of the positive and negative sequence components. The results were compared with the direct measured efficiencies (using the torque/speed sensor), as shown in Fig. 3.12 and Table 3.8 for the first scenario.

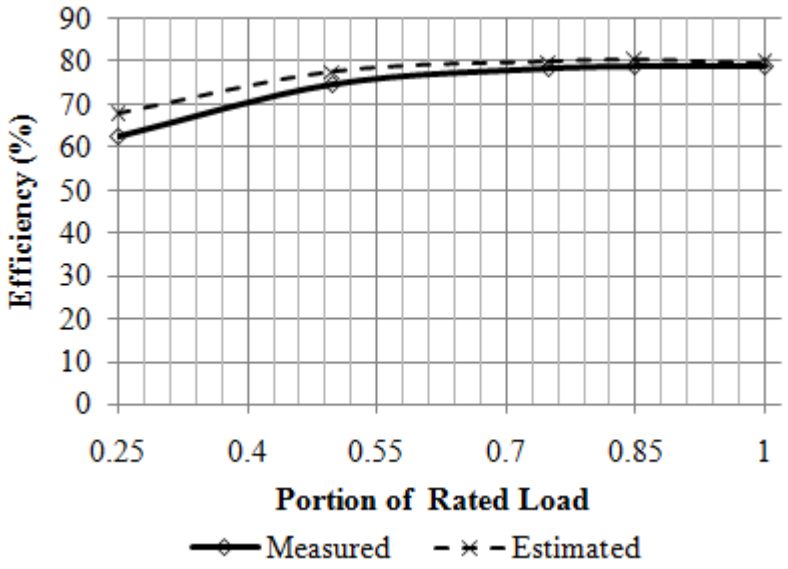

Fig. 3.12 Comparison of the estimated and measured efficiencies with 5% VUF under the first working scenario

Table 3.8 Comparison of measured and estimated efficiencies under the first scenario

% of rated load	25	50	75	85	100
Measured efficiencies (%)	62.30	74.55	78.13	78.93	78.63
Estimated efficiencies (%)	67.61	77.59	79.98	80.25	79.69
Error (%)	5.31	3.04	1.85	1.32	1.06

The estimated efficiencies under the second working scenario were compared with the direct measured values, as shown in Fig. 3.14 and Table 3.9.

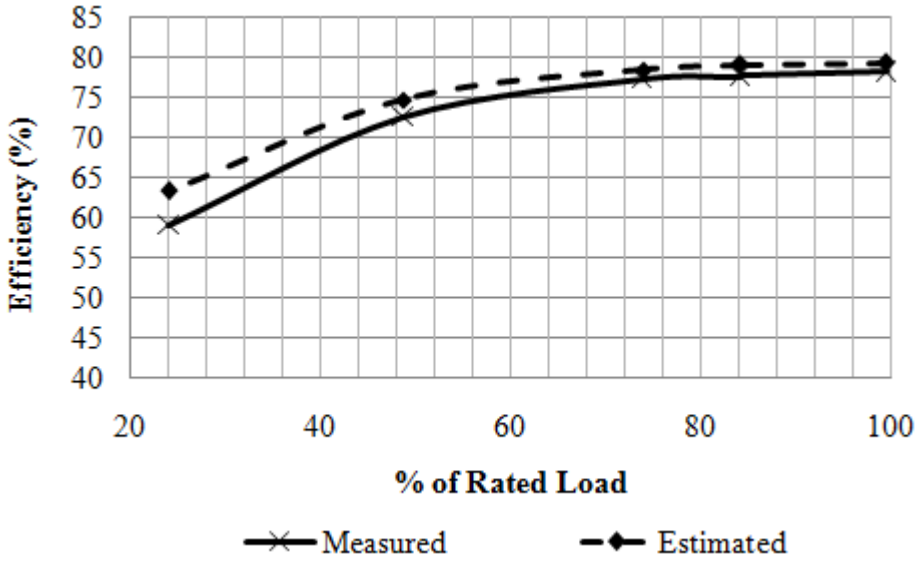

Fig. 3.13 Comparison of the estimated and measured efficiencies with 5% VUF under the second working scenario

Table 3.9 Comparison of measured and estimated efficiencies under the second scenario

% of rated load	25	50	75	85	100
Measured efficiencies (%)	59.17	72.57	77.43	77.64	78.23
Estimated efficiencies (%)	63.42	74.82	78.55	79.17	79.42
Error (%)	4.25	2.25	1.12	1.53	1.19

Based on the achieved results, it can be concluded that the proposed algorithm is capable of estimating the efficiency of an induction machine under unbalanced supplies within acceptable range of error.

3.8 Effects of the Input Data on Efficiency Estimation Accuracy

As can be seen from the previous sections, the data of multiple operating points was used in the efficiency estimation process. To be able to compare different cases and arrive at a set of conclusions, four different cases were defined as follows:

Case 1: Data of five operating points were used. These points were: no-load with shaft still coupled to the load, 50%, 75%, 85%, and 100% of the rated load.

Case 2: Data of five operating points were used. These points were: 25%, 50%, 75%, 85%, and 100% of the rated load.

Case 3: Data of five operating points were used. These points were: 50%, 65%, 75%, 85%, and 100% of the rated load.

Case 4: Data of three operating points were used. These points were: no-load with shaft still coupled to the load, 75% and 100% of the rated load.

The estimated efficiencies of all the cases were compared with the measured values at three important operating points, i.e., 50%, 75%, and 100% of rated load, as shown in Table 3.10 as well as Fig. 3.14.

The algorithm was terminated after 5000 generations in all cases to be able to compare the accuracy of the results. The trend of the accuracy of the cases is shown below:

Case 1 > Case 4 > Case 2 > Case 3

Table 3.10 Comparison of estimated efficiencies at three operating points for the four cases

% of rated load	50	75	100
Measured efficiencies (%)	74.55	78.13	78.63
Estimated efficiencies at Case 1 (%)	76.91	79.55	79.45
Error at Case 1 (%)	2.36	1.42	0.82
Estimated efficiencies at Case 2 (%)	77.59	79.98	79.69
Error at Case 2 (%)	3.04	1.85	1.06
Estimated efficiencies at Case 3 (%)	81.10	82.38	81.36
Error at Case 3 (%)	6.55	4.25	2.73
Estimated efficiencies at Case 4 (%)	77.07	79.66	79.52
Error at Case 4 (%)	2.52	1.53	0.89

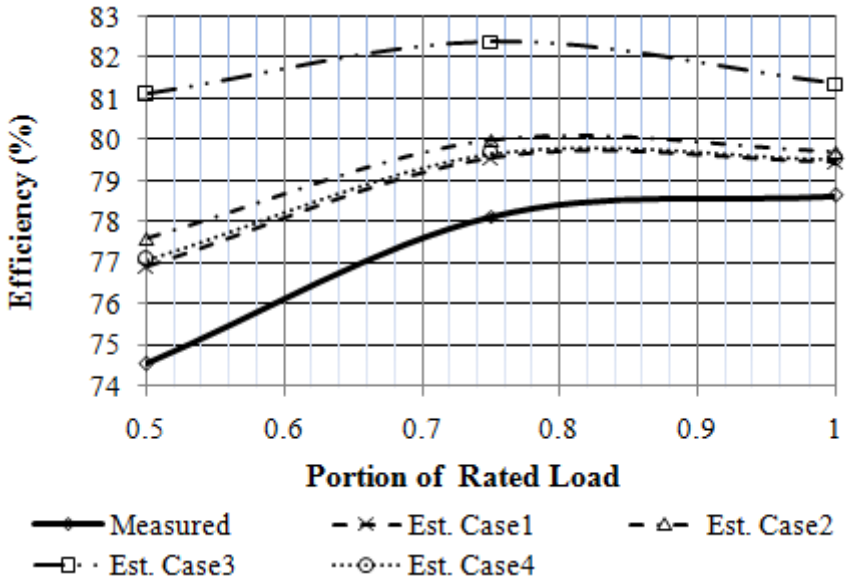

Fig. 3.14 Comparison of the estimated and measured efficiencies with 5% VUF for the four different cases

Based on these observations, the following conclusions were made:

1) The algorithm is capable of estimating the efficiency without the requirement of decoupling the shaft and performing the intrusive no-load test (Case 1 and Case 2).
2) At least one light load operating point, e.g., 25% of the rated load in Case 2, is required in order to have an acceptable efficiency estimation (based on Case 3).
3) The closer the light load point is to the no-load condition, the more accurate the efficiency estimation result (comparing Case 1 and Case 2).
4) A higher number of data points will not bring a significant advantage if at least one light load and one heavy load point are included (comparing Case 1 and Case 4).

3.9 Effects of the Assumptions on the Estimated Efficiencies

In this section, the sensitivity of the algorithm to each of the assumptions in section 3.3 are investigated.

To see the effect of the assumed rated temperature rise on the performance of the algorithm and the final estimated efficiencies, the rated temperature rise was first assumed to be 70° (based on the recommendation of IEEE standard 112 for insulation class B), and then equal to 59° (the obtained rated temperature rise from the rated temperature rise test). The estimated efficiencies are shown in Fig. 3.15.

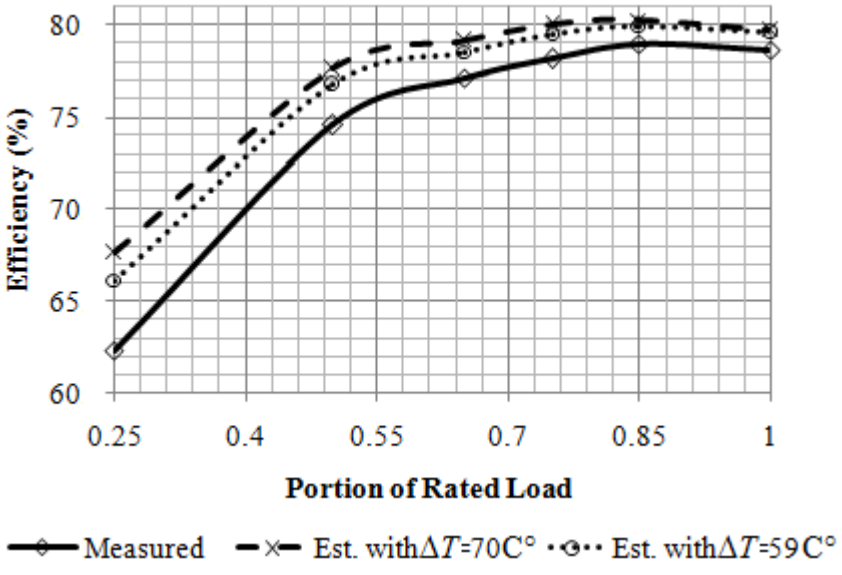

Fig. 3.15 Comparison of the estimated efficiencies with two different values of assumed rated temperature rise and measured values

As can be seen, using the right temperature rise improved the efficiency estimation slightly. However, there was no way to know the rated temperature rise of a loaded machine in situ. Thus, this was the best that could be achieved without measurement, while still maintaining compliance with the IEEE standard 112.

To see the effect of the X_1/X_2 ratio on the performance of the algorithm, three different values (0.43, 0.67 and 1) were assumed for this ratio and the results are compared in Fig. 3.16. As can be seen, the algorithm was not sensitive to this ratio.

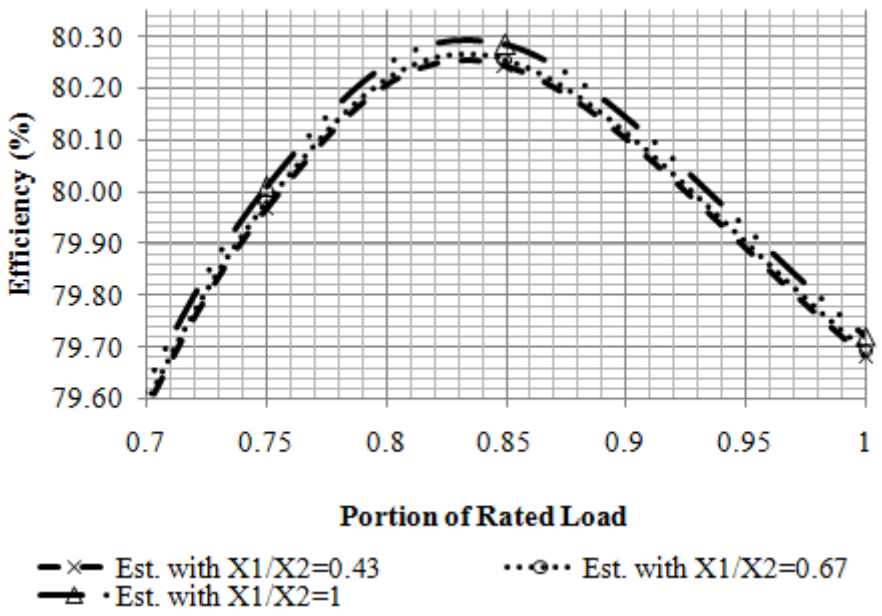

Fig. 3.16 Comparison of the estimated efficiencies with three different values of the X_1/X_2 ratio

The effect of the stray load loss was investigated by considering ±25% change to the suggested value of the IEEE standard 112, which was 1.8% of the rated power for the rated loading conditions. Fig. 3.17 suggests that the efficiencies were not really affected even with 25% change in the assumed value. In addition, as expected, the effect of changes on stray load loss was more evident in heavier loads.

Fig. 3.18 shows the effect of ±25% change in the value of the friction and windage losses, which were assumed equal to 1.2% of the input power, based on [54]. As can be seen, the change in efficiency was not significant.

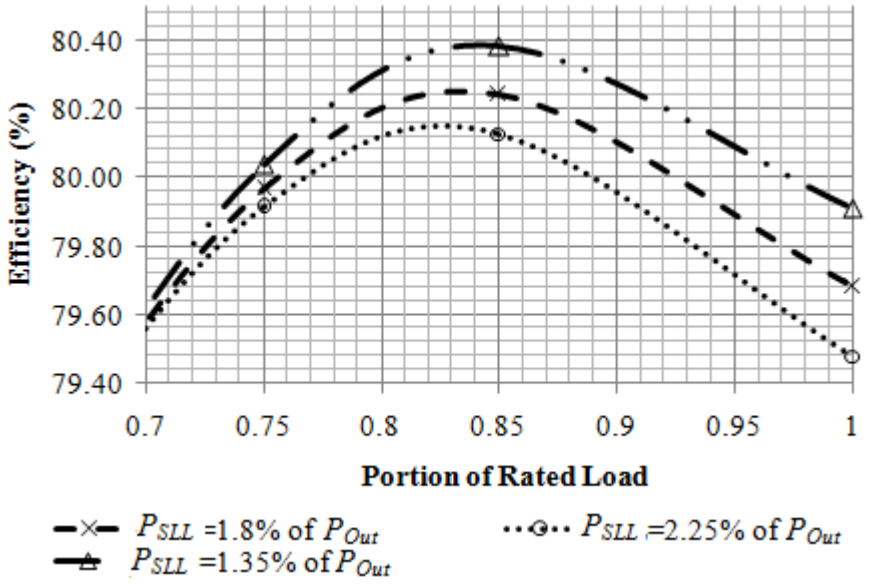

Fig. 3.17 Comparison of the estimated efficiencies for ±25% change in the suggested value of the IEEE standard 112 for stray load loss (1.8% of rated power)

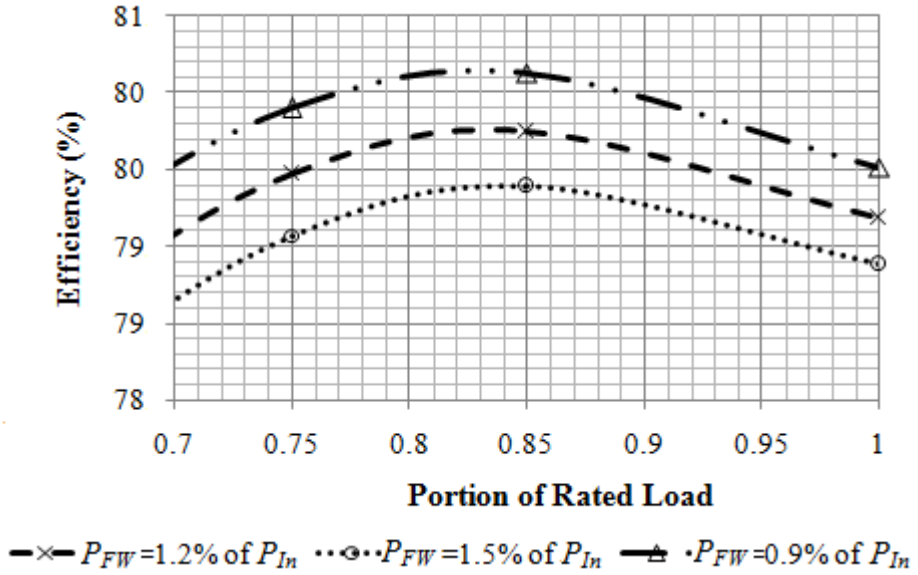

Fig. 3.18 Comparison of the estimated efficiencies for ±25% change in the assumed value of the friction and windage losses

3.10 Testing Generality of the Proposed Method

The proposed efficiency estimation algorithm was tested with another 10 hp induction motor with nameplate data as shown in Table 2.3. It should be mentioned that, going forward, all tests were done based on the second scenario of data acquisition, which was discussed in the previous section.

The recorded voltage and current signals of the tested 10 hp induction machine at full load condition with about 6% voltage unbalance factor (VUF) are shown as an example in Fig. 3.19 and Fig. 3.20. The proposed algorithm in Chapter 2 was used to extract all the required data used in the efficiency estimation process, as shown in

Table 3.11. The extracted data of the five operating points was imported into the developed floating point evolutionary-based efficiency estimation algorithm as a set of input data.

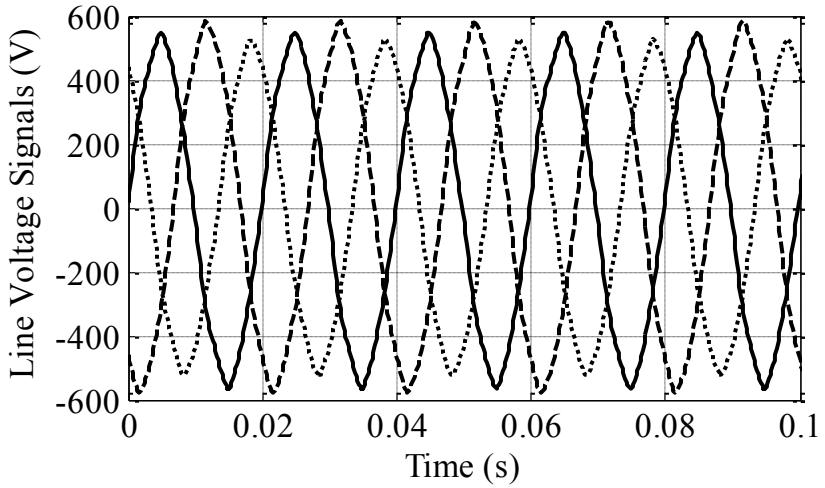

Fig. 3.19 Line voltage signals with 6% VUF at full load condition

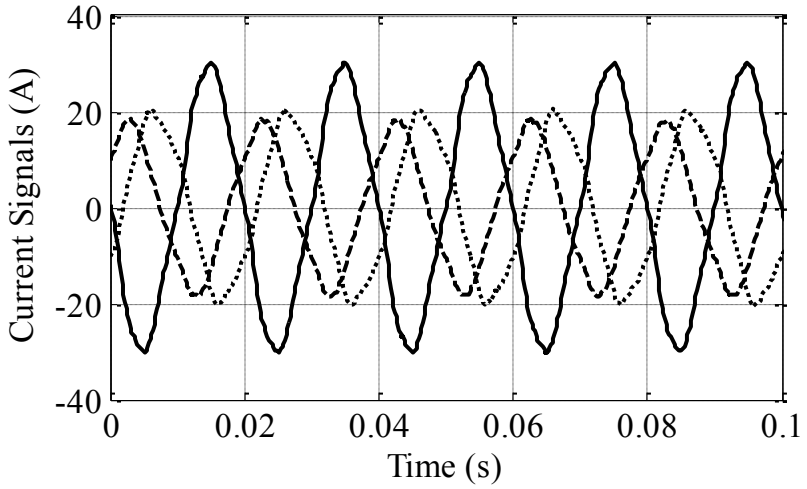

Fig. 3.20 Line current signals with 6% VUF at full load condition

Table 3.11 Five different operating points with around 6% VUF for a 10 hp machine

% of rated load	**25**	**50**	**75**	**85**	**100**
$V_{In,P}$ (V)	379.78	382.04	380.35	378.80	378.12
$V_{In,N}$ (V)	22.68	23.30	22.54	22.57	22.31
$I_{In,P}$ (A)	3.52	4.86	6.46	7.31	8.50
$I_{In,N}$ (A)	2.26	2.91	3.12	3.20	3.25
$P_{In,P}$ (W)	2463.42	4392.26	6347.52	7311.23	8630.89
$P_{In,N}$ (W)	54.06	87.60	95.71	101.39	103.32
Speed (rpm)	1493.9	1486.5	1482.1	1474.9	1467.0

The trend of the improvement of the fitness value (after each generation) is illustrated in Fig. 3.21. The value of the average error between the estimated and measured positive sequence currents and the powers at different operating points was around 0.76% after the convergence of the algorithm.

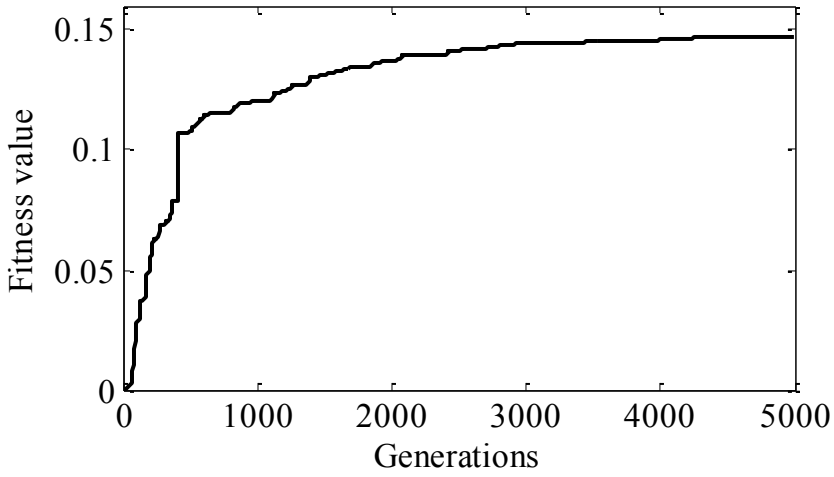

Fig. 3.21 Trend of the improvement of the fitness value for the 10 hp machine

The efficiency of the machine was calculated after estimation of the positive and negative sequence components. The results were compared with the direct measured efficiency values (with torque/speed sensor) as shown in Fig. 3.22 and Table 3.12.

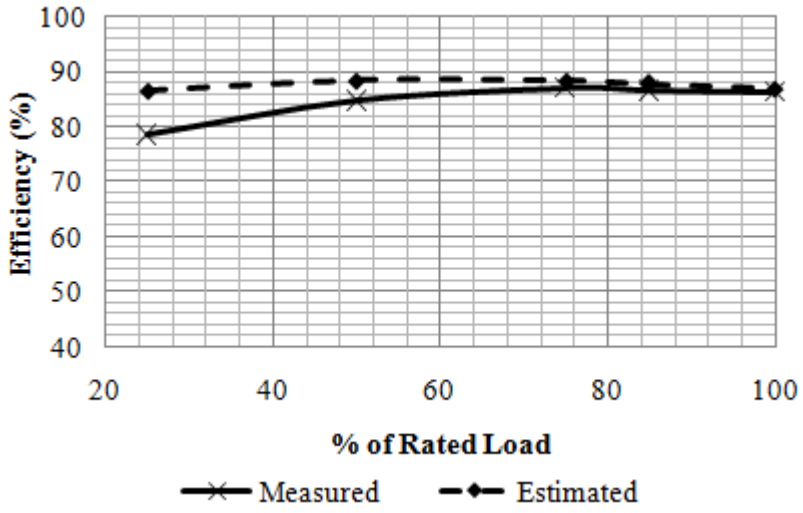

Fig. 3.22 Comparison of the estimated and measured efficiencies for the tested 10 hp machine with 6% voltage unbalance factor

Table 3.12 Estimated efficiencies vs. measured efficiencies for the 10 hp machine

% of rated load	25	50	75	85	100
Measured efficiencies (%)	78.55	84.70	86.94	86.51	86.22
Estimated efficiencies (%)	86.45	88.42	88.31	87.74	86.84
Error (%)	7.90	3.73	1.37	1.23	0.62

3.11 Measurement Error Analysis

In the previous sections, comparison of the estimated efficiencies with the measured values was used to validate the effectiveness of the proposed in-situ efficiency estimation algorithm. However, the accuracy of the measured values must be guaranteed in order to be able to use them as a reference for comparison.

In a typical experiment, three types of errors may exist. The first is methodological error, the second is human error, and the third is caused by instrument error. Instrument error is the most common type of error for the efficiency estimation problem, and it can be calculated with three common error evaluation techniques, which are presented below [56]-[57]:

1) Maximum error estimation (MEE)
2) Worst case error estimation (WCEE)
3) Realistic error estimation (REE)

The MEE technique gives the maximum possible error and is defined with the following equation:

$$\varepsilon_\eta = \max\left|\frac{1 \pm \varepsilon_{Pout}}{1 \pm \varepsilon_{Pin}}\right| - 1 = \max\left|\frac{(1 \pm \varepsilon_T).(1 \pm \varepsilon_S)}{(1 \pm \varepsilon_V).(1 \pm \varepsilon_I)}\right| - 1 \tag{3.27}$$

where

ε_η : is the relative error of the measured efficiency

ε_{Pout} : is the relative error of the measured output power

ε_{Pin} : is the relative error of the measured input power

ε_T : is the relative error of the measured torque

ε_S : is the relative error of the measured speed

ε_V : is the relative error of the measured voltage

ε_I : is the relative error of the measured current

The relative error for a parameter is defined as the ratio of the absolute error to the true value of the parameter. The relative errors of the instruments, used in the efficiency measurement of a 10 hp machine, are as follows:

- Torque sensor: ±0.2%
- Speed sensor: ±0.05%
- Voltage sensors: ±0.2%

- Current sensors: ±0.2%

Using the provided data on the accuracy of the used instruments and (3.27), the maximum possible error in the efficiency measurement can be calculated as follows:

$$\varepsilon_\eta = \max\left|\frac{(1\pm 0.2\%).(1\pm 0.05\%)}{(1\pm 0.2\%).(1\pm 0.2\%)}\right| - 1 = \pm 0.65\% \tag{3.28}$$

This is the maximum value of the error that can exist in the measured efficiency values. However, it is unrealistic to expect all the errors to happen in a way that leads to the calculated maximum error.

The WCEE is another way of handling the error calculation problem. In this method, the effect of each error source on the measured component (in this case, efficiency) is handled separately and its influence is considered with an influence coefficient (*IC*) as shown in (3.29) [56].

$$\varepsilon_\eta = \sum IC_I.\varepsilon_I + IC_V.\varepsilon_V + IC_T.\varepsilon_T + IC_S.\varepsilon_S \tag{3.29}$$

Where IC_I is the influence coefficient of the current, IC_V is the influence coefficient of the voltage, IC_T is the influence coefficient of the torque, and IC_S is the influence coefficient of the speed. The value of the influence coefficient for each parameter is determined based on a perturbation method, where the relative deviation of the output parameter (efficiency) is found for a known perturbation in an input parameter, as shown in (3.30) for the current [56].

$$IC_I = \frac{\varepsilon_\eta}{\varepsilon_I} \tag{3.30}$$

As shown in [56] and [57], the influence coefficient of all the parameters in (3.29) is almost equal to 1 for the direct efficiency measurement technique. This means that the error of each instrument has the same influence on the final error of the measured efficiency. Therefore, the worst case error for the efficiency measurement with the direct method will be as follows:

$$\varepsilon_\eta = \sum 1.(\pm 0.2\%) + 1.(\pm 0.2\%) + 1.(\pm 0.2\%) + 1.(\pm 0.05\%) = \pm 0.65\% \tag{3.31}$$

As can be seen, the WCEE method gives almost the same result as the MEE method. This is due to the similar nature of both methods, which assumes a simultaneous existence of maximum possible errors in all measured parameters. To have a more realistic value of the error, the REE method should be used. With the assumption of the uniformly distributed error for each parameter, the relative distribution of the output can be found based on (3.32) [56].

$$\varepsilon_\eta = \sqrt{\sum (IC_I.\varepsilon_I)^2 + (IC_V.\varepsilon_V)^2 + (IC_T.\varepsilon_T)^2 + (IC_S.\varepsilon_S)^2} \tag{3.32}$$

Using the same influence coefficients, the error of the measurement based on the REE method was found, as shown in (3.33).

$$\varepsilon_\eta = \sqrt{\sum (1.\pm 0.2\%)^2 + (1.\pm 0.2\%)^2 + + (1.\pm 0.2\%)^2 + (1.\pm 0.05\%)^2} = \pm 0.35\% \tag{3.33}$$

In reality it is expected to have a distribution of error more concentrated around the original value rather than uniformly distributed one. Thus Guassian distribution may even better represent the real condition. It is expected to have even better accuracies using a Gaussian distribution.

Based on the achieved results, one can be assured that the measurements were done within an acceptable range of error.

3.12 Repeatability of the Results

In order to guarantee the consistency of the results, the test with a 3 hp machine was repeated three times, and the results are compared in Fig. 3.23 and Fig. 3.24.

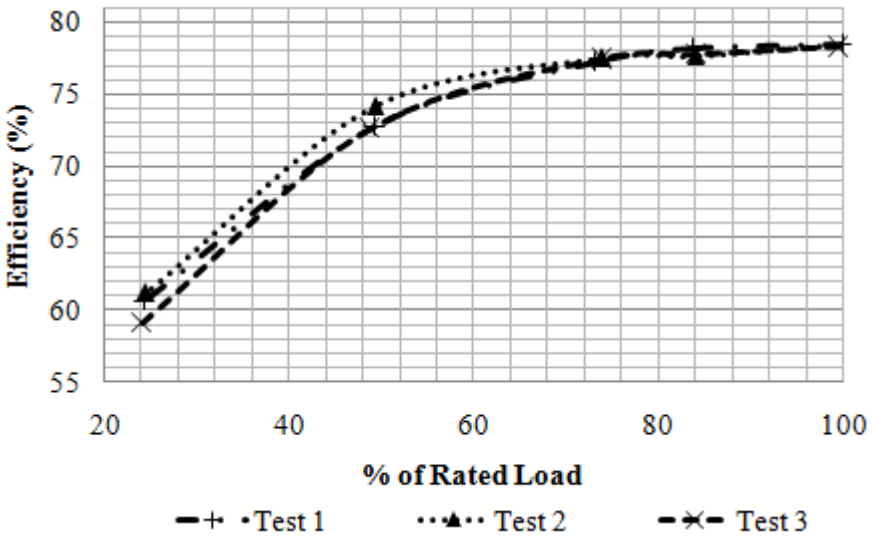

Fig. 3.23 Repeatability of the measured efficiencies of a 3 hp machine

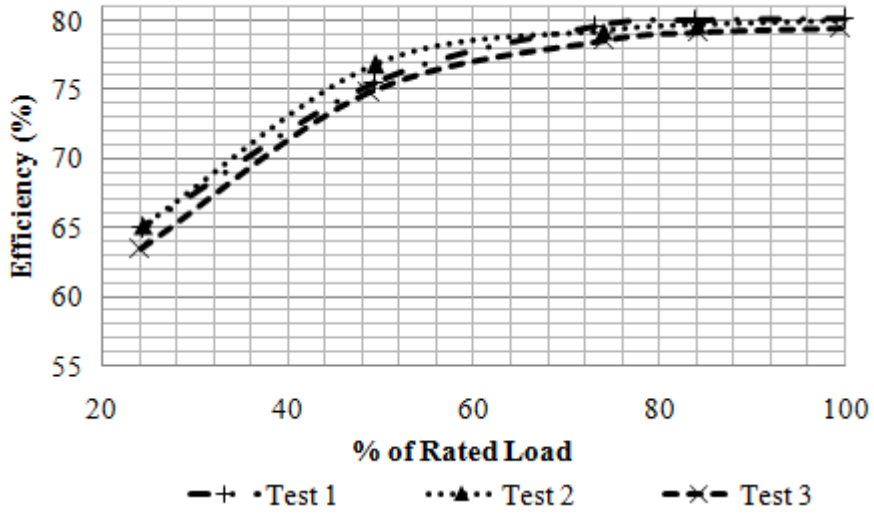

Fig. 3.24 Repeatability of the estimated efficiencies of a 3 hp machine

As can be seen, the consistency of the achieved results proves the reliability of the proposed method.

3.13 Conclusions

In this chapter, a new evolutionary-based in-situ efficiency estimation algorithm was developed for unbalanced supply conditions. In addition, a non-linear temperature estimation algorithm was presented to estimate the temperature of a machine in the event of a partial loading condition.

The proposed method was validated through simulation results. It was shown that the parameters of a machine can be accurately estimated based on the input power and the current of the multiple operating points.

Experimental results with two different induction machines under two different working scenarios were used to prove the effectiveness and generality of the proposed method.

The effect of the input data on the accuracy of the final estimated efficiencies was investigated in detail. It was shown that the algorithm is capable of estimating efficiency without decoupling the shaft or performing an intrusive no-load test. However, at least one light load operating point is required in order to attain an acceptable efficiency estimation. It was also concluded that a higher number of data points will not bring a significant advantage if at least one light and one heavy load point are included.

The sensitivity of the results to the assumptions was interrogated in detail. It was shown that the final estimated efficiencies are not really influenced by the assumptions.

A measurement error analysis was done to guarantee the accuracy of the measured efficiencies so that they could be used as reference values. Based on the provided analysis, it was shown that the measurements were done within an acceptable range of error.

Finally repeatability tests were performed to assure consistency of the results.

4. EFFICIENCY ESTIMATION UNDER OVER- OR UNDERVOLTAGE UNBALANCED SUPPLY CONDITIONS

4.1 Introduction

The real working efficiency of installed induction motors in industry is generally different from their rated efficiencies. This is due to the fact that these motors operate at 60% or less of their rated load conditions mainly because of oversized installations [21]. In addition, the efficiency of a motor changes due to aging, over- or undervoltage conditions, unbalanced supplies, and operating conditions.

As discussed in previous chapters, in-situ efficiency monitoring of installed motors provides the opportunity to detect motors with poor efficiencies and to evaluate the perceived benefit of replacing them with newer more efficient ones. In order to minimize the cost of this evaluation, the efficiency of existing machines should be measured with the lowest intrusion level and highest accuracy under real operating conditions. The real operating conditions are generally different from standard conditions in terms of supply voltage magnitude, supply voltage unbalance, and loading conditions. Since the efficiency of new machines is only available for the standard test condition, the efficiency comparison, the evaluation of energy saving, and the calculation of the payback period will only be meaningful if the efficiency of the existing machine in the plant can also be estimated under standard test conditions. However, plant operating conditions rarely meet standard test conditions. Thus it is necessary to devise an algorithm that is capable of

estimating the motor's efficiency under standard test conditions using the data acquired under plant conditions. This is a very critical issue which is often neglected in literature.

In this chapter, an extension is proposed for the developed optimization-based algorithm (of the previous chapter) in order to make it compatible for in-situ efficiency estimation of induction machines operating with over- or undervoltage and unbalanced supplies. The capability of the proposed algorithm is demonstrated in the estimation of the standard condition efficiency from the measured data of plant conditions.

In addition, a comprehensive study was done on the functionality and accuracy of the non-intrusive air-gap torque (NAGT) method, which is claimed in literature to be one of the most promising methods. It was shown that the efficiency calculated by this method under field conditions is only valid for the measured operating conditions, and no conclusion can be made regarding its efficiency under standard conditions. Thus the estimated efficiencies of this method under field conditions cannot be used in the decision-making process regarding the replacement of existing machines or calculations regarding their payback period. This research is supported by the experimental results of two different induction machines.

The chapter is organized as follows: the proposed extension to the evolutionary-based efficiency estimation algorithm is presented in section 4.2. The fundamentals of the air-gap torque method are discussed briefly in section 4.3. In the same section, the NAGT method is discussed in detail, and a comprehensive study is presented on its functionality and accuracy. In section 4.4, the proposed evolutionary-based efficiency estimation

algorithm is used to estimate the efficiency of a 3 hp squirrel cage induction machine under unbalanced rated, unbalanced overvoltage and unbalanced undervoltage conditions. Unbalanced rated voltage and undervoltage tests have been repeated with a 7.5 hp energy-efficient induction machine to verify the generality of the proposed method. The experimental results of the efficiency estimation with the NAGT method and its modified version (MNAGT) under the same conditions are presented in section 4.5, and they are compared with the results of the proposed evolutionary-based method and the direct measured efficiencies from an installed torque/speed sensor. The effect of assuming an empirical value for no-load losses in the NAGT method is also investigated in this section. A summary of the conclusions, which are based on the obtained results, is presented in section 4.6.

4.2 Extension of the Proposed Method for Unbalanced and Over- or Undervoltage Conditions

In this section, the fundamentals of the proposed evolutionary-based efficiency estimation algorithm are discussed in detail. This algorithm is designed for efficiency estimation under real industrial conditions where machines work with over- or undervoltage and unbalanced supplies. The operation of a machine in an over- or undervoltage condition alters the saturation level of the motor and thus changes the magnitude of the no-load magnetizing current, as shown in Fig. 4.1 for a 3 hp induction motor with nameplate data (shown previously in Table 2.1).

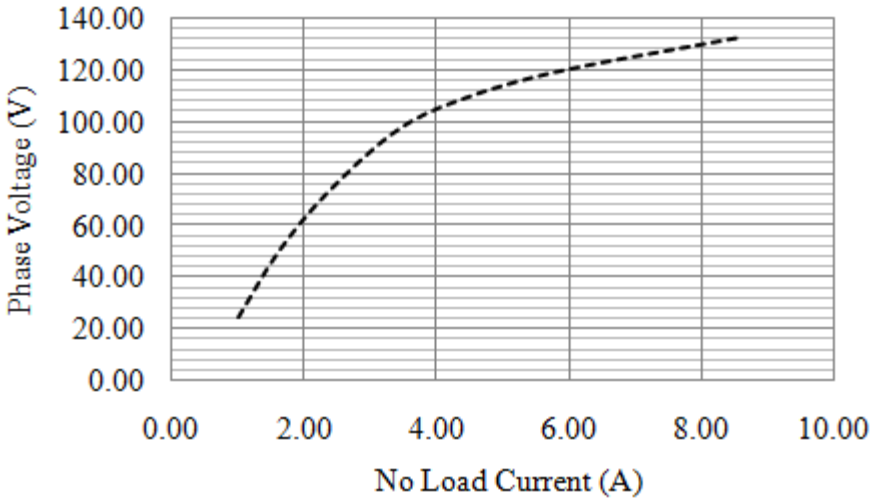

Fig. 4.1 No-load phase voltage vs. no-load current curve of a 3 hp machine

The change in magnetizing current was due to a change in the core loss and the mutual reactance, as shown in Fig. 4.2, for the tested 3 hp machine. In this figure, V_M is the voltage across the magnetizing branch.

As explained before, in the presence of an unbalanced supply condition, unbalanced currents are produced in the machine. The unbalanced currents generate positive sequence and negative sequence fluxes that lead to the positive and negative sequence torque components, which act against each other.

The performance of an induction machine working under different magnitudes of voltage and with some level of voltage unbalance can be presented by the positive and negative sequence equivalent circuits, shown in Fig. 4.3, where the mutual reactance was considered to be a variable component. More specifically, this component was considered

to be a function of "V_M", which is the voltage across the magnetizing branch. This is to model the change in core saturation level due to over- or undervoltage conditions.

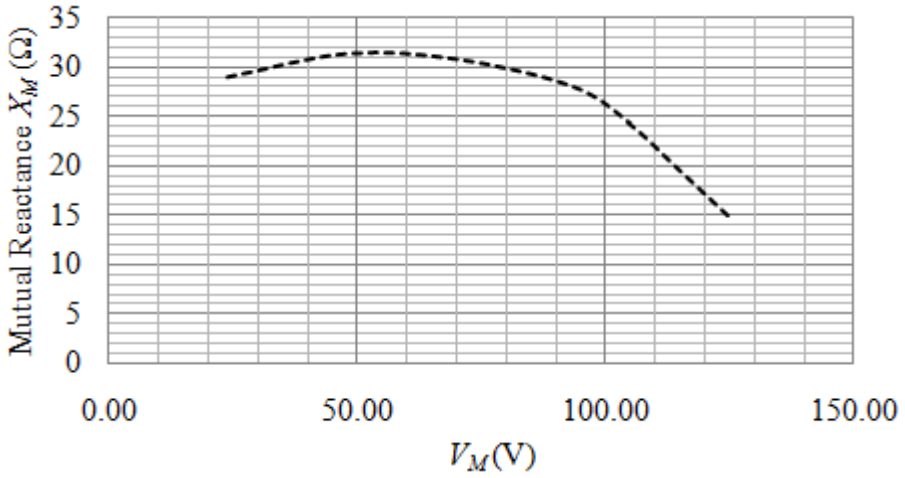

(a)

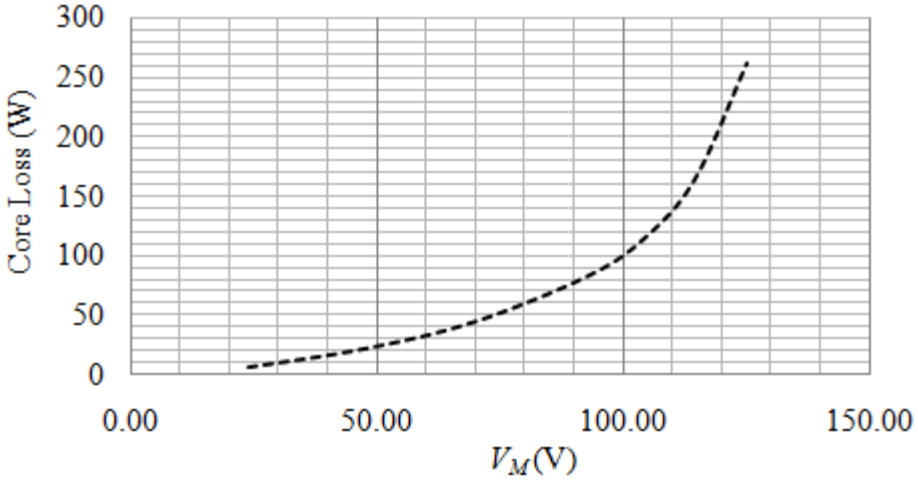

(b)

Fig. 4.2 (a) Mutual reactance and (b) core losses vs. V_M for the 3 hp machine

As discussed previously, if all the parameters of the positive and negative sequence equivalent circuits are known, the efficiency of the machine can be estimated simply by

solving the circuit and calculating the converted power at the known slip. To consider the effects of the voltage variation on the efficiency estimation process, the change in the mutual reactance (X_M) with voltage must be known. Based on the IEEE standard 112 [8], the accuracy of this value is critical for the accurate estimation of the efficiency.

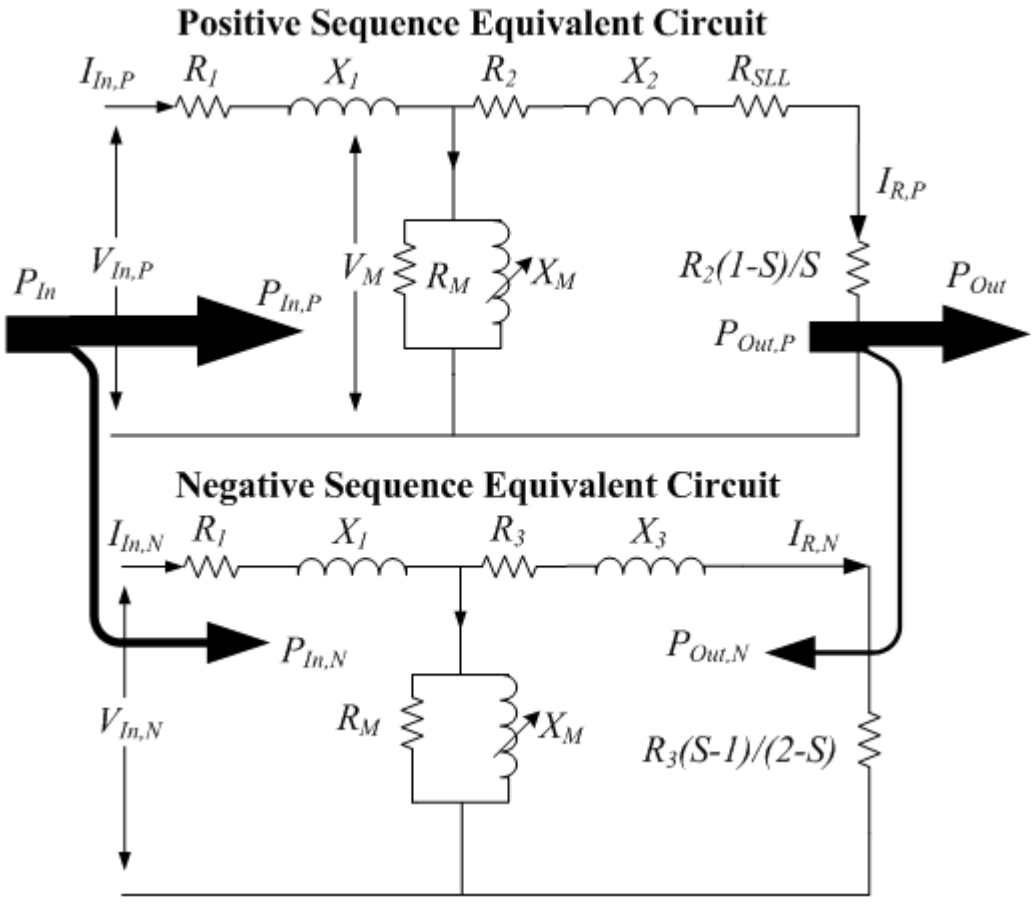

Fig. 4.3 Positive and negative sequence equivalent circuits of an induction machine with variable mutual reactance

where

R_1 : is the stator resistance

X_1 : is the stator leakage reactance

R_2 : is the rotor positive sequence resistance

X_2 : is the rotor positive sequence leakage reactance

R_3 : is the rotor negative sequence resistance

X_3 : is the rotor negative sequence leakage reactance

X_M : is the mutual reactance of the machine

R_M : is the representative of the core loss

R_{SLL} : is the representative of the stray load loss defined, based on the IEEE standard 112 [8]

S : is the slip of the induction motor

Normally, at most, ±10% voltage variation is expected in an industrial facility. As shown in Fig. 4.4 for the case of a 3 hp motor, the mutual reactance changes almost linearly with voltage in that limited range. Considering the trend of change of the mutual reactance with voltage, it seems reasonable to assume a linear relationship for this limited range of voltage variation. Thus the mutual reactance is represented as a linear function of the voltage, as shown in (4.1).

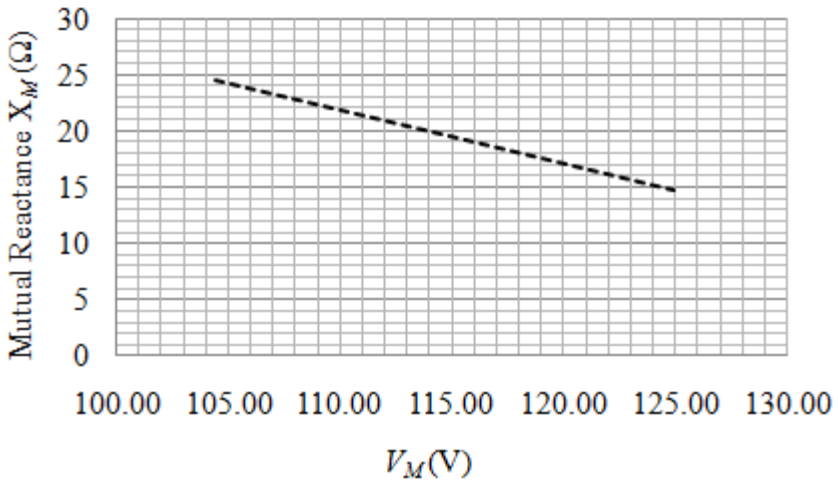

Fig. 4.4 Mutual reactance vs. V_M for the 3 hp machine

$$X_M = a.V_M + b \tag{4.1}$$

The proposed evolutionary-based search algorithm can be used to estimate these unknown parameters (a and b) in order to define this relationship, using the measured current and voltage signals at multiple operating points without the requirement for a no-load test at different voltage levels.

The core loss can be assumed based on a simple representation of sum of hysteresis (P_H) and eddy current (P_E) loss components, shown in (4.2).

$$P_C = P_H + P_E = K_H.B^n f + K_E.B^2 f^2 \tag{4.2}$$

Where

f: is the frequency

B : is the flux density

K_H : is the constant coefficient of the hysteresis losses

K_E : is the constant coefficient of the eddy current losses

N : is the constant changing in the range 1.6 to 2.0

For fixed frequency operation and by accepting the error caused by assuming n = 2, it is possible to simplify the above equation:

$$P_{\mathrm{C}} \approx K_1.B^2 \tag{4.3}$$

where

K_1 : is a constant value

Since flux density is directly proportional to the voltage of the magnetization branch (V_M), the core loss changes with the square of this voltage, and therefore the value of R_M is independent of the voltage variation, as shown in (4.4).

$$P_{\mathrm{C}} \approx K_2.{V_{\mathrm{M}}}^2 = \frac{{V_{\mathrm{M}}}^2}{R_{\mathrm{M}}} \Rightarrow R_{\mathrm{M}} = \frac{1}{K_2} = const. \tag{4.4}$$

where

K_2 : is a constant value

Based on (4.4), core loss can be estimated with a parallel resistor "R_M", as shown in the equivalent circuit of the machine. The value of the loss will be changed with the square of the voltage.

In real life "R_M", also varies to some extent with the voltage of the magnetization branch. However, for the limited variation of the voltage around the rated value (±10% voltage variation), where the variation of the "R_M" flattens out, it is possible to assume a fixed value.

Based on the performed experiments, it was noted that using a more complex model would not necessarily improve the core loss estimation since the losses should be estimated only based on the measured voltage and current signals under loaded conditions.

The proposed evolutionary-based search algorithm of Chapter 3 can be used to find the parameters of the equivalent circuits of the machine and the unknown coefficients "a, b" that define the relation between "X_M" and the magnetizing voltage "V_M". The estimation of parameters should be done with help of the limited electrical data, non-intrusively. As mentioned previously, for the purpose of this work, non-intrusiveness refers to electrical measurements at the terminals only with no mechanical measurements, not even speed. Therefore no-load and locked rotor tests were not permitted. As discussed in Chapter 3, data of multiple operating points should be used to find a unique set of solution. In this case, the data of two light load operating points with different voltage levels, and some

other partially and fully loaded operating points is required, and it should be extracted from the field measurements in order to estimate the unknown parameters.

In order to make the proposed algorithm of Chapter 3 compatible with over- or undervoltage unbalanced conditions, each individual is modified as shown in below:

X_2	R_2	R_M	K_{Th}	a	b

Fig. 4.5 One individual of the population for the modified algorithm

Knowing the parameters of the machine and the unknown coefficients of (4.1), the efficiency of the machine can be calculated for the measured field condition or any other condition of interest. This means the efficiency of the machine under standard test conditions can be estimated even when the in-situ measurements have been done under field conditions that are considerably different from standard conditions. Thus the estimated efficiency of this method can be compared with other new machines, and it can also be used for energy-saving calculations and estimations of the payback period. This is the main advantage of the proposed method. The flowchart of the proposed method is shown in Fig. 4.6.

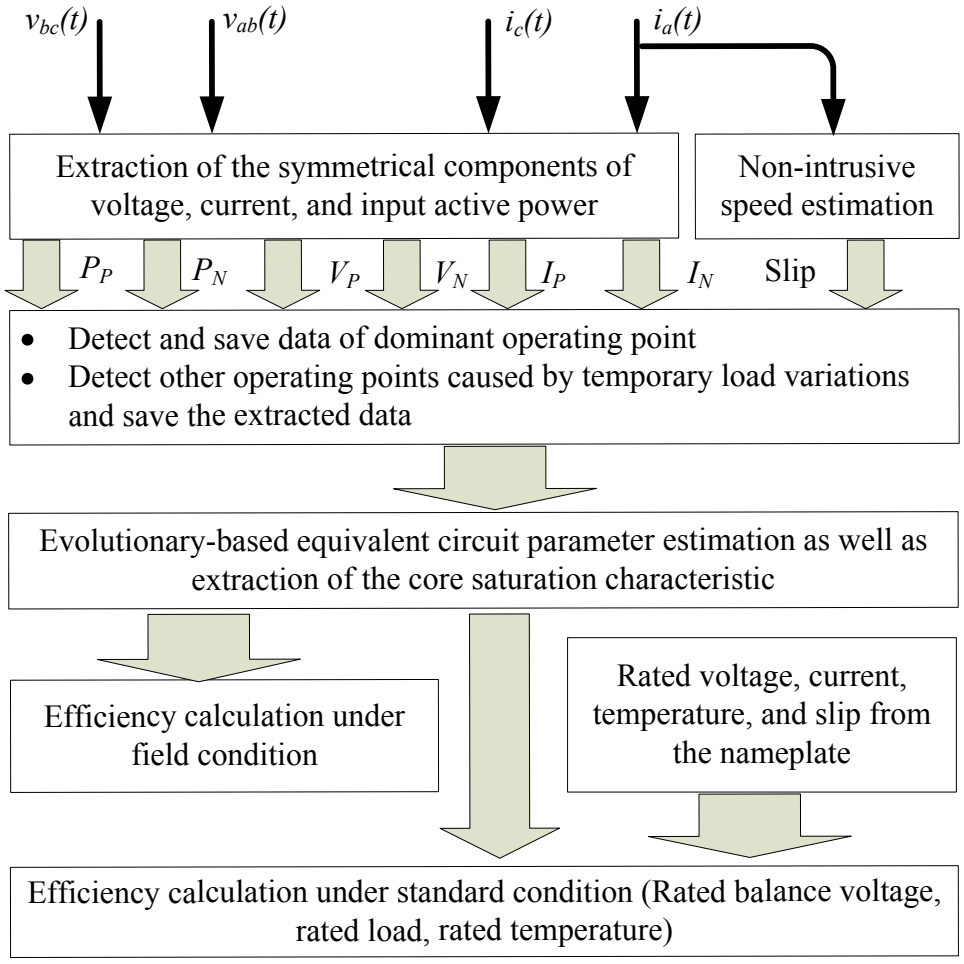

Fig. 4.6 Flowchart of the proposed efficiency estimation technique

4.3 Non Intrusive Air-Gap Torque (NAGT) Method

As discussed briefly in Chapter 1, the air-gap torque (AGT) method was proposed for the first time in [19] and [20] for the in-situ efficiency estimation process. In this method, the air-gap torque was calculated based on (1.8) with the use of the voltage and current signals as well as the magnitude of the stator's resistance at operating temperature. The efficiency (η) was then calculated using (1.9).

In [19], it is suggested that the core losses as well as friction and windage losses can be calculated with the air-gap torque calculation while the motor is working under no-load condition. The stray load loss at the rated load is assumed as a fixed percentage of the rated output power based on recommendations of the IEEE standard 112.

The efficiency calculation with this method requires a no-load test that imposes a high level of intrusion on the process. In addition, the resistance of the machine was measured at the operating point, which required a shutdown of the motor. In spite of these facts, the method led to a very accurate estimation of efficiency as shown in [20] and in section 4.5 of this chapter.

In [21], the non-intrusive version of the air-gap torque method (NAGT) was proposed. In this work, it is suggested that some empirical values for core losses, as well as friction and windage losses, be used in order to avoid the intrusiveness of the no-load test. In addition, a DC injection circuit is proposed and employed for the measurement of the stator's resistance.

Although the idea sounds promising, it creates some questions:

1) Is adding a circuit for online measurement of the stator resistance less intrusive than measuring the resistance itself?
2) Is considering a fixed value (3.5% of the output power [21]) for the sum of the core, and friction and windage losses accurate for all machines with different sizes?
3) In real life, some level of under- or overvoltage exists. What will happen in these cases?

4) Is considering a fixed value for stray load loss acceptable under partially loaded conditions?
5) What is the meaning of the calculated efficiency under field conditions? Is the calculated value useful for comparison purposes, or for estimation of the payback period in order to justify the replacement of an existing motor with a new one?

These important concerns are addressed below.

Adding a DC injection circuit requires an unpowered machine, and this imposes an additional intrusion level beyond the direct resistance measurement from the terminals of an unpowered machine.

The answer to the second concern is reported in [57] and [58] where no-load tests were performed with three different machines of different sizes. It was concluded in the testing that the assumption of 3.5% of the rated output power for a combination of the core, friction, and windage losses at the rated condition is not accurate for different machines. A similar conclusion has been made in section 4.5 of this chapter.

Moreover, as is stated in the third concern, the core loss is dependent on the magnitude of the input voltage of the machine. An assumption of a fixed value may lead to a significant error in estimated efficiencies where an under- or overvoltage problem exists.

As suggested in [20], the stray load loss is assumed based on the recommendations of the IEEE standard 112. It is also stated in this standard that the stray load loss must be

corrected for different loading conditions, as shown in (4.5), based on the rotor's current, which can be estimated with (4.6) if the no-load current of the machine is known [8].

$$P_{SLL} = P_{SLL,Rated}\left(\frac{I_R}{I_{R,Rated}}\right)^2 \tag{4.5}$$

$$I_R = \sqrt{I_{In,Meas}{}^2 - I_{In,Noload}{}^2} \tag{4.6}$$

where

$P_{SLL,Rated}$: is the stray load loss at the rated load

P_{SLL} : is the stray load loss at partial load

$I_{R,\ Rated}$: is the rotor current at the rated load

I_R : is the rotor current at partial load

$I_{In,\ Meas}$: is the input current at partial load

$I_{In,Noload}$: is the input current at no-load

In the NAGT method, neither the no-load current nor the rotor's current is known at different loading condition as the no-load test is basically avoided. In [21], the value of the stray load loss at different loading conditions is simply considered equal to the rated condition. In the same work, it is mentioned that, on average, motors work at no more than 60% of their rated load due to oversized installation or under-loaded conditions.

Considering the rated stray loss to be equal to 1.8% of the rated output, the stray load loss for a machine that works with a rotor current equal to 60% of the rated current is shown in (4.7).

$$P_{SLL} = P_{SLL,Rated}\left(\frac{0.6I_{R,Rated}}{I_{R,Rated}}\right)^2 = 0.36P_{SLL,Rated} = 0.36 \times 1.8\% \times P_{Out,Rated} \tag{4.7}$$

As can be seen, the assumption of a stray load loss being equal to the rated value will lead to an overestimation of this loss by around (1-0.36) x 1.8% = 1.15% of the rated output power. Considering a roughly linear relationship between the output power and rotor current for the sake of simplicity, the relative error in efficiency can be calculated as shown in (4.8).

$$\varepsilon_\eta = \frac{\Delta\eta}{\eta} = \frac{1.15\% \times \frac{P_{Out}}{0.6}}{\frac{P_{In}}{\frac{P_{Out}}{P_{In}}}} = 1.92\% \tag{4.8}$$

In [57], a linear regression method is proposed for the improvement of the stray load loss estimation in partially loaded conditions. The stray load loss is considered as a function of the square of the torque for each load. Therefore a straight line, passing through the origin and the assumed value of the stray load loss at the rated conditions, is used to estimate the improved value of the stray load loss in partially loaded conditions. The effect of this modification is shown in section 4.5.

Based on discussions to this point, it can be concluded that the efficiency estimated by the NAGT method is only valid for field conditions in which the measurement is done. Thus there is no way to calculate the efficiency of the machine under standard conditions when the measurements are done in field conditions. Consequently, a comparison of the estimated efficiency of the tested machine with other machines is meaningless. This is the main weakness of the NAGT method.

As discussed in the previous section, in contrast to the NAGT method, the optimization-based method is capable of estimating the efficiency of the machine under standard conditions even when the in-situ measurement has been done under field conditions. This is due to the fact that the parameters of the machine are extracted in this method and therefore the equivalent circuits can be used for efficiency estimations under any condition. This is the main advantage of the equivalent circuit-based method over the NAGT method.

4.4 Experimental Results of the Proposed Algorithm in Unbalanced and Over-Undervoltage Conditions

In this section, the proposed evolutionary-based efficiency estimation method was used to estimate the efficiency of 3 hp and 7.5 hp squirrel cage induction motors with nameplate data, as shown in Table 2.1 and Table 4.1, respectively. The same experimental setup of Fig. 3.8 was used for these tests.

Table 4.1 Nameplate data of 7.5 hp induction machine

f	60 Hz	Design class	C
V_{LL}	230/460 V	Insulation class	F
I	17.7/8.85 A	Nominal speed	1755 rpm
Connection	Δ	Poles	4

The proposed evolutionary-based efficiency estimation algorithm was used to estimate the efficiency of the tested 3 hp induction machine under three different scenarios:

1) Rated voltage unbalanced (RVU) operation: The positive sequence component of the voltage was equal to the rated value (208 V) and the voltage unbalance factor (VUF) was around 5%.
2) Under voltage unbalanced (UVU) operation: The positive sequence component of the voltage was around 90% of the rated value and the VUF was around 5%.
3) Overvoltage unbalanced (OVU) operation: The positive sequence component of the voltage was around 105% of the rated value and the VUF was around 5%.

In all three cases, the induction machine worked at 75 % of the rated load until the thermal steady state operating point was achieved. Then short term load fluctuations, e.g., with a one minute duration, were applied to the motor in order to obtain the additional load points for the efficiency estimation process. In this case, the temperature of all short term operating points was considered equal to the temperature of the main operating point. The extracted data after measurement is shown in Table 4.2, Table 4.3, and Table 4.4 for the unbalanced rated, under- and overvoltage conditions, respectively.

Table 4.2 Different operating points with around 5% VUF and rated voltage for a 3hp machine (RVU)

% of rated load	25	50	75	85	100
$V_{In,P}$ (V)	120.30	119.82	119.25	118.58	118.53
$V_{In,N}$ (V)	7.47	7.39	7.24	7.32	7.25
$I_{In,P}$ (A)	6.26	7.00	8.21	8.81	9.85
$I_{In,N}$ (A)	3.41	3.43	3.43	3.47	3.46
$P_{In,P}$ (W)	872.94	1468.32	2087.04	2359.50	2765.63
$P_{In,N}$ (W)	47.47	48.90	49.48	51.63	51.86
Speed (rpm)	1786.0	1773.1	1760.0	1751.9	1742.3

Table 4.3 Different operating points with around 5% VUF and 10% undervoltage for a 3hp machine (UVU)

% of rated load	25	50	75	85	100
$V_{In,P}$ (V)	109.32	108.71	108.05	107.39	106.84
$V_{In,N}$ (V)	6.02	5.92	5.80	5.79	5.66
$I_{In,P}$ (A)	4.93	6.15	7.91	8.77	10.09
$I_{In,N}$ (A)	2.64	2.78	2.86	2.85	2.83
$P_{In,P}$ (W)	790.75	1400.44	2051.87	2342.17	2755.39
$P_{In,N}$ (W)	25.89	30.23	32.45	33.32	33.18
Speed (rpm)	1784.3	1768.1	1750.3	1740.1	1727.2

Table 4.4 Different operating points with around 5% VUF and 5% overvoltage for a 3 hp machine (OVU)

% of rated load	**25**	**50**	**75**	**85**	**100**
$V_{In,P}$ (V)	126.76	126.06	125.67	125.36	125.17
$V_{In,N}$ (V)	7.24	7.14	7.12	7.06	7.01
$I_{In,P}$ (A)	7.38	7.84	8.81	9.27	10.12
$I_{In,N}$ (A)	3.49	3.45	3.49	3.46	3.45
$P_{In,P}$ (W)	950.26	1527.34	2145.46	2400.06	2797.06
$P_{In,N}$ (W)	49.87	49.57	51.04	51.03	51.25
Speed (rpm)	1787.1	1775.8	1762.9	1756.6	1748.6

As an aside, from the measured data of Table 4.3 and in the case of 75% of the rated load, it can be shown that:

$$\frac{V_{In,P}}{V_{In,Rated}} = \frac{108.05\,V}{120.00\,V} \times 100 = 90\% \tag{4.9}$$

$$\frac{V_{In,N}}{V_{In,P}} = \frac{5.80\,V}{108.05\,V} \times 100 = 5.3\% \tag{4.10}$$

So it can be reasoned that the machine was working with 10% undervoltage and around 5% VUF. The estimated efficiencies after convergence of the algorithm were compared with the measured values as shown in Table 4.5 to Table 4.7 for RVU, UVU, and OVU cases, respectively. It should be emphasized that the estimated efficiencies in these cases were efficiencies under field conditions.

Table 4.5 Estimated vs. measured efficiencies for a 3 hp machine with rated voltage and 5% VUF (RVU)

% of rated load	25	50	75	85	100
Measured efficiencies (%)	59.17	72.57	77.43	77.64	78.23
Estimated efficiencies (%)	64.87	75.92	79.30	79.76	79.79
Error (%)	5.70	3.35	1.87	2.12	1.56

Table 4.6 Estimated vs. measured efficiencies for a 3 hp machine with 10% undervoltage and 5% VUF (UVU)

% of rated load	25	50	75	85	100
Measured efficiencies (%)	67.85	77.58	79.59	79.71	78.67
Estimated efficiencies (%)	70.86	79.35	80.92	80.61	79.83
Error (%)	3.01	1.77	1.33	0.90	1.16

Table 4.7 Estimated efficiencies vs. measured efficiencies for a 3 hp machine with 5% overvoltage and 5% VUF (OVU)

% of rated load	25	50	75	85	100
Measured efficiencies (%)	55.55	70.25	75.75	76.78	77.85
Estimated efficiencies (%)	61.88	74.02	78.09	78.90	79.35
Error (%)	6.33	3.77	2.34	2.12	1.50

As can be seen from the results, the proposed algorithm is capable of estimating the efficiency of the tested machine in situ within an acceptable range of error under unbalanced over- or undervoltage conditions. However, what is important is to be able to

estimate the efficiency of the machine under standard supply and load conditions even when the in-situ measurement has been done under field conditions (unbalanced supply, under- or overvoltage condition, partially loaded machine). To verify this capability, the data of the UVU condition was used to estimate the efficiency of the machine under standard conditions. The results were compared with the measured values of the efficiencies under standard conditions (balanced rated voltage and rated load), as shown in Fig. 4.7.

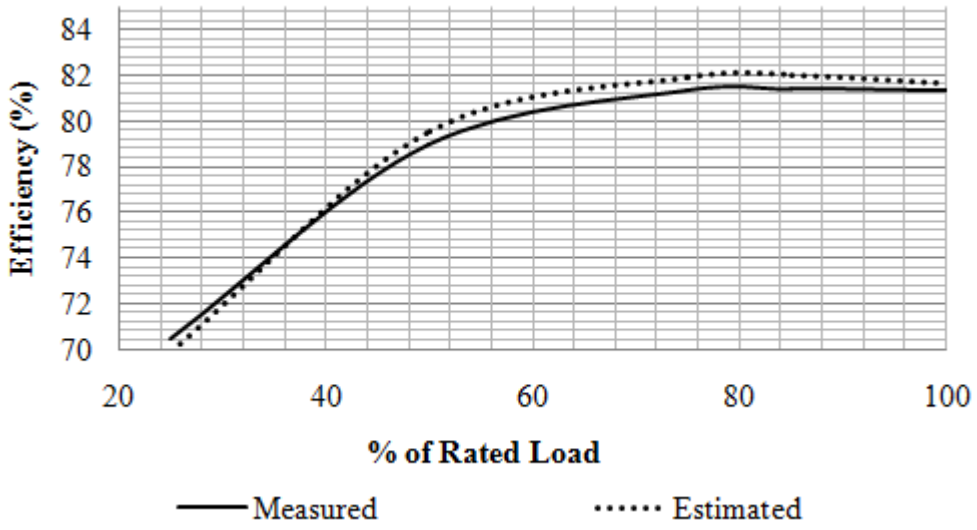

Fig. 4.7 Estimated efficiencies for standard conditions from UVU measurements vs. measured efficiencies in standard conditions

In case of the 7.5 hp machine, the test was only performed for the following two cases.

1) RVU operation: The positive sequence component of the voltage was equal to the rated value (230 V) and the VUF was around 6%.

2) UVU operation: The positive sequence component of the voltage was around 90% of the rated value and the VUF was around 6%.

In both cases, the induction machine worked at 65% of the rated load until the thermal steady state operating point was achieved. Short term load fluctuations, e.g., with a one minute duration, were then applied to the motor in order to achieve the extra load points for the efficiency estimation process. The extracted data, after measurements, is shown in Table 4.8 and Table 4.9 for the unbalanced rated and undervoltage conditions, respectively. The test in an overvoltage unbalanced condition was not performed for this machine due to power supply limitations in the laboratory.

Table 4.8 Different operating points with around 6% VUF and rated voltage for a 7.5hp machine (RVU)

% of rated load	**25**	**50**	**65**	**85**	**100**
$V_{In,P}$ (V)	234.16	231.98	230.69	229.81	228.43
$V_{In,N}$ (V)	14.24	13.72	13.46	13.21	13.07
$I_{In,P}$ (A)	4.19	5.86	7.03	8.67	10.10
$I_{In,N}$ (A)	3.17	3.66	3.89	4.09	4.21
$P_{In,P}$ (W)	1613.87	3118.62	3987.63	5125.57	6064.13
$P_{In,N}$ (W)	44.60	56.23	62.65	68.35	71.77
Speed (rpm)	1790.7	1780.6	1775.1	1766.9	1759.5

The estimated efficiencies under field conditions were compared with the measured values as shown in Table 4.10 and Table 4.11.

Table 4.9 Different operating points with around 6% VUF and 10% undervoltage for a 7.5hp machine (UVU)

% of rated load	25	50	65	85	100
$V_{In,P}$ (V)	210.47	208.54	206.09	205.13	203.83
$V_{In,N}$ (V)	12.79	12.13	12.01	11.93	11.83
$I_{In,P}$ (A)	3.97	6.08	7.53	9.58	11.22
$I_{In,N}$ (A)	2.74	3.36	3.57	3.77	3.85
$P_{In,P}$ (W)	1598.26	3114.83	4002.21	5208.29	6117.94
$P_{In,N}$ (W)	33.66	47.39	53.11	58.45	61.02
Speed (rpm)	1788.0	1775.4	1767.4	1756.2	1746.0

Table 4.10 Estimated vs. measured efficiencies for a 7.5 hp machine with rated voltage and 6% VUF (RVU)

% of rated load	25	50	65	85	100
Measured efficiencies (%)	83.43	88.31	88.57	88.70	88.32
Estimated efficiencies (%)	85.94	89.78	89.89	89.45	88.73
Error (%)	2.51	1.47	1.32	0.76	0.41

Table 4.11 Estimated vs. measured efficiencies for a 7.5 hp machine with 10% undervoltage and 6% VUF (UVU)

% of rated load	25	50	65	85	100
Measured efficiencies (%)	86.25	88.64	88.53	87.86	86.97
Estimated efficiencies (%)	84.48	88.15	88.13	87.35	86.25
Error (%)	-1.77	-0.49	-0.40	-0.50	-0.73

The data of the UVU condition was used to estimate the efficiency of the machine under standard conditions. The results were compared to the available values of the efficiencies for standard conditions provided by the manufacturer of the machine (Fig. 4.8).

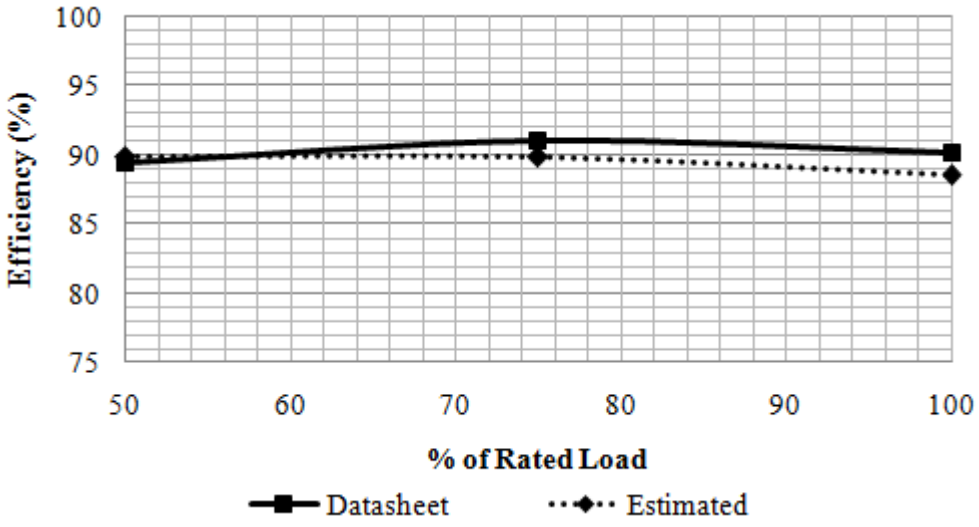

Fig. 4.8 Estimated efficiencies for standard conditions from the UVU measurements vs. efficiencies from data sheet measurements

The experimental results verified the generality and effectiveness of the proposed efficiency estimation algorithm.

4.5 Experimental Results of the NAGT Method

The non-intrusive air-gap torque method of [21] and its modified version (MNAGT), [57] and [58], were used to estimate the efficiency of the same machines under the same conditions. In fact, the same recorded data was used with these methods. The efficiency estimation results are shown in Fig. 4.9 to Fig. 4.11 for the 3 hp machine and Fig. 4.12 to Fig. 4.13 for the 7.5 hp machine. In these figures, the results of NAGT, MNAGT and the

proposed evolutionary-based (EVB) efficiency estimation methods are compared with the direct measured efficiencies (using the torque/speed sensor).

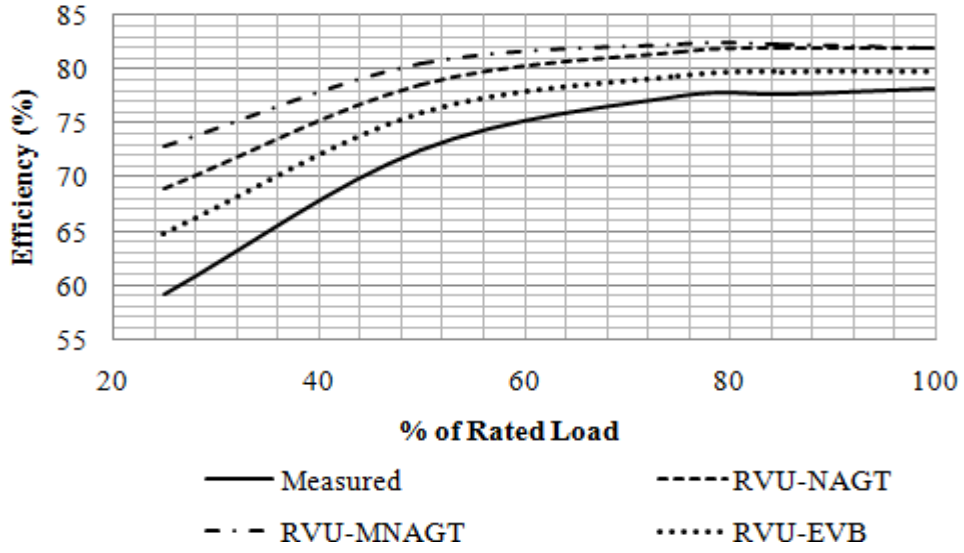

Fig. 4.9 Estimated efficiencies vs. measured values for the 3 hp machine at rated voltage unbalanced supply condition (RVU)

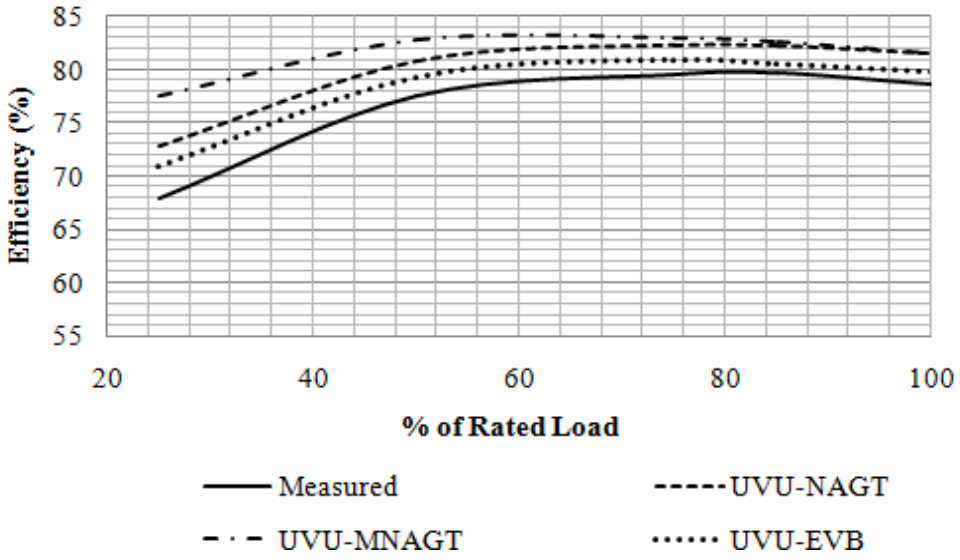

Fig. 4.10 Estimated efficiencies vs. measured values for the 3 hp machine in UVU supply conditions

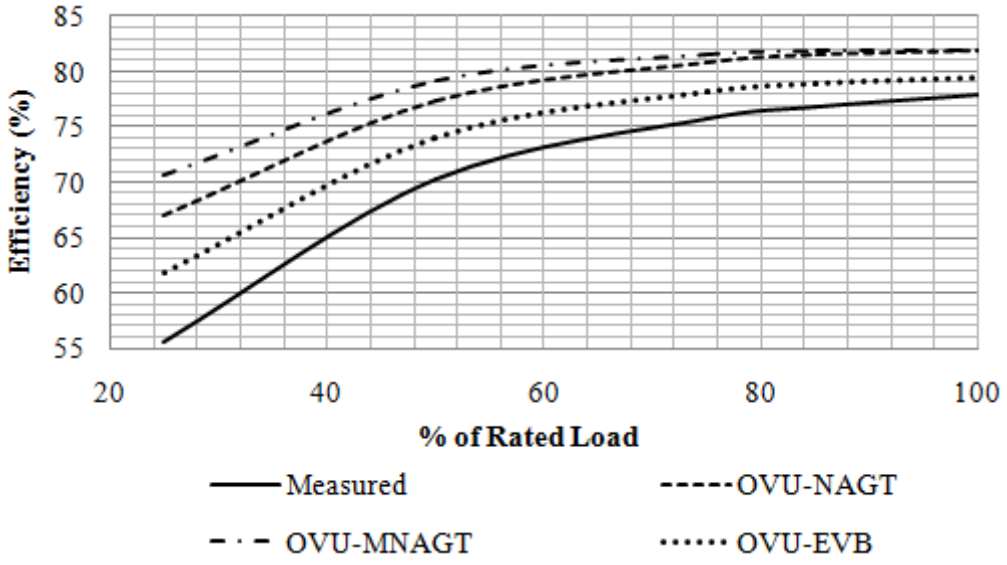

Fig. 4.11 Estimated efficiencies vs. measured values for the 3 hp machine in OVU supply conditions

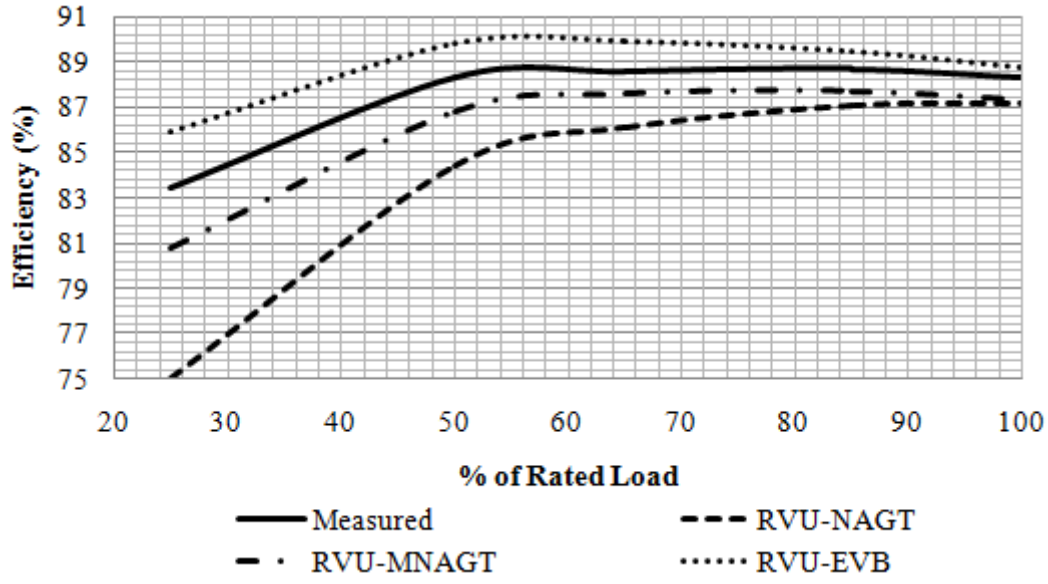

Fig. 4.12 Estimated efficiencies vs. measured values for the 7.5 hp machine in RVU supply conditions

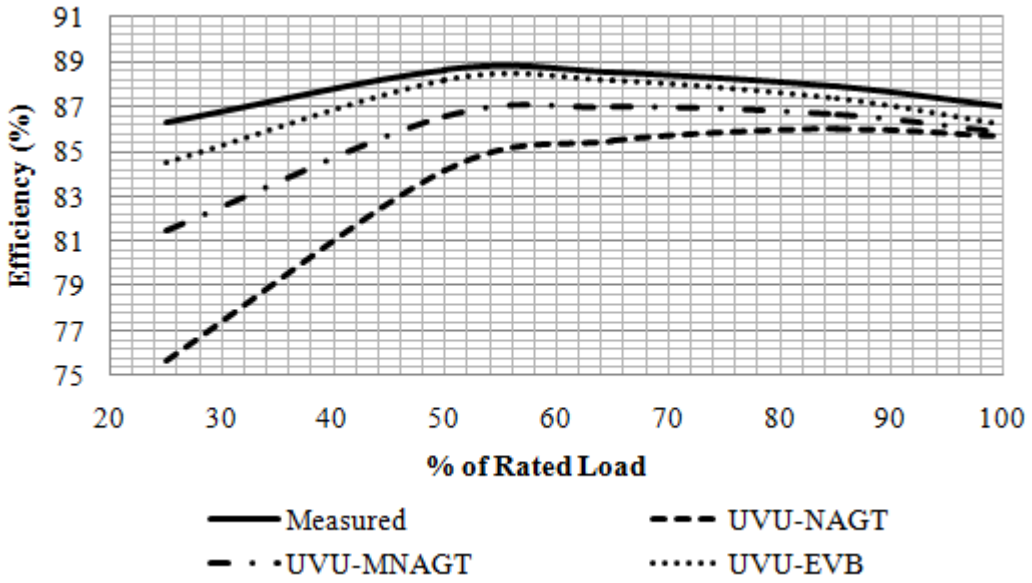

Fig. 4.13 Estimated efficiencies vs. measured values for the 7.5 hp machine in UVU supply conditions

As can be seen, the error of efficiency estimation with the NAGT method is higher, specifically for partially loaded conditions. In addition, in the case of the 3 hp machine, the modified method (MNAGT), which should have provided a better estimation in partially loaded conditions, led to a greater error.

Based on the performed no-load tests, the total no-load losses minus the copper losses in the rated load condition were around 196 W and 125 W for the 3 hp and 7.5 hp machines, respectively.

Based on the assumptions of the NAGT method [21], the total no-load losses minus the stator copper losses of a machine were considered to be 3.5% of the output power, which is around 78 W for a 3 hp and 195 W for a 7.5 hp machine. These differences created an

over-estimation of the efficiency in the case of the 3 hp machine and an underestimation for the 7.5 hp machine.

The results of the AGT method with the real values of the no-load losses of the 3 hp and 7.5 hp machines under the rated unbalanced condition are shown in Fig. 4.14 and Fig. 4.15, respectively. As can be seen, the efficiency estimation results are improved dramatically in comparison to Fig. 4.9 and Fig. 4.12. Notwithstanding, the modified method (MAGT) gives a more accurate estimation.

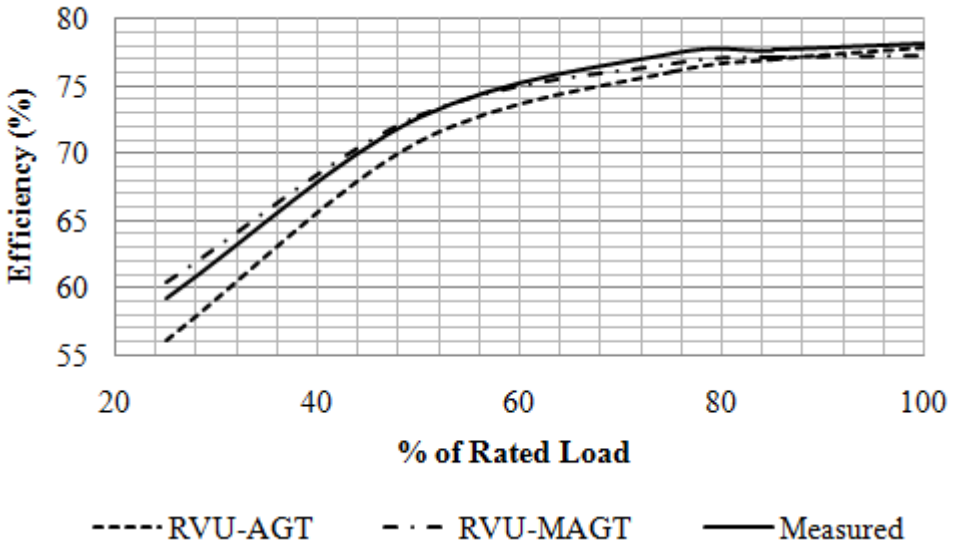

Fig. 4.14 . Estimated efficiencies with real no-load values vs. measured values for the 3 hp machine in RVU supply conditions

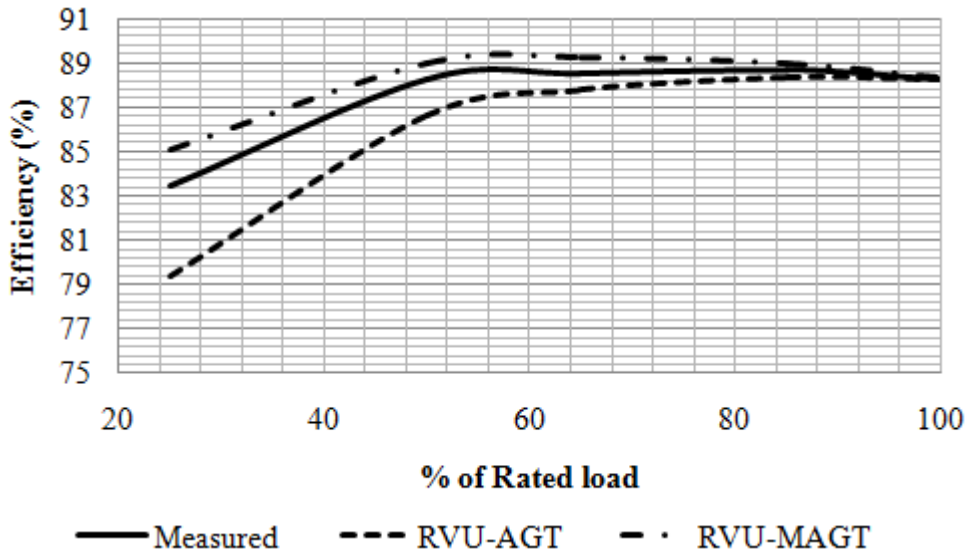

Fig. 4.15 Comparison of the estimated efficiencies with real no-load values of the 7.5 hp machine vs. measured values for the RVU supply

Based on the achieved results, it can be concluded that, although the AGT method is very accurate, the NAGT method, which is a non-intrusive version of the AGT method, lacks accuracy due to the fixed assumption of the no-load losses.

Even assuming an accurate estimation for the NAGT method, there is no way to calculate the efficiency of the machine in standard conditions from field measurements. This may lead to a significant error when assessing the benefits of replacing an existing motor with a new one.

4.6 Conclusions

In this chapter, an extension was proposed for the developed optimization-based in-situ efficiency estimation algorithm (outlined in the previous chapter) in order to make it compatible with over- or undervoltage and unbalanced supplies. The capability of the

proposed algorithm was demonstrated through experimental results with two different induction machines.

In addition, a comprehensive study was done on the functionality and accuracy of the NAGT method, which is claimed in literature to be one of the most promising methods. The details of the MNAGT method were reviewed, and it was shown that it leads to a better efficiency estimation by comparison to the NAGT method.

The results of the proposed method were compared with the NAGT method, and it was shown that the efficiency calculated by the NAGT method or its modified version is only valid under tested field conditions. Thus it cannot be used in the decision-making process regarding the replacement of existing machines or in calculations regarding the payback period. However, it was shown that the proposed method is capable of estimating the efficiency of the machine under standard conditions, even when the in-situ measurement has been done under field conditions.

Finally, it was demonstrated that the modified version of the air-gap torque method (MAGT) has the best accuracy, as claimed in literature. However, this method cannot be used for non-intrusive in-situ efficiency estimation due to its requirement for the intrusive no-load test. In addition, the efficiency calculated under this method is only valid under tested field conditions.

5. FULL LOAD EFFICIENCY ESTIMATION OF REFURBISHED INDUCTION MACHINES FROM NO-LOAD TESTING

5.1 Introduction

Quite a significant number of induction machines in industry are repaired at least once in their lifetime. Studies have shown that repaired and rewound motors suffer from efficiency changes. Various techniques have been proposed for efficiency estimation with different requirements. Standard routine tests are discussed in the IEEE standard 112 [8] and IEC 60034-2 standard [59]. Numerous other works have also been published with the aim of estimating the efficiency of the machines in situ, while they are working under load without interruption. However, very little has been done to find a simple yet reliable approach to estimate the efficiency of machines after the refurbishment process in workshops.

Being able to estimate the full load efficiency of a machine after its repair can help machine repair facilities to assess the quality of their work. Furthermore, it can also assist industrial facilities to make more informed decisions regarding the future replacement or repair of their existing machines. The majority of electrical machine refurbishment centers cannot afford to test machines with the well-accepted efficiency test method IEEE standard 112 method B, which requires dynamometer testing. In fact, these facilities are only able to start up the machine with an auto-transformer and run it at the rated no-load condition. Thus, typically they do not provide any information regarding the full load efficiency of the machine following its repair.

In this thesis, a simple method is proposed for the full load efficiency estimation from uncoupled no-load testing. This method is a modified version of IEEE standard 112 method F/F1, which incorporates the available data from uncoupled no-load testing, namely:

1. Voltage and current signals in a no-load testing condition.
2. Value of the stator resistance at the ambient temperature.
3. Nameplate data of the machine.

This chapter is organized as follows: the principles of the equivalent circuit based method of the IEEE standard 112 and, more specifically, details of the third impedance testing routine are reviewed in section 5.2. In section 5.3, this testing routine is used to find the parameters and efficiency of two different induction machines. As is shown, the achieved results are not satisfactory due to the existence of a problem in the method, which leads to an error in the estimated parameters. In section 5.4, a simple test is added to the proposed method in order to modify the existing problem. In section 5.5, the modified method is used to calculate the parameters and efficiency of the two tested induction machines, and the results are compared with the real measured efficiencies. The conclusions are presented in section 5.6.

5.2 Fundamentals of the Equivalent Circuit-Based Efficiency Estimation Method

In this section, the fundamentals of the equivalent circuit-based efficiency estimation method, IEEE standard 112 method F/F1 are reviewed, and the details of the third impedance testing routine are discussed.

As suggested in the IEEE standard 112, the efficiency of a machine can be found based on the following steps, using the method F/F1:

1) Measure the stator resistance at the ambient temperature.
2) Perform the variable voltage no-load test and measure the core losses as well as the friction and windage losses.
3) Perform the impedance test, and identify the rotor resistance and leakage reactance.
4) Determine the equivalent circuit parameters from the information of the previous steps.
5) Correct the value of the stator and the rotor resistances for the specified (rated) temperature.
6) Estimate the value of the stray load loss.
7) Solve the equivalent circuit iteratively and find the proper value of the slip for the desired output.
8) Estimate the efficiency.

The first two steps are the well-known routine DC measurement and no-load tests. Therefore they are not discussed here. The third step, which is the impedance test, is the most important part of this method. The third impedance testing routine of the IEEE

standard 112 has been chosen since it does not require a low frequency locked rotor test, and it can be applied simply in workshop applications.

In this method, the voltage of the machine is reduced until the full load slip is achieved. Then the parameters of the rotor are calculated based on an iterative approach.

A few typo errors were found in the equations of the standard. The corrected version is presented here and the details are explained.

In this method, the total per-phase reactance of the machine is calculated from the no-load saturation test, and the curve of the total per-phase reactance vs. no-load voltage is drawn, as shown in Fig. 5.1, in the case of a typical machine.

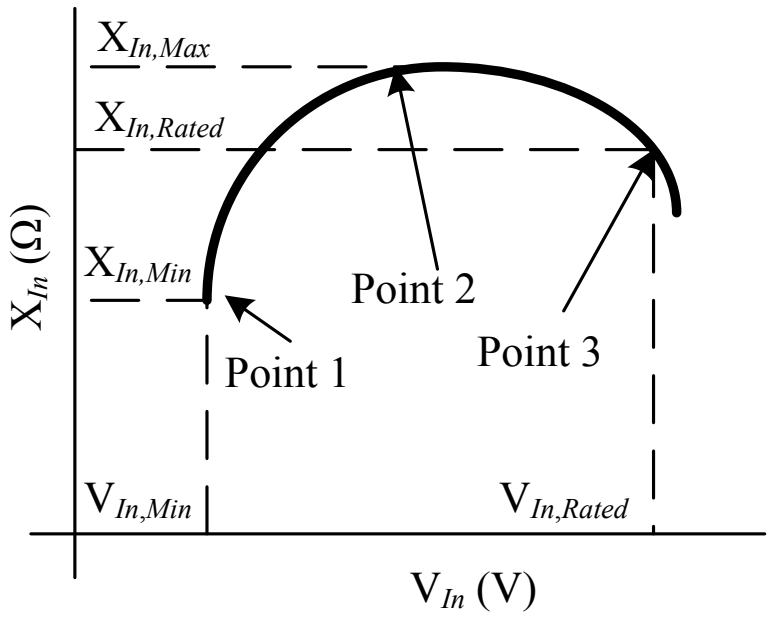

Fig. 5.1 Total no-load per-phase input reactance vs. no-load per-phase voltage [8]

where

$V_{In,Rated}$: is the rated voltage of the machine

$V_{In,Min}$: is the minimum voltage which gives the largest possible slip

$X_{In,Rated}$: is the input reactance at the rated voltage

$X_{In,Min}$: is the input reactance at minimum voltage

$X_{In,Max}$: is the maximum input reactance

To better understand the concept of the method, it is important to grasp the reason for the input reactance vs. voltage curve being almost circular. The input reactance of the machine was calculated based on Fig. 5.2, as shown in (5.1). In (5.1), R_M was neglected for the sake of simplicity.

$$X_{In} = X_1 + \left(\frac{\left(\frac{R_2}{S}\right)^2 + X_2\left(X_M + X_2\right)}{\left(\frac{R_2}{S}\right)^2 + \left(X_M + X_2\right)^2} \right) . X_M = X_1 + K.X_M \tag{5.1}$$

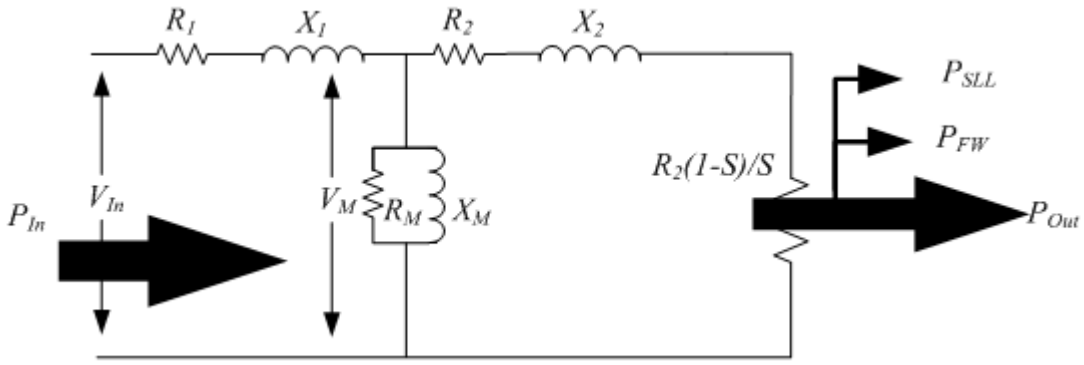

Fig. 5.2 Equivalent circuit of an induction machine

where

R_1 : is the stator resistance

X_1 : is the stator leakage reactance

R_2 : is the rotor resistance

X_2 : is the rotor leakage reactance

X_M : is the mutual reactance of the machine

R_M : is representative of the core loss

S : is the slip of the induction motor

P_{SLL} : is the stray load loss

P_{FW} : is the friction and windage loss

P_{In} : is the electrical input power

P_{Out} : is the mechanical output power on the shaft

K : is the constant defined in (5.1)

Three different regions can be assumed on this curve:

1) High voltage region: In this region, the slip of the machine is very close to zero and therefore the constant K will be very close to 1, as shown in (5.2).

$$Lim_{S\to 0}\, K = Lim_{S\to 0}\left(\frac{\left(\frac{R_2}{S}\right)^2 + X_2\left(X_M + X_2\right)}{\left(\frac{R_2}{S}\right)^2 + \left(X_M + X_2\right)^2}\right) \approx \frac{\left(\frac{R_2}{S}\right)^2}{\left(\frac{R_2}{S}\right)^2} = 1 \tag{5.2}$$

Consequently, X_{In} can be written as follows:

$$X_{In} = X_1 + X_M \tag{5.3}$$

Since the machine is saturated in this region, X_M and consequently X_{In} are decreased by increasing the voltage.

2) Medium voltage region: In this region slip is still close to zero and thus (5.3) is still valid. However, the machine is not saturated and the value of X_M is the same as one in the low voltage region.
3) Low voltage region: In this section of the curve, the slip of the machine starts increasing with the reduction in the voltage to compensate for friction and windage losses and, therefore, K is not equal to 1 anymore. Based on (5.4), it is possible to show that K is smaller than 1 and its value decreases with the increase of the slip.

$$\left(X_M + X_2\right)^2 > X_2\left(X_M + X_2\right) \Rightarrow K < 1 \tag{5.4}$$

So based on (5.1) and (5.4), it can be concluded that X_{In} will be decreased by the reduction of the voltage, as shown in Fig. 5.1.

According to the above explanation, it can be concluded that the values of the mutual reactance at point 1 and 2 are almost equal, since the machine is not yet saturated. Hence the data of these two points can be used to find the parameters of the machine in the low voltage region.

The following iterative approach, which is proposed in the IEEE standard 112, was used to find the parameters of the machine. The initial value for the sum of the stator and the rotor leakage reactances ($X_{Sum} = X_1 + X_2$) was assumed to be equal to $X_{In,Min}$. The stator leakage reactance was found based on (5.5).

$$X_1 = X_{Sum} \frac{\left(\frac{X_1}{X_2}\right)}{1+\left(\frac{X_1}{X_2}\right)} \tag{5.5}$$

The ratio of X_1/X_2 was assumed, based on the design class of the machine and the recommendation of IEEE standard 112, as shown in Table 3.1 in Chapter 3.

Other parameters of the machine were found based on (5.6) to (5.15). These equations should be repeated iteratively until stable values of X_1 and X_2 are achieved.

$$X_M = X_{In,Max} - X_1 \tag{5.6}$$

$$\theta_1 = -\arccos\left(\frac{P_{In}}{3V_{In}I_{In}}\right) \tag{5.7}$$

$$V_M = \sqrt{\left[V_{In} - I_{In}\left(R_1 \cos\theta_1 - X_1 \sin\theta_1\right)\right]^2 + \left[I_{In}\left(R_1 \sin\theta_1 + X_1 \cos\theta_1\right)\right]^2} \tag{5.8}$$

$$\theta_2 = \arctan\frac{-I_{In}\left(R_1 \sin\theta_1 + X_1 \cos\theta_1\right)}{V_{In} - I_{In}\left(R_1 \cos\theta_1 - X_1 \sin\theta_1\right)} \tag{5.9}$$

$$I_M = \frac{V_M}{X_M} \tag{5.10}$$

$$R_M = \frac{{V_M}^2}{\frac{P_C}{3}} \tag{5.11}$$

$$I_C = \frac{V_M}{R_M} \tag{5.12}$$

$$I_R = \sqrt{\left[I_{In}\cos\theta_1 - I_M \sin\theta_2 - I_C \cos\theta_2\right]^2 + \left[I_{In}\sin\theta_1 + I_M \cos\theta_2 - I_C \sin\theta_2\right]^2} \tag{5.13}$$

$$X_2 = \frac{-V_{In} I_{In} \sin\theta_1 - {I_{In}}^2 X_1 - {I_M}^2 X_M}{{I_R}^2} \tag{5.14}$$

$$X = X_1 + X_2 \tag{5.15}$$

After converging to the stable values of the reactances, the rotor resistance can be found using (5.16) [8] and the slip of the motor at point 1.

$$R_2 = S\sqrt{\left(\left(\frac{V_2}{I_2}\right)^2 - {X_2}^2\right)} \tag{5.16}$$

To make the method simple and applicable in a workshop environment and to avoid the coupling issues, the proposed machine current signature analysis-based speed estimation technique (Chapter 2) is employed for speed measurements.

In [8], it is assumed that the stable value of X_1, determined from the iterative solution of the previous equations, can be used for the rated voltage condition. Thus (5.17) can be employed to find the mutual reactance of a machine at the rated voltage condition.

$$X_{M,Rated} = X_{In,Rated} - X_1 \tag{5.17}$$

After estimating the machine parameters at the ambient temperature, the calculated values of the stator and the rotor resistances should be corrected for the specified (rated) temperature. The standard temperature rise test requires the rated loading of the machine, thus it cannot be easily carried out in refurbishments centers. If the data of the rated temperature rise is available, it should be used for the purpose of correction. If not, the only possible solution is to assume a value based on the insulation class of the machine and the recommendations of the IEEE standard 112, as shown in Table 3.2 of Chapter 3. Equation (5.18) can be used to correct the value of each resistance [8]:

$$R_{Rated} = \frac{R_a\left(T_{Rated} + K\right)}{\left(T_a + K\right)} \tag{5.18}$$

where

R_a : is the value of resistance at the ambient temperature

R_{Rated} : is the value of resistance at the rated temperature

T_a : is the ambient temperature

T_{Rated} : is the known rated temperature, based on the available data or Table 3.2

K : is 234.5 for stator resistance and 225 for rotor resistance [8]

The indirect measurement of the stray load loss requires the dynamometer test, and the direct measurement involves the reverse rotational test. Neither of these requirements is achieved easily in a workshop environment. Therefore, as for method F1, an empirical value is assumed for the stray load loss. In this work, the value was assumed based on the IEC 60034-2-1 standard [59], as shown in (5.19), for machines with an output power greater than 1 kW and smaller than 10 MW. The value from the IEC standard was chosen over that of IEEE standard 112 due to its improved accuracy.

$$P_{SLL} = P_{In} \times [0.025 - 0.005 \log_{10} (\frac{P_{Out}}{1\,kW})] \tag{5.19}$$

After the estimation and correction of all parameters, the slip of the machine at each loading condition was found iteratively. This means that the slip of the machine at any load and voltage condition was found by changing the slip and solving the equivalent circuit until the desired output power was obtained. The proper value of the slip was used

in the calculation of the input power, input current, and power factor. The efficiency was calculated based on these slips.

The abovementioned equivalent circuit-based efficiency estimation algorithm is coded in the Matlab/Simulink software package, and it is used to find the efficiency of a 3 hp and a 7.5 hp induction machine. The results are discussed in the next section.

5.3 Experimental Results of the IEEE Method

In this section, the abovementioned testing routine was used to find the efficiency of a 3 hp and a 7.5 hp induction machine in the laboratory. The nameplate data of these machines is shown in Table 2.1 and Table 4.1, respectively. Each step of the discussed efficiency estimation process is shown below.

Step 1: DC measurement test to find the stator resistance.

3 hp machine: 0.67 Ω/phase

7.5 hp machine: 0.71 Ω/phase

Step 2: No-load test to find the core loss, and friction and windage losses.

The input power minus the stator copper losses vs. voltage square curve is shown for the tested 3 hp and 7.5 hp induction machines in Fig. 5.3 and Fig. 5.4, respectively. The core loss at the rated voltage condition, and the friction and windage losses were calculated from the following figures.

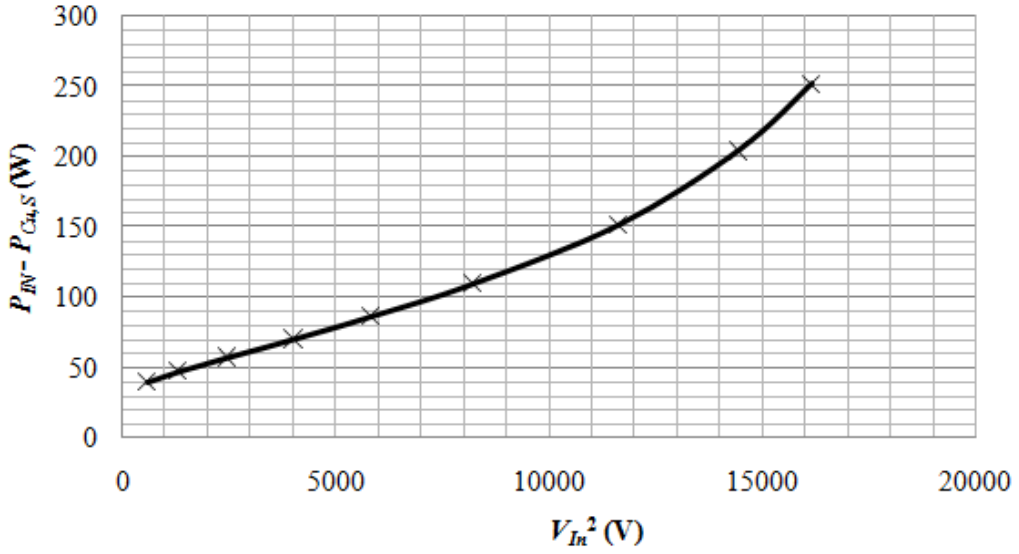

Fig. 5.3 No-load input power vs. no-load voltage square curve for the 3 hp machine

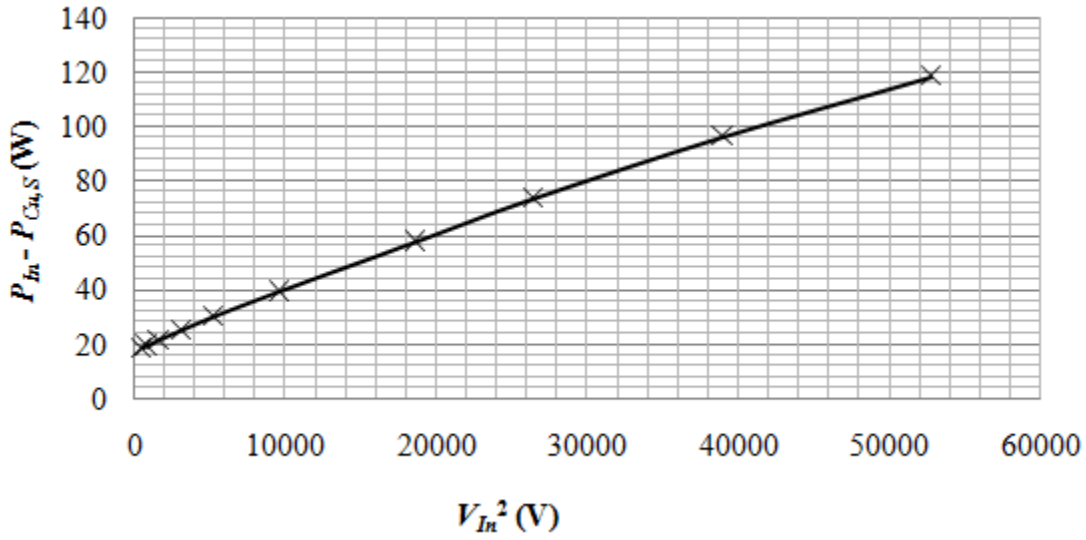

Fig. 5.4 No-load input power vs. no-load voltage square curve for the 7.5 hp machine

Step 3: The impedance test was performed for the tested two machines. The curves of the total no-load per-phase input reactance vs. no-load per-phase voltage were obtained and shown for the two tested machines in Fig. 5.5 and Fig. 5.6, respectively.

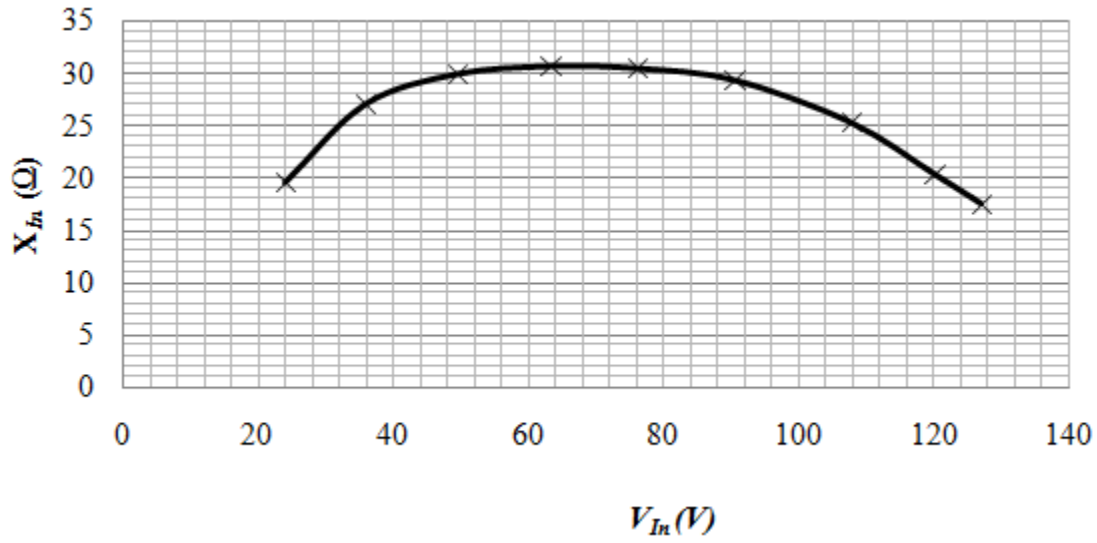

Fig. 5.5 No-load input reactcance vs. voltage curve for the 3 hp machine

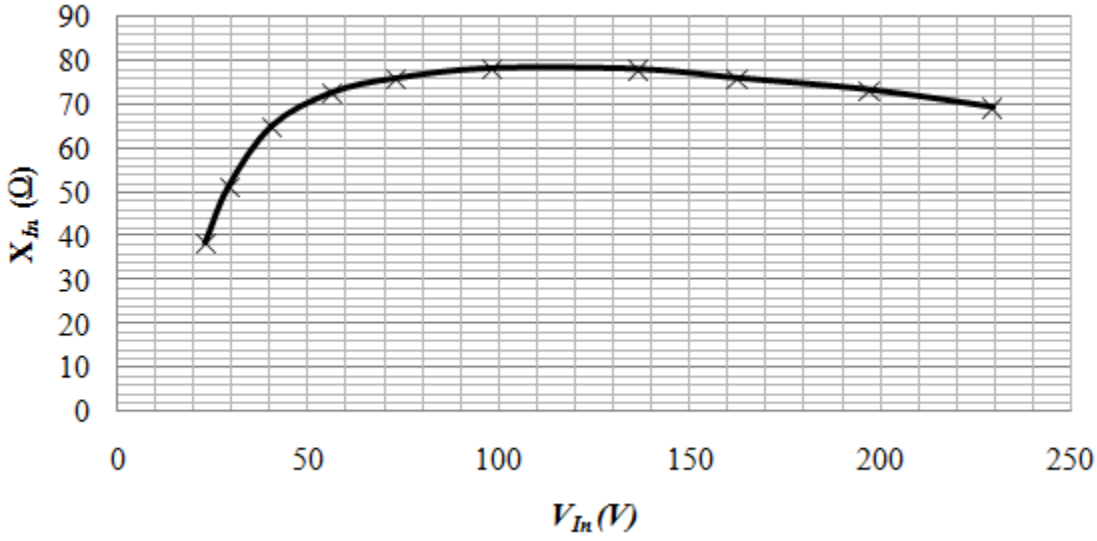

Fig. 5.6 No-load input reactance vs. voltage curve for the 7.5 hp machine

As can be seen, the curves of these two machines are quite different in the high voltage region. This is due to the fact that the first machine was a standard machine with a noticeable saturation rate in the high voltage region, while the second was an energy-efficient machine with a very low saturation rate.

The slip of the machines at minimum voltage was extracted from the current signal, as shown in Fig. 5.7 and Fig. 5.8 for the 3 hp and 7.5 hp machines, respectively.

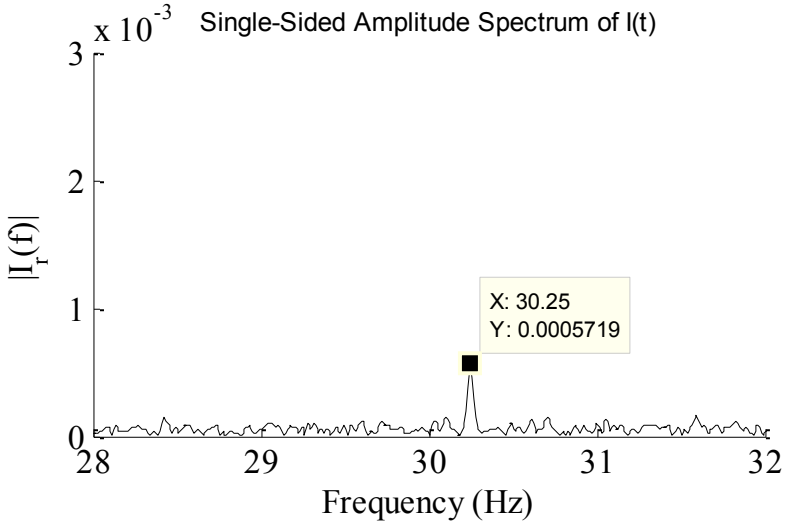

Fig. 5.7 Speed-dependent current harmonic of the 3 hp machine at low voltage point

Considering (2.23) from Chapter 2, the number of pole pairs (equal to 2), the supply frequency (60 Hz), and the possible slip range from 0 to 0.055 (1700 rpm), it was anticipated that the speed-dependent current harmonic would be somewhere between 30 Hz and 31.67 Hz. As shown in Fig. 5.7 and Fig. 5.8, the frequency of this harmonic was found to be equal to 30.25 Hz in the case of the 3 hp machine and 30.21 Hz in the case of the 7.5 hp machine. Using (2.23), 30.25 Hz was found to be equivalent to 1785.8 rpm and

30.21 Hz to 1787.5 rpm. The slip estimation was based on 60 seconds of data acquisition with 5 kHz sampling rate.

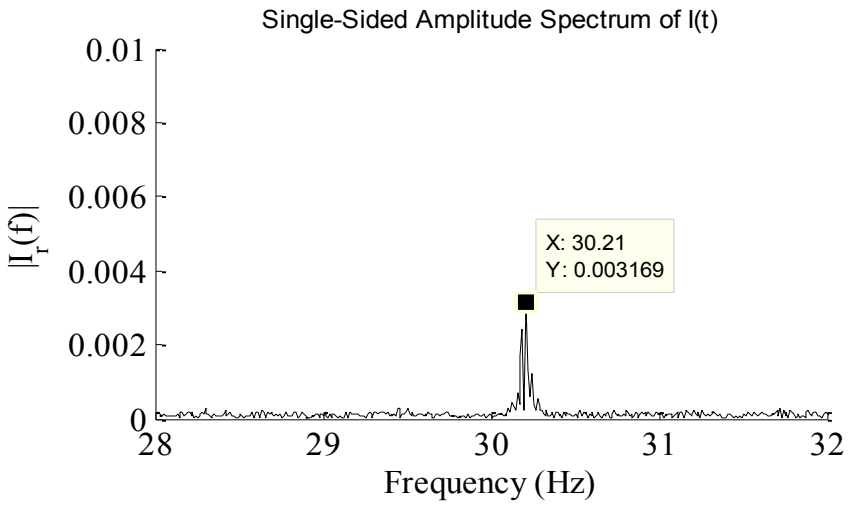

Fig. 5.8 Speed-dependent current harmonic of the 7.5 hp machine at low voltage point

Step 4: The discussed iterative approach of the IEEE standard 112 has been coded in the Matlab/Simulink software package, and it was used with the data obtained from the previous steps to find the parameters of the machines. The estimated parameters are shown below.

Table 5.1 Estimated parameters of the 3 hp and 7.5 hp machines

Parameters	3 hp	7.5 hp
R_1	0.67 Ω	0.71 Ω
X_1	2.37 Ω	8.77 Ω
X_2	3.54 Ω	20.41 Ω
R_2	0.32 Ω	0.38 Ω
X_M	17.94 Ω	60.56 Ω
R_M	198.7 Ω	1214Ω

Step 5: The value of the stator and rotor resistances were corrected to the specified temperature. The specified temperature of each machine was assumed based on the insulation class of the machine and Table 3.2 of Chapter 3. The results are shown below.

Table 5.2 Corrected resistances of the 3 hp and 7.5 hp machines

Parameters	3 hp	7.5 hp
R_1	0.85 Ω	0.96 Ω
R_2	0.41 Ω	0.52 Ω

Step 6: The stray load losses were assumed based on (5.19).

Step 7: Based on the estimated parameters, the equivalent circuit was solved iteratively to find the slip in which the machine provided the rated output power. Surprisingly, no slip was found with these parameters. This means that the value of the estimated parameters was not correct.

To better understand the problem, the equivalent circuit of the machine was solved using the rated speed from the nameplate. The output powers, the input currents and the power factor were found as follows:

3 hp machine: I_{In} = 10.63 A, P_{Out} = 2.56 hp, PF=0.65

7.5 hp machine: I_{In} = 7.89 A, P_{Out} = 2.46 hp, PF=0.41

By comparing the results with the nameplate values, it was concluded that the input impedance of the machines was estimated to be much bigger than their real values.

More investigation into the parameters and the source of the error made it clear that the problem was the value of the stator and rotor leakage reactances. Consequently, the inaccurate value of the stator leakage reactance in (5.17) led to the erroneous value of the mutual reactance at the rated voltage condition.

In fact, the problem lies in the assumption of the IEEE standard 112, which considers that the stator and rotor leakage reactance determined from the proposed impedance test method in the low voltage region can also be used for the rated voltage condition. As is shown in Fig. 5.9 and Fig. 5.10 for the tested 3 hp and 7.5 hp induction machines respectively, the value of the current in the low voltage region is very small. Due to the small value of the current and consequently the non-saturated teeth of the machine, the reluctance of the leakage flux path in the machine is much smaller than the rated condition. Consequently, the reactance is much bigger than the rated condition where the value of the current is higher.

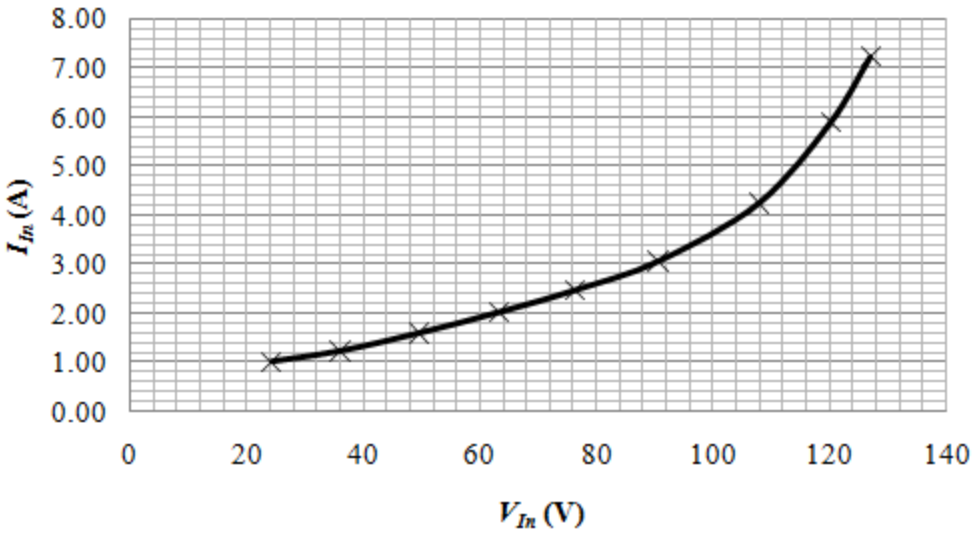

Fig. 5.9 No-load current vs. no-load voltage curve of the 3 hp machine

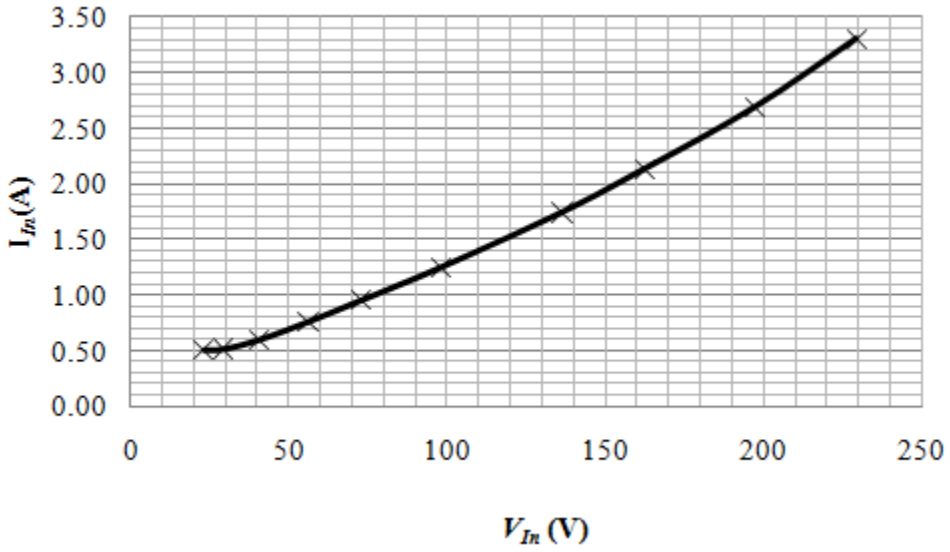

Fig. 5.10 No-load current vs. no-load voltage curve of the 7.5 hp machine

Based on this explanation, the value obtained for the leakage reactance at the low voltage region is not valid for the rated voltage condition, and another method should be used to estimate these parameters. It should be mentioned that the value of the rotor resistance

obtained in this method was still valid for the rated condition, since the rotor resistance was not dependent on the current.

5.4 Proposed Modification to the IEEE Method

In this section, a simple test was proposed in order to find the values of the leakage reactances that can later be used to find the mutual reactance of the machine at the rated voltage level and, finally, the efficiency at any loading condition. This test was called the "virtual locked rotor test".

As is known, in the very first cycles before the machine starts to rotate, the situation is very similar to the locked rotor test. Consequently, it should be possible to use the data of these cycles to find the leakage reactances. However, two main points should be considered:

1) In the case of the rated voltage start-up, the machine accelerates very fast, and there is a significant electrical transient in the current. Therefore it is almost impossible to extract the locked rotor parameters. However, in the case of a low voltage start-up, the electrical transient is smaller, the current is adequate, and, in addition, it takes quite a significant number of cycles before the machine starts up. Even after start-up, the machine accelerates very slowly, so there are a sufficient number of electrical cycles in which to extract the locked rotor parameters.
2) Since, in this condition, the frequency of the rotor current is 60 Hz, the rotor resistance calculated here cannot be used in the efficiency estimation process. However, the leakage reactance of the rotor is less dependent on the frequency than

the level of the current, as discussed before, and thus the accuracy of its value is sufficient for the efficiency estimation process. Moreover, the value of the rotor resistance is more critical for the efficiency estimation process in comparison to rotor leakage reactance, since R_2/s is always much greater than X_2 in the normal operation range of a motor.

The data of the voltage, current, and input power is required to find the leakage reactance of the machine from the virtual locked rotor test. In this case, two line voltage and current signals were used to obtain the required data. With knowledge of these values, the sum of the stator and rotor leakage reactance can be found based on (5.20).

$$X_1 + X_2 = \frac{V_{In,VLR}}{I_{In,VLR}} \times \sqrt{1 - \left(\frac{P_{In,VLR}}{3V_{In,VLR} I_{In,VLR}} \right)^2} \tag{5.20}$$

where

$V_{In,VLR}$: Phase voltage at low voltage virtual locked rotor test

$I_{In,VLR}$: Input current at low voltage virtual locked rotor test

$P_{In,VLR}$: Input power at low voltage virtual locked rotor test

After this step, (5.5) can be used to separate rotor and stator leakage reactances, and (5.17) can be employed to find the value of the mutual reactance at the rated voltage condition.

The proposed test was performed with the 3 hp and 7.5 hp induction machines, and the results are shown in Fig. 5.11 and Fig. 5.12, respectively.

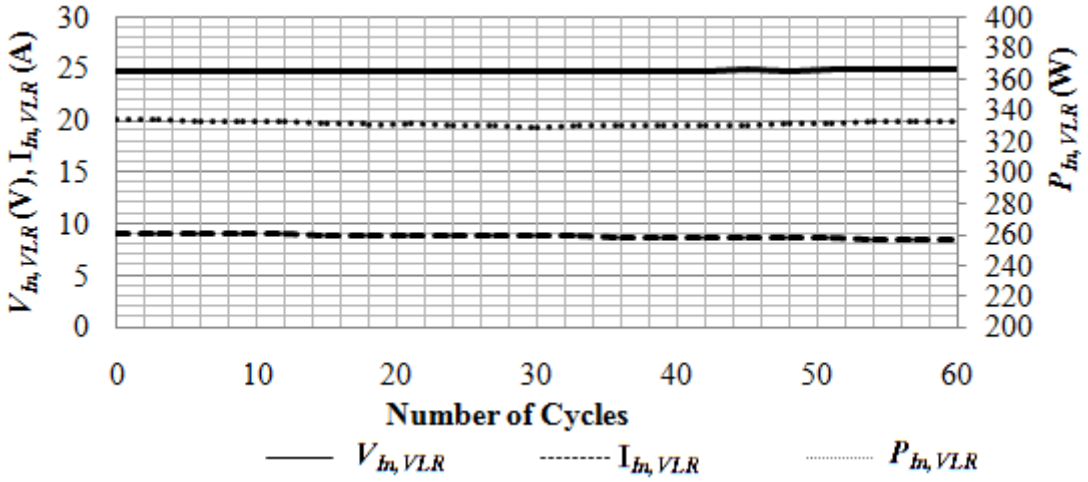

Fig. 5.11 The average rms voltage, average rms current, and input power at low voltage virtual locked rotor test for the 3 hp machine

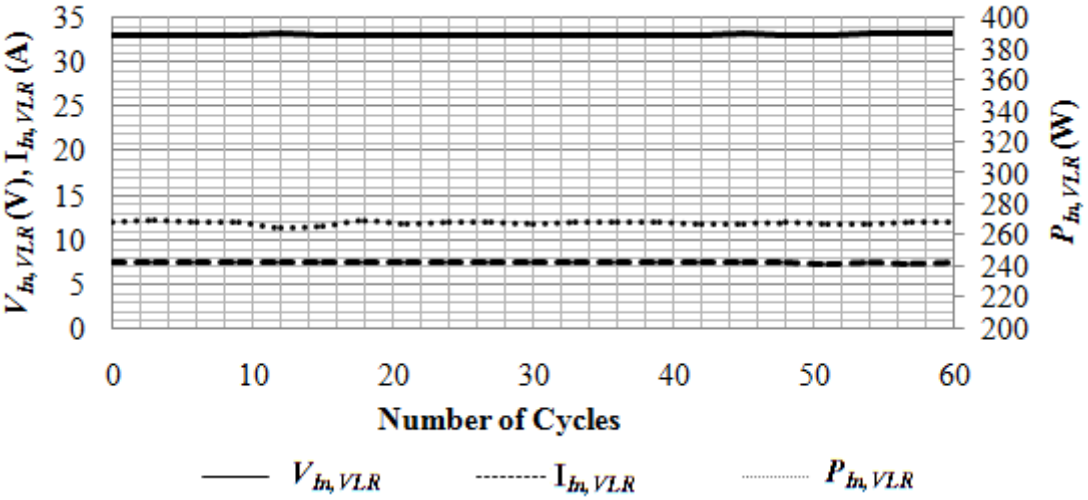

Fig. 5.12 The average rms voltage, average rms current, and input power at low voltage virtual locked rotor test for the 7.5 hp machine

As can be seen, the rms value of the current and voltage signals were almost constant during the 60 cycles following the low voltage start-up. The sum of the leakage reactance was calculated for the tested machines, and is shown in Fig. 5.13 and Fig. 5.14.

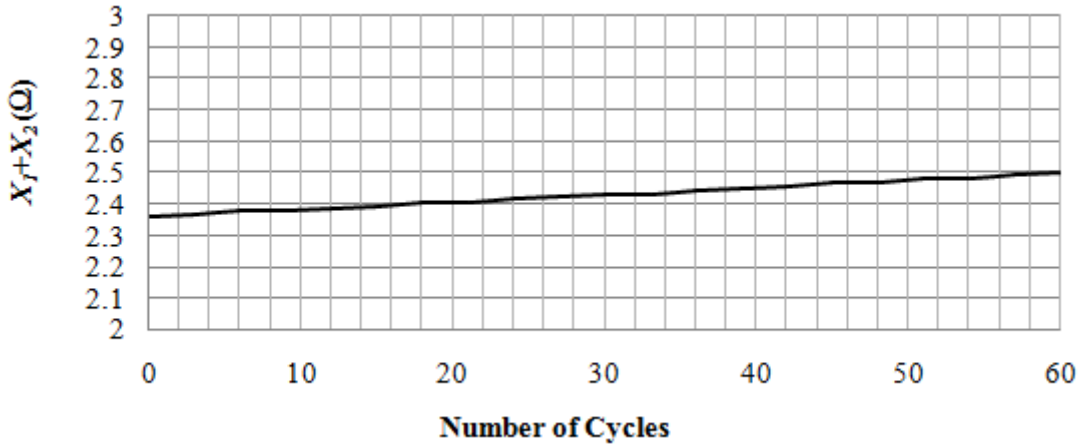

Fig. 5.13 The calculated sum of the leakage reactances based on data from the low voltage virtual locked rotor test of the 3 hp machine

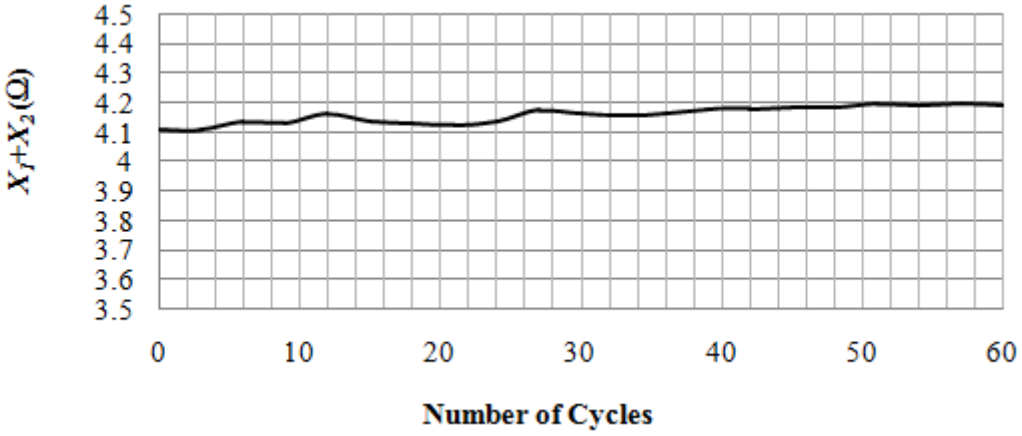

Fig. 5.14 The calculated sum of the leakage reactances based on data from the low voltage virtual locked rotor test of the 7.5 hp machine

The new parameters were calculated based on the results of the virtual locked rotor test, and they are shown in Table 5.3. It is evident that the parameters were significantly different from those found by the third impedance testing method of the IEEE standard 112 (shown in Table 5.1).

Table 5.3 Corrected parameters of the 3 hp and 7.5 hp machines

Parameters	3 hp	7.5 hp
X_1	0.94 Ω	1.23 Ω
X_2	1.41 Ω	2.87 Ω
X_M	19.36 Ω	68.10 Ω
R_M	231.2 Ω	1534 Ω

In the next section, the corrected parameters are used to estimate the efficiency of the tested machines.

5.5 Experimental Validation of the Modified Efficiency Estimation Method

In this section, the proposed efficiency estimation method was used to estimate the efficiency of the tested 3 hp and 7.5 hp squirrel cage induction machines. The same experimental setup of Fig. 3.8 was used to measure the real efficiency of the tested machines. As explained in Chapter 3, a torque/speed sensor was used to measure the accurate speed and torque values at each loading point. The measured values of the efficiencies were calculated based on these measurements, and they were used as a reference to validate the estimated efficiencies of the no-load uncoupled testing with the proposed method.

The measured efficiency values were compared with the estimated values from the no-load uncoupled testing shown in Table 5.4 and Table 5.5 for the tested 3 hp and 7.5 hp machines, respectively. In the case of the 3 hp motor, the machine was at the rated thermal steady state condition. In the case of the 7.5 hp motor, the rated thermal condition was not achieved because the dynamometer was not capable of absorbing 7.5 hp of continuous power. To validate the proposed method, the machine was run at 0.75% of the rated load until the thermal steady state condition was obtained. The temperature of the machine at this operating point (77 C°) was then used in the algorithm.

Table 5.4 Estimated efficiencies vs. measured efficiencies for the 3 hp machine

% of rated load	**50**	**75**	**100**
Measured efficiencies (%)	77.27	80.15	80.48
Estimated efficiencies (%)	76.29	79.14	79.40
Error (%)	-0.98	-1.01	-1.08

Table 5.5 Estimated efficiencies vs. measured efficiencies for the 7.5 hp machine

% of rated load	**50**	**75**	**100**
Measured efficiencies (%)	91.43	91.33	90.45
Estimated efficiencies (%)	91.77	91.38	90.00
Error (%)	0.34	0.05	-0.45

5.6 Conclusions

In this chapter, a simple method was proposed for the full load efficiency estimation of induction machines from uncoupled no-load testing, which can be used in refurbishment facilities where standard dynamometer testing is not viable. The proposed method is a modified version of the equivalent circuit-based method, IEEE standard 112 method F/F1, which requires only the uncoupled no-load testing.

It was shown that the third impedance testing method of the IEEE standard 112 has some problems, and it cannot be used directly to find the parameters and efficiency of a machine.

A new test routine called the virtual locked rotor test is proposed to modify the IEEE method.

The method was validated by experimental results, and it was shown that the proposed method is capable of estimating the efficiency of machines within an acceptable range of error based on the data from no-load uncoupled testing.

6. CONCLUSIONS AND FUTURE WORK

6.1 Conclusions

In-situ machine efficiency estimation techniques are increasing in importance due to pressures to improve performance and demand side energy management. Numerous techniques have been proposed to estimate the efficiency of an induction motor in situ; however, very little has been done to make these methods compatible with unbalanced and over- or undervoltage supply conditions that exist in most industrial applications. In this thesis, a new evolutionary-based in-situ efficiency estimation technique, capable of dealing with unbalanced and over- or undervoltage supply conditions is proposed, which does not require an intrusive no-load test.

In the second chapter of the thesis, the non-intrusive speed detection technique and the symmetrical components extraction algorithm were proposed, based on a non-linear filter developed in [41].

From experimental results, it was concluded that the speed of the machine can be estimated non-intrusively only from the current signal.

It was also shown that the combination of the proposed filter and the Fortescue transformation can be used to extract the symmetrical components of the voltage, current, and input active power from the line voltage and current signals.

The extracted speed information, and the positive and negative sequence components are used as a set of input data for the developed efficiency estimation algorithms.

The new evolutionary-based in-situ efficiency estimation algorithm, which is capable of dealing with unbalanced supply conditions, was proposed in Chapter 3.

The proposed concept has been verified through simulation results. It was concluded that the parameters of a machine can be accurately estimated based on the input power and current information at multiple operating points.

Experimental results with two different machines were used to validate the effectiveness and generality of the proposed method. It was concluded that the algorithm is capable of estimating the efficiency in unbalanced supply conditions within an acceptable margin of error.

Based on the performed analysis, it was concluded that the final estimated efficiencies are not really sensitive to the assumptions.

Measurement error analysis was done to guarantee the accuracy of the measured efficiencies. Based on the provided analysis, it was concluded that the measurements were done within an acceptable range of error, and thus they can be used as reference values.

Repeatability tests were performed, and it was concluded that the results were consistent.

The effect of the input data on the accuracy of the final estimated efficiencies was investigated in detail. It was concluded that the algorithm is capable of estimating efficiency without the requirement of decoupling the shaft and performing an intrusive no-load test. However, at least one light load operating point is required in order to have

acceptable efficiency estimation. It was also concluded that a higher number of data points will not bring a significant advantage if at least one light and one heavy load point are included.

In Chapter 4, the algorithm was extended to be able to estimate the efficiency in unbalanced and over- or undervoltage conditions. It was shown that the changes in mutual reactance due to saturation should be included in the method in order to have an acceptable estimation of the efficiency.

In addition, a comprehensive study was done on the functionality and accuracy of the non-intrusive air-gap torque (NAGT) method, which is claimed in literature to be one of the most promising methods. The details of the modified non-intrusive air-gap torque (MNAGT) method were reviewed, and it was shown that it leads to improved efficiency estimation when compared to the NAGT method.

The experimental results of the proposed method with two different machines were compared to the NAGT method, and it was shown that the efficiency calculated by the NAGT method or its modified version is only valid under the tested field conditions. Consequently, it was concluded that these methods cannot be used in the decision-making process regarding the replacement of existing machines or the relevant calculations regarding the payback period.

It was shown that, unlike the NAGT method, the proposed method is capable of estimating the efficiency of a machine under standard conditions even when the in-situ measurement has been completed under field conditions.

Finally, it was observed that the modified version of the air-gap torque method (MAGT) has the best accuracy, as claimed in the reviewed literature. However, this method cannot be used for non-intrusive in-situ efficiency estimation due to the requirement for an intrusive no-load test.

A simple method is proposed for full load efficiency estimation of induction machines from the uncoupled no-load testing in Chapter 5. The method is specifically designed for efficiency estimation in motor workshops. The proposed method is a modified version of the equivalent circuit-based method, IEEE standard 112 method F/F1, which requires only uncoupled no-load testing.

The problems with the third impedance testing method of the IEEE standard 112 were discussed, and it was concluded that this method cannot be used directly to find the parameters and efficiency of a machine.

A new test routine called a virtual locked rotor test was proposed to modify the IEEE method. The method was validated by experimental results, and it was concluded that the method is capable of estimating the efficiency of machines within an acceptable range of error, based on the data from no-load uncoupled testing.

6.2 Proposed Future Work

In this section, some suggestions are made for future studies based on experiences during this work.

6.2.1 Improvement in Non-Intrusive Speed Detection Technique

As mentioned in the thesis, at least 60-seconds of data acquisition are required in order to have an estimated speed with acceptable accuracy for efficiency estimation process. This is mainly due to the inherent limitation of the Fast Fourier Transformation.

One subject of research could be to use other techniques in order to reduce the required data acquisition time and still conserve the same level of accuracy in speed estimation.

6.2.2 Estimation of the Stator Resistance

As discussed in Chapter 3, the value of stator resistance at an ambient temperature is assumed to be known through measurements from the motor control center when the motor is in shutdown mode.

It would be useful if a technique could be developed to estimate stator resistance from only the current and voltage signals of a loaded machine without adding any circuit to measure this resistance.

6.2.3 Improvement in Temperature Estimation Algorithm

In this work, the working temperature of the machine under a partially loaded condition is estimated based on an assumed rated temperature rise. This rise is assumed based on the insulation class of the machine and the recommendations of the IEEE standard 112. It is evident that an empirical value cannot be accurate for different machines.

It would be valuable if a non-intrusive way of estimating the temperature, which does not depend on the assumed rated temperature rise, could be found.

6.2.4 Effects of Harmonics

In this work, it is assumed that the grid is not a significant source of harmonics. This is not necessarily true for different power systems.

It would be beneficial to add the effect of harmonics into the efficiency estimation algorithm.

6.2.5 Investigation on the Effects of Fluctuating Power Component on the Efficiency

Under unbalance voltage conditions, the input and output powers contain average and time varying components which oscillate at a frequency equal to double of the fundamental frequency. Due to the existence of time varying components in the input and output powers, the efficiency which is defined as the ratio of the output power to the input power will also contain a time varying component. It would be beneficial to investigate the possible effects of the fluctuating component on the machine's efficiency.

6.2.6 Building the Efficiency Estimation Tool

The application of the efficiency estimation tool based on the proposed algorithm in a real industrial environment with different machines will lead to new directions in order to

modify the limitations of the proposed method. Thus, it would be highly advantageous to build an industrial version of this tool.

REFERENCES

[1] P. Pillay, K. A. Fendley, "The contribution of energy efficient motors to demand and energy savings in the petrochemical industry," *IEEE Trans. Power Syst*., vol. 10, pp. 1085–1093, May 1995.

[2] H.R.776, Energy Policy Act of 1992, sec. 122. "Energy conservation requirements for certain commercial and industrial equipment, energy conservation standards for high-intensity discharge lamps, distribution transformers, and small electric motors" [online], Available: http://thomas.loc.gov

[3] U. S. DOE Energy Efficiency and Renewable Energy (EERE), DOE Industry Tools. DOE Motor Master+ Website, [Online], Available: http://www1.eere.energy.gov/industry /bestpractices/software.html

[4] Ching-Yin Lee, Bin-Kwie Chen, Wei-Jen Lee, Yen-Feng Hsu, "Effects of various unbalanced voltages on the operation performance of an induction motor under the same voltage unbalance factor condition," in *Proc. IEEE Technical Conf. on Industrial and Commercial Power Systems*, 1997, pp. 51-59.

[5] P. Pillay, P. Hofmann, M. Manyage, "Derating of induction motors operating with a combination of unbalanced voltages and over or under voltages," *IEEE Trans. Energy Convers.*, vol. 17, no. 4, pp. 485- 491, Dec 2002.

[6] H. M. Mzungu, P. Barendse, M. A. Khan and M. Manyage, "Determination of effects on induction motor efficiency", *ICUE Conference*, South Africa, Cape Town, May 2008.

[7] H. M. Mzungu, M. J. Manyage, M. A. Khan, P. Barendse, T. L. Mthombeni,; P. Pillay, "Application of induction machine efficiency testing standards in South Africa," in *Proc. IEEE Int. Conf Electric Machines and Drives* , 2009. pp. 1455-1462.

[8] " IEEE Standard Test Procedure for Polyphase Induction Motors and Generators", *IEEE Standard 112*, 2004.

[9] NEMA standard Publication MG1-1987

[10] A. Siddique, G. S. Yadava, B. Singh "Effects of voltage unbalance on induction motors," in *Proc. IEEE Int. Symposium. Electrical Insulation*, 2004, pp. 26- 29

[11] Ching-Yin Lee, "Effects of unbalanced voltage on the operation performance of a three-phase induction motor," *IEEE Trans. Energy Conversion*, vol. 14, no. 2, pp. 202-208, Jun 1999

[12] J. S. Hsu, J. D. Kueck, M. Olszewski, D. A. Casada, P. J. Otaduy, L. M. Tolbert, "Comparison of induction motor field efficiency evaluation methods, " *IEEE Tran. Ind. Appl.*, vol. 34, no. 1, pp. 117-125, Feb. 1998.

[13] F. Ferreira, A. T. de Almeida, "Considerations on in-field induction motor load estimation methods", in *Proc. IEEE Int. Conf.* Electrical Machines, 2008, pp. 1-8.

[14] J. R. Holmquist, J. A. Rooks, M. E. Richter, "Practical approach for determining motor efficiency in the field using calculated and measured values," *IEEE Trans. Ind. Appl.,* vol. 40, no. 1, pp. 242- 248, Feb. 2004

[15] Bin Lu, T. G. Habetler, R. G. Harley, "A survey of efficiency-estimation methods for in-service induction motors," *IEEE Tran. Ind. Appl.*, vol. 42, no. 4, pp. 924-933, Aug. 2006.

[16] J. D. Kueck, M. Olszewski, D. A. Casada, J. Hsu, P. J. Otaduy, and L. M. Tolbert, "Assessment of methods for estimating motor efficiency, and load under field conditions," Oak Ridge National Laboratory Rep., ORNL/ TM-13165, pp. 1- 47, 1996.

[17] Y. El-Ibiary, "An accurate low-cost method for determining electric motors' efficiency for the purpose of plant energy management," *IEEE Tran. Ind. Appl*., vol. 39, no. 4, pp. 1205-1210, Aug. 2003.

[18] "In-plant electric motor loading and efficiency techniques," Ontario Hydro Rep., TSDD-90-043, 1990.

[19] J. S. Hsu, B. P. Scoggins, "Field test of motor efficiency and load changes through air-gap torque," *IEEE Trans. Energy Convers.*, vol. 10, no. 3, pp. 477-483, Sep. 1995.

[20] J. S. Hsu, P. L. Sorenson, "Field assessment of induction motor efficiency through air-gap torque," *IEEE Trans. Energy Convers.*, vol. 11, no. 3, pp. 489-494, Sep. 1996.

[21] Bin Lu, T. G. Habetler, R. G. Harley, "A nonintrusive and in-service motor-efficiency estimation method using air-gap torque with considerations of condition monitoring," *IEEE Trans. Ind. Appl.*, vol. 44, no. 6, pp. 1666-1674, Dec. 2008

[22] P. Pillay, V. Levin, P. Otaduy, J. Kueck, "In situ induction motor efficiency determination using the genetic algorithm," *IEEE Trans. Energy Convers.*, vol. 13, no. 4, pp. 326-333, Dec 1998.

[23] A. Charette, J. Xu, A. Ba-Razzouk, P. Pillay, V. Rajagopalan, "The use of the genetic algorithm for in situ efficiency measurement of an induction motor," in *Conf. Rec. IEEE Power Engineering Society Winter Meeting*, 2000, pp. 392-397.

[24] T. Phumiphak, C. Chat-uthai, "Estimation of induction motor parameters based on field test coupled with genetic algorithm," in *Proc. IEEE Int. Conf. Power System Technology*, 2002, pp. 1199- 120.

[25] M. S. Aspalli, S. B. Shetagar, S. F. Kodad, "Estimation of induction motor field efficiency for energy audit and management using genetic algorithm," in *Proc. Int. Conf. Sensing Technology*, 2008, pp. 440-445

[26] T. Phumiphak, C. Chat-uthai, "An economical method for induction motor field efficiency estimation for use in on-site energy audit and management," in *Proc. IEEE Int. Conf. Power System Technology*, 2004, pp. 1250- 1254.

[27] Bin Lu, Cao Wenping; I. French, K. J. Bradley, T. G. Habetler, "Non-intrusive efficiency determination of in-service induction motors using genetic algorithm and air-gap torque methods," in *Conf. Rec. IEEE 42nd IAS Annual Meeting*, 2007, pp. 1186-1192.

[28] M. Cunkas, T. Sag, “Efficiency determination of induction motors using multi-objective evolutionary algorithms”, *Elsevier J. Advances in Engineering Software*, vol. 41, pp. 255-261, Feb. 2010.

[29] V. P. Sakthivel, R. Bhuvaneswari, S. Subramanian, "Non-intrusive efficiency estimation method for energy auditing and management of in-service induction motor using bacterial foraging algorithm," *IET Electr. Power Appl*.,vol.4, pp.579-590, Sept. 2010.

[30] E. B. Agamloh, A. K.Wallace, A. von Jouanne, K. J. Anderson, J. A. Rooks, "Assessment of nonintrusive motor efficiency estimators," *IEEE Tran. Ind. Appl.*, vol. 41, no. 1, pp. 127- 133, Jan.-Feb. 2005

[31] P. Pillay, P. Hofmann, M. Manyage, "Derating of induction motors operating with a combination of unbalanced voltages and over or undervoltages," *IEEE Trans. Energy Convers.*, vol.17, no. 4, pp. 485- 491, Dec. 2002.

[32] J. Faiz, H. Ebrahimpour, P. Pillay, "Influence of unbalanced voltage on the steady-state performance of a three-phase squirrel-cage induction motor," *IEEE Trans. Energy Convers.*, vol.19, no. 4, pp. 657- 662, Dec. 2004

[33] Yaw-Juen Wang, "Analysis of effects of three-phase voltage unbalance on induction motors with emphasis on the angle of the complex voltage unbalance factor," *IEEE Trans. Energy Convers.*, vol.16, no. 3, pp.270-275, Sep 2001

[34] M. Anwari, A. Hiendro, "New unbalance factor for estimating performance of a three-phase induction motor with under- and overvoltage unbalance," *IEEE Trans. Energy Convers.*, vol.25, no. 3, pp.619-625, Sept. 2010

[35] P. Gnacinski, " Derating of an induction machine under voltage unbalance combined with over or undervoltages", *Elsevier J. Energy Conversion and Management,* 2009*,* vol. 50, pp. 1101-1107

[36] P. Pillay, M. Manyage, "Loss of life in induction machines operating with unbalanced supplies," *IEEE Trans. Energy Convers.*, vol. 21, no. 4, pp. 813-822, Dec. 2006.

[37] J. R. Gomez, E. C. Quispe, M. A. de Armas, P. R. Viego, "Estimation of induction motor efficiency in situ under unbalanced voltages using genetic algorithms," *in Proc. IEEE Int. Conf. Electrical Machines,* 2008, pp. 1-4.

[38] F. Waldhart, J. P. Bache, "Online efficiency determination of three phase asynchronous machines by start-up data," *in Proc. IEEE Int. Conf. Diagnostics for Electric Machines, Power Electronics and Drives*, 2009, pp. 1-6.

[39] C. Grantham, H. Tabatanaei-Yazdi, M.F. Rahman, "A novel method for rapid efficiency measurement of three phase induction motors," *IEEE Trans. Energy Convers*., vol. 14, no. 4, pp. 1236-1240, Dec 1999

[40] D. J. McKinnon, C. Grantham, "Improved efficiency test methods for three-phase induction machines," *in Conf. Rec. IEEE 40th IAS Annual Meeting*, 2005 , pp. 466- 473.

[41] A. K. Ziarani, "Extraction of Non-stationary Sinusoids", *Ph.D. thesis*, *University of Toronto, Toronto*, Canada, 2002.

[42] A. Gharakhani Siraki, P. Pillay, "A novel evolutionary based in-situ efficiency estimation technique for induction machines working with unbalanced supplies," *in Conf. Rec. IEEE Electric Machines & Drives*, 2011, pp. 1563-1568

[43] A. Siraki, P. Pillay, "An in situ efficiency estimation technique for induction machines working with unbalanced supplies," *IEEE Trans. Energy Convers*., vol. 27, no. 1, pp. 85-95, March 2012

[44] A. Gharakhani Siraki, C. Gajjar, M.A. Khan, P. Barendse, P. Pillay, "An algorithm for non-intrusive in-situ efficiency estimation of induction machines operating with unbalanced supply conditions", *IEEE Tran. Ind. Appl.,* vol. 48, no. 6, Nov/Dec 2012.

[45] A. Gharakhani Siraki, P. Pillay, “Comparison of two methods for full load in situ induction machine efficiency estimation from field testing in the presence of over/under voltages and unbalanced supplies", *IEEE Tran. Ind. Appl.,* vol. 48, no. 6, Nov/Dec 2012.

[46] A. Gharakhani Siraki, P. Pillay, “Full load efficiency estimation of refurbished induction machines from no load test", *submitted to IEEE Tran. Energy Convers.*

[47] R. Naidoo, "A nonlinear adaptive filter for improved operation and protection of power systems ", *Ph.D. thesis*, *University of Cape Town, Cape Town*, South Africa, 2008.

[48] H. Douglas, P. Pillay, A.K. Ziarani, "A new algorithm for transient motor current signature analysis using wavelets," *IEEE Trans. Ind. Appl.*, vol. 40, no. 5, pp. 1361- 1368, Oct. 2004.

[49] P. S. Barendse, P. Pillay, "A new algorithm for the detection of faults in permanent magnet machines," *in Proc. IEEE Int. Conf. Industrial Electronics*, 2006, pp. 823-828.

[50] B. W. Williams, J. K. Goodfellow, T. C. Green, "Sensorless speed measurement of inverter driven squirrel cage induction motors," in *Proc. IEEE Int. Conf. Power Electronics and Variable-Speed Drives*, 1991, pp. 297-300

[51] P. Pillay, Z. Xu, "Labview implementation of speed detection for mains-fed motors using motor current signature analysis," *IEEE Power Eng. Review*, vol. 18, pp. 47- 48, June 1998.

[52] K. D. Hurst, T.G. Habetler, " Sensorless speed measurement using current harmonic spectral estimation in induction machine drives " *IEEE Trans. Power Electronics*, vol. 11, no. 1, pp. 66-73, Jan 1996.

[53] S. E. Zocholl, E. O. Schweitzer, A. Aliaga-Zegarra, "Thermal protection of induction motors enhanced by interactive electrical and thermal models," *IEEE Trans. Power App. and Syst.*, vol. PER-4, no. 7, pp. 1749-1755, July 1984

[54] J. S. Hsu, J. D. Kueck, M. Olszewski, D. A. Casada, P. J. Otaduy, L. M.Tolbert, "Comparison of induction motor field efficiency evaluation methods ," in *Conf. Rec. IEEE Ind. Appl. Annual Meeting*, 1996, pp. 703-712

[55] A. E. Eiben, J. E. Smith, “Introduction to evolutionary computing”, Natural Computing Series, 2nd printing, New York: Springer-Verlag, 2007, ch. 3.

[56] Bin Lu, Cao Wenping, T. G. Habetler, "Error analysis of motor-efficiency estimation and measurement*," in Conf. Rec. IEEE Power Electronics Specialists*, 2007, pp. 612-618.

[57] B. Herndler, P. Barendse, M. A. Khan, "Considerations for improving the non-intrusive efficiency estimation of induction machines using the air gap torque method," *in Conf. Rec. IEEE Electric Machines & Drives*, 2011, pp. 1516-1521.

[58] B. L. Herndler, "Non-intrusive efficiency estimation of induction machines," M.S. thesis, Dept. Elect. Eng., Cape Town Univ., Cape Town, South Africa, 2010.

[59] IEC 60034-2 International Standard, Rotating electrical machines – Part 2: "Standard methods for determining losses and efficiency from tests (excluding machines for traction vehicles)", IEC, Geneva, Switzerland, 2007.